POLITECNICO DI TORINO

Dipartimento Scienza Applicata e Tecnologia
Dottorato di Ricerca in Fisica

Nonlinear relativistic equation of state and phase transitions in nuclear matter at finite temperature and baryon density

Tesi di Dottorato

<table>
<tr><td>

Relatore:
Prof.
Andrea Lavagno
</td><td>

Candidato:
Daniele Pigato
</td></tr>
</table>

XXV ciclo
Anno Accademico 2010-2012

Abstract

The main goal of this Thesis, is the study of the thermodynamic properties of strongly interacting and dense nuclear matter, away from the nuclear ground state. This analysis constitutes one of the most interesting aspect and one of the major tasks in the modern high-energy nuclear physics.

The first part of this dissertation, addresses the phenomenological and theoretical study of the nuclear matter equation of state, under the extreme conditions reached in high energy heavy ion collision experiments and in astrophysical object, such as for example neutron stars.

Of particular interest is the determination of the microscopic hadronic and quark-gluon plasma equation of state in the framework of a relativistic mean field theory and in regime of high density and temperature. This is realized by means of a theoretical-computational approach and comparing the results with the recent experimental data obtained from the relativistic heavy ion collisions experiments. We adopt and develop a method based on the so-called non-extensive statistical mechanics to derive momentum and energy distribution functions to simply evaluate the physical quantities, taking into account of the correlations among the strongly interacting particles of the medium.

Deconfinement phase transition is investigated by applying the Gibbs condition on a system of two (B, C) or three (B, C, S) conserved charges, by requiring the global conservation of each charges in the total phase. A multi-component system, in fact, implies a global and not a local charge conservation. Therefore, the charge densities ρ_B, ρ_C and ρ_S are fixed only as long as the system remains in one of the two pure phases. In the mixed phase, the charge concentration in each of the regions of one phase or the other may be different.

We also study the strangeness production at finite temperature and baryon density by means of an effective relativistic mean-field model, with the inclusion of the full baryon octet and the meson degrees of freedom. In this context, lightest pseudo-scalar $(\pi, K, \overline{K}, \eta, \eta^{'})$ and vector mesons $(\rho, \omega, K^*, \overline{K}^*, \phi)$ are introduced in the QHD-Lagrangian density through an effective chemical potential depending on the self-consistent interaction between baryons. Hence, the obtained results are compared with those of minimal coupling scheme. The different meson ratios, strangeness production and possible kaon condensation are deeply investigated.

Finally, in the last part of this dissertation, we investigate the possible thermodynamical instabilities in a warm $(T \leq 50 \text{ MeV})$ and dense nuclear medium $(\rho_0 \leq \rho_B \leq 3\rho_0)$, where a phase transition from nucleonic matter to resonance-dominated Δ matter can take place. This analysis is performed by requiring the global conservation of baryon and electric

charge numbers in the framework of a relativistic equation of state. Similarly to the liquid-gas phase transition, we show that the nucleon-Δ matter phase transition is characterized by both mechanical instability (fluctuations on the baryon density) and by chemical-diffusive instability (fluctuations on the charge concentration) in asymmetric nuclear matter. We then perform an investigation and a comparative study on the different nature of such instabilities and phase transitions.

In this context, the liquid-gas phase transition is also investigated in the framework of nonextensive statistical effects and in the last part of this analysis we also investigate the possible onset of strangeness-diffusive instability (fluctuation on the strangeness density) in a hot ($70 \leq T \leq 140$ MeV) and dense nuclear medium ($\rho_0 \leq \rho_B \leq 4\rho_0$).

The goal of this thesis, is therefore a deeper knowledge of the proprieties of nuclear matter at high density and finite temperature, with the study and the implementation of the nuclear equation of state through effective models (non-extensive statistical mechanics and effective relativistic mean-field model), through which overcome some theoretical and experimental difficulties in the determination of the physical parameters of the system.

Finally, the study of the thermodynamical proprieties of strongly interacting nuclear matter, away from the nuclear ground state, allow us to deal and respond to one of the major questions of modern high-energy nuclear physics.

Contents

List of Tables

List of Figures

Acknowledgements

I would like to say a big thanks to Prof. Andrea Lavagno, who accompanied me in these three years of PhD, believing in me and giving me always new ideas and suggestions for my studies and researches. I would also like to thank my parents for their patience and help and the Politecnico di Torino, who gave me this opportunity of growth.

Introduction

The determination of the properties of nuclear matter as functions of density and temperature, is a fundamental task in nuclear and subnuclear physics.
In this context, heavy-ion collision experiments, open the possibility to investigate strongly interacting compressed nuclear matter by exploring in the laboratory the structure of the QCD phase diagram [1, 2, 3, 4].

In the early 1960's, with the construction of the first proton accelerators with energies well above the threshold for anti-proton production, a veritable zoo of new particles and resonances was discovered [5]. Gell-Mann [6] and Neeman [7] noticed that particles sharing the same quantum numbers (spin, parity) follow the symmetry of the mathematical group $SU(3)$ which is based on 3 elementary generators, up, down, strange (u, d, s), with spin 1/2 and fractional electrical charge, [8, 9] which Gell-Mann called quarks. Mesons are described as states made of a quark-anti-quark ($\bar{q}q$) pair and baryons as states of 3 quarks (qqq). This led to the prediction of a new baryon (Ω^-), as a state of (sss) quarks, with strangeness -3, which was observed shortly thereafter [10]. However, the Ω^- had a problem: 3 identical s quarks in the same state, apparently violating the Pauli Exclusion Principle. To avoid this problem, it was proposed [11] that quarks come in 3 colors, i.e. distinguishing characteristics which would allow 3 otherwise identical quarks to occupy the same state (formally, para-Fermi statistics of rank 3). A major breakthrough was the realization that the real SU(3) symmetry was not the original 3 quarks uds (now called flavor), but the 3 colors; and that color-charged gluons are the quanta of the asymtotically-free strong interaction which binds hadrons [12].
Following this line, from the early 1970's, it was generally accepted that the nucleon was not an elementary particle, but was composed of a substructure of 3 valence quarks confined into a bound state by a strong interaction, Quantum Chromo Dynamics (QCD), which is mediated by the exchange of color-charged vector gluons [12]. In sharp distinction to the behavior of the uncharged quanta of quantum electrodynamics (QED), the color-charged gluons of QCD interact with each other. This leads to the property of asymptotic freedom [13, 14], the reduction of the effective coupling constant at short distances, and is believed to provide the confinement property at long distances where the quarks and gluons behave as if attached to each other by a color string.
In the following decades, by increasing of the energy of the relativistic heavy ion collision experiments, other quark degrees of freedom have been discovered. For example, the first charmed particle (a particle containing a charm quark) to be discovered was the J/ψ meson,

Name	Mass (MeV)	q	B	J	I_3
Up (u)	1.5-3.3	+2/3	+1/3	+1/2	+1/2
Down (d)	3.5-6	-1/3	+1/3	+1/2	+1/2
Strange (s)	80-150	-1/3	+1/3	+1/2	0
Charm (c)	1150-1350	+2/3	+1/3	+1/2	0
Bottom (b)	4100-4400	-1/3	+1/3	+1/2	0
Top (t)	≈173000	+2/3	+1/3	+1/2	0

Table 1: Quarks mass, charge (q), baryon number (B), angular momentum (J) and isospin number (I_3).

in the early 1970's. It was detected by a team at the Stanford Linear Accelerator Center (SLAC), led by Burton Richter [15], and one at the Brookhaven National Laboratory (BNL), led by Samuel Ting. [16]. The 1974 discovery of the J/ψ (and thus the charm quark) ushered in a series of breakthroughs which are collectively known as the November Revolution.
At present, quarks appear as the real degrees of freedom of hadrons and are present in six flavors (up, down, strange, charm, beauty and top), represented through the $SU(3)$ gauge group, obtained by taking the color charge to define a local symmetry. In Tab. (1) we report the main quarks quantum numbers.

In order to study the properties of nuclear matter at finite temperature and baryon density, is of great importance to develop statistical approaches in order to treat the complexity of the many-body nuclear interactions. In this context, the relativistic mean-field theory are especially suitable for the description of hadronic matter. The nuclear force is mediated by the exchange of mesons and the coupling constant of the model are related with the bulk proprieties of nuclear matter. Furthermore, in the mean field approximation, we suppose the medium static and uniform, therefore, the quantum fluctuation of the mesons fields are removed and we can express them as classical field through their expectation values [17]
In this sense, the relativistic mean field theory, will provide a relativistically covariant theory of hot and dense hadronic matter.
However, the extraction of information about the equation of state (EOS) at different densities and temperatures by means of intermediate- and high-energy heavy-ion collisions is a very difficult task and can be realized only indirectly by comparing the experimental data with different theoretical models, such as, for example, fluid-dynamical models. The EOS at density below the saturation density of nuclear matter ($\rho_B \approx 0.153$ fm^{-3}) is relatively well known due to the large amount of experimental nuclear data available. At larger density there are many uncertainties; the strong repulsion at short distances of nuclear force makes, in fact, the compression of nuclear matter quite difficult. Furthermore, in relativistic heavy-ion collisions the baryon density can reaches values of a few times the saturation nuclear density and/or high temperatures.
In these conditions, phase transition phenomena in the hot and dense fireball created during the collisions may take place [1]. However, since the process of deconfinement and the equa-

tion of state (EOS) of hot and dense nuclear matter can in principle be described by QCD, such a theory is highly non-perturbative in the energy density range involved in relativistic heavy-ion collisions. The generated quark-gluon plasma (QGP) in the early stages of the collisions does not at all resemble a quasi-ideal gas of quarks and gluons because strongly dynamical correlations are present, including long-range interactions [18, 2, 19]. Therefore, in the absence of a converging method to approach QCD at finite density one has often to resort to effective and phenomenological model investigations to obtain qualitative results.

For this reason, in Chapters 2, 3 and 4, we will study and implement the nuclear equation of state in the context of an effective statistical model, known as nonextensive statistical mechanics. This model, was firstly proposed by Tsallis [20, 21, 22], in order to deal systems where strong dynamical correlation, long-range color interaction and memory effects are presents. In this direction, in the last years, several authors have outlined the possibility that experimental observations in relativistic heavy ion collisions can reflect nonextensive statistical behaviors [23, 24, 25, 26, 27, 28, 28, 29].

The nonextensive statistical mechanics, will also be used in Chapter 3, in order to study the mechanical and the thermodynamical proprieties of protoneutron stars. In this context, a detailed study of the finite-temperature equation of state of a β-stable matter in presence and in absence of hyperons and trapped neutrinos will be made.

As we will show in Chapters 2, 3 and 4, the onset of nonextensive statistical effects should strongly affect the finite temperature and density nuclear EOS [30, 31, 32, 33, 34, 35, 36, 37]. In fact, by varying temperature and density, the EOS reflects in terms of the macroscopic thermodynamical variables the microscopic interactions of the different phases of nuclear matter.

Therefore, the variation in the thermodynamical proprieties of the nuclear equation of state, together with the alteration in the particles concentration, due to the variation in the many-body interaction at microscopic level, may be important indicators of the possible onset of nonextensive effects in the nuclear medium.

Another of the major research fields of modern physics, at the energy of relativistic heavy ion collision experiments, regard the production of strange particles (hyperons and strange mesons), first discovered more than a quarter of century ago [38, 39].

In this context, especially in the last years, there was a growing interest in the study of the kaons and anti-kaons proprieties in finite nuclear matter as well as in compact stars.

As known, strange particles interact with the hadronic medium not only by collisions but also by potential interaction. At finite densities, this interaction is commonly investigated by extending the chiral perturbation theory to the $SU(3)$ sector. This procedure allowed to predict how the K^+ mesons are modified in matter but failed for the description of the K^- properties. The K^- spectra, in fact, carry a very complex information on the system which to reproduce is a challenge for every theoretical approach.

What makes the situation even more complicated is the very complex potential interaction with the hadronic environment. In contradistinction to the K^+ mesons, K^- can produce baryonic resonances in the nuclear medium which render mean field approaches very tricky and require self-consistent multi-channel Brĺuckner G-matrix calculations. These calculations have not reached stable conclusions yet and the depth of the K^- N potential as a function

of the nuclear density is still very much debated. To this regard, recent analysis of kaonic atom data leads to the real part of anti-kaon optical potential close to $U_{K^-} = -180\pm20$ MeV at the saturation nuclear matter density [40, 41, 42, 43, 44, 45]. Contrariwise, chiral-models and coupled-channel G-matrix theory, seem to suggest a strength of the optical potential close to $U_{K^-} = -(50 \div 80)$ MeV [46, 47, 48].

If the interaction is strong enough, a kaon condensate could be created, with important implication for the nuclear equation of state, in particular in astrophysical systems. In this direction, many studies have shown the possibility that these particles may condensate in neutron stars, whereas the situation seems to be more uncertain in the physical conditions reachable in relativistic heavy ion collision [49, 50, 51, 52, 40, 53].

These uncertainties in the estimation of the anti-kaon potential depth, imply some difficulties in the calculation of the effective kaon mass in-medium. Furthermore, different mean field models predict negative or imaginary effective kaon mass at sufficiently large values of the σ-meson field, responsible of the medium range attraction [44, 45, 54]. Regarding this, due to overcome these theoretical and experimental difficulties in order to determinate the correct coupling constants to the meson-fields, in Chapter 1.4.1, we introduce a self consistent formulation, taking into account an effective chemical potential depending on the self-consistent interaction between baryons. From a phenomenological point of view, we can take into account the meson degrees of freedom by adding their one-body contribution to the thermodynamical potential, that is, the contribution of an ideal Bose gas with an effective chemical potential μ_j^* , depending self-consistently from the meson fields. In this way, the hadronic system is still regarded as an ideal gas but here we have a (quasifree) meson gas with an effective chemical potential that contains the self-consistent interaction of the meson fields. To this regard, the future CBM (Compressed Baryonic Matter) experiment of FAIR (Facility of Antiproton and Ion Research) at GSI Darmstadt, will be of great importance to create compressed baryonic matter with a high net baryon density and finite temperature [55, 56, 57, 58] and make possible an accurate analysis of the proprieties of kaons and, more in general, of the strangeness production at high baryon density.

Finally, in the last part of this dissertation, we investigate the thermodynamical properties of strongly interacting nuclear matter away from the nuclear ground state. This constitutes, one of the most interesting aspects and one of the most difficult task of modern high-energy physics.

At this regard, it is generally accepted that the nuclear multifragmentation, observed in intermediate-energy nuclear reactions, is indicating a nuclear liquid-gas phase transition [59].

More specifically, nuclear transport models predict that, after the projectile and target touch themselves, a fast compression stage ($\approx 20 fm/c$) starts and light particles are emitted (pre-equilibrium emission). The system subsequently expands, correlations develop, and after a few tens of fm/c surfaces appear inside the inhomogeneous medium. Once the fragment surfaces are separated by a distance overcoming the nuclear interaction range, inter-fragment interactions are inhibited and the chemical and energetic fragment content is fixed (freeze-out stage). These fragments are typically not in their ground state, and they undergo a slow light particles decay in vacuum, in some hundreds of fm/c. Finally, after a time of

the order of nanoseconds $\approx 10^{14}$ fm/c, the final (cold) products impinge on the detecting system, keeping the same identity reached after the secondary decays [60].

At present, the liquid-gas phase transition was experimentally observed at intermediate-energy in many nuclear reactions [61, 62], for temperature of the order of $T \approx 10$ MeV and baryon density below the nuclear saturation density.

Furthermore, by increasing of the temperature of the system, many other degrees of freedom appear. In particular, at moderate temperature $(20 < T \leq 50$ MeV$)$ and hight baryon density $(\rho_B \leq 3\rho_0)$, a state of high density resonance matter may be formed and the $\Delta(1232)$-isobar degrees of freedom are expected to play a central role in relativistic heavy ion collisions and in the physics of compact stars [63, 64, 65, 66, 67]. In this context, transport model calculations and experimental results indicate that an excited state of baryonic matter is dominated by the Δ-resonance at the energy from AGS to RHIC [68, 69, 70, 71]. In order to study the thermodynamical proprieties of the nuclear medium, for this range of temperatures and baryon densities, many theoretical works have been done in the framework of nonlinear Walecka model. In this context, in symmetric nuclear matter, it has been predicted that a phase transition from nucleonic matter to Δ-excited nuclear matter can take place and the occurrence of this transition sensibly depends on the Δ-meson coupling constants [72, 73].

As for the case of the liquid-gas phase transition, in presence of only one conserved "charge" (baryon number), the region of the phase transition develops when the incompressibility becomes negative and therefore only mechanical instabilities (fluctuations in the baryon density) is present.

However, the information coming from experiments with heavy ions in intermediate and high-energy collisions is that the nuclear equation of state, depends on the energy beam but also sensibly on the electric charge fraction of the colliding nuclei, especially at not too high temperature [74, 75].

For this reason, in this thesis, we investigate the thermodynamical proprieties of the liquid-gas and of the Δ-matter phase transition, in a binary system, where both the baryon number (B) and the electric charge (C) are conserved, following and developing the very relevant results obtained by Müller and Serot [76]

In this context, a relevant aspect of a system with two conserved charges (baryon and isospin numbers) is that the phase transition is of second order from the viewpoint of EhrenfestŠs definition. At variance with the so-called Maxwell construction for one conserved charge, the pressure is not constant in the mixed phase and therefore the incompressibility does not vanish [76, 77]. Such feature plays a crucial role in the structure and in the possible hadron-quark phase transition in compact star objects [78, 79]. Moreover, for a binary system with two phases, the binodal coexistence surface is two dimensional and the instabilities in the mixed liquid-gas phase arise from fluctuations in the charge concentration (chemical instability) and in the baryon density (mechanical instability) [76, 80, 81, 82].

Finally, we would like to present a preliminary study of the proprieties of the nuclear environment at high temperature $(T > 70$ MeV$)$ and baryon density $(\rho_B > 2\rho_0)$, where strange particles start to be abundantly produced. In this context, during the extreme conditions reached in relativistic heavy ion collision experiments, a net strangeness excess could be generated and chemical fluctuation in the strangeness concentration may take place.

This in-depth analysis of the thermodynamical proprieties of strongly interacting nuclear matter, will be made in Chapter 5. Phase transitions will be investigated in the framework of nonlinear relativistic Walecka type model, by requiring the Gibbs conditions on the global conservation of baryon number, net electric charge and strangeness number.

The analysis will be done through effective models and, due to the simplicity of the system (only two degrees of freedom are present), we will also analyze the possible influence of nonextensive effects on the liquid-gas phase transition.

In this sense, the future CBM (compressed baryonic matter) experiment of the FAIR (Facility of Antiproton and Ion Research) project at GSI Darmstadt will make it possible to create compressed baryonic matter with a high net baryon density [55, 58, 57], allowing the experimental identification of such phase transitions and a precise measure of the strangeness production and of the quark-gluon plasma phase transition at high temperature and finite baryon density.

Chapter 1

Lagrangian formalism and relativistic mean-field equation of state

In this chapter, we introduce the basic formalism of quantum hydrodynamics, in the framework of nonlinear relativistic mean-field model and we are planning to investigate the nuclear equation of state, at finite temperature and baryon density, through statistical and effective models. In this context, strangeness production, at high temperature and finite baryon density, will be investigated by effective relativistic mean-field model.

1.1 Lagrangian formalism

The Lagrangian formalism is one of the main tools of the description of the dynamics of a vast variety of physical systems including systems with finite (particles) and infinite number of degrees of freedom (strings, membranes, fields). As known, Lagrangian mechanics does not contain any new physics, but is simply an alternative expression of the physical laws governing the equations of motion of objects. It is based on the action principle, a fundamental theoretical concept which, in particular, for more than a century has been a leading principle for the construction and development of the theory of fundamental (electromagnetic, weak, strong and gravitational) interactions of elementary particles based on Quantum Field Theory.
The form of the action determines the equations of motion (Euler-Lagrange equations) of the physical system, its symmetries and (via Noether's theorem) the corresponding conserved quantities, the integrals of motion.

In order to be able to study the proprieties of nuclear matter at finite density and temperature, the lagrangian formalism is the natural candidate to obtain a relativistic and covariant formulation of the equation of motion of the system. In fact, the Lagrangian density is a lorentz scalar (it has the dimension of lengh^{-4} (fm^{-4})) and because it is construct only from the scalar functions of the fields and their derivatives, its relativistic covariance is manifest.
In particular, in the field theory, the Lagrangian would be defined in terms of the Lagrangian density as: $\mathcal{L} = [\phi(x), \partial_\mu \phi(x)]$, where $\phi(x)$ is the field operator. In this context, the equation

of motion is obtained in the usual way, from the minimization of the action S applied to the lagrangian density $\mathcal{L}$, and it gives:

$$S = \int_{t_1}^{t_2} d^4x \mathcal{L}[\phi(x), \partial_\mu \phi(x)]\,. \tag{1.1}$$

The variation of the action is given by:

$$
\begin{aligned}
\delta S &= \int_{t_1}^{t_2} d^4x \{\frac{\partial \mathcal{L}}{\partial \phi}\delta\phi + \frac{\partial \mathcal{L}}{\partial(\partial_\mu \phi)}\delta(\partial_\mu \phi)\} \\
&= \int_{t_1}^{t_2} d^4x \{(\frac{\partial \mathcal{L}}{\partial \phi} - \partial_\mu \frac{\partial \mathcal{L}}{\partial(\partial_\mu \phi)})\delta\phi + \partial_\mu(\frac{\partial \mathcal{L}}{\partial(\partial_\mu \phi)}\delta\phi)\} \\
&= \int_{t_1}^{t_2} d^4x (\frac{\partial \mathcal{L}}{\partial \phi} - \partial_\mu \frac{\partial \mathcal{L}}{\partial(\partial_\mu \phi)})\delta\phi(x)\,.
\end{aligned}
\tag{1.2}
$$

So, the relative equation of motion (Euler-Lagrangian equation) for the field $\phi(x)$, can be written as [17]:

$$\frac{\partial \mathcal{L}}{\partial \phi(x)} - \partial_\mu \frac{\partial \mathcal{L}}{\partial(\partial_\mu \phi(x))} = 0\,. \tag{1.3}$$

If $\mathcal{L} = [\phi(x), \partial_\mu \phi(x)]$ depends on several fields, we obtain n-equation of motion associated to this Lagrangian (one for each field).

Furthermore, by Noether's theorem, it is possible to demonstrate the invariance of the lagrangian density under rotation and spatial translation, due to the presence of conserved quantities (currents).

In particular, the theorem states that, if a generic field transformation $\phi_\alpha(x) \to \phi'_\alpha(x') = \phi_\alpha(x) + \delta\phi_\alpha(x)$ is continuous and the Lagrangian density is invariant under this transformation, then the following equation (Noether equation) must be satisfied and a conserved quantity (current) must exist:

$$J_j^\mu(x) \equiv \frac{\mathcal{L}}{\partial(\partial_\mu \phi_i)} F_i^j\,, \tag{1.4}$$

where $\delta\phi_i = \lambda_j F_i^j$ represent a continuous symmetry transformation of the field ϕ_i and λ_j are infinitesimal parameters that are space-time independent [17]. The conserved quantities (currents) take the form: $\partial_\mu J_j^\mu = 0$. In this sense the Lagrangian formalism is manifestly covariant under the Lorentz group, due to the presence of space-time symmetries.

1.2   Quantum hadrodynamics I

Quantum hadrodynamics I (QHD-I), also known as the σ-ω model, is the original and simplest parameter set of QHD. In this model, the nuclear force is mediated by the exchange of two mesons: a neutral isoscalar-scalar sigma (σ) mesons and a neutral isoscalar-vector omega (ω) mesons. These mesons have been found to be the most important in describing

the properties of nuclei and nuclear matter [17]. In this context, the scalar meson gives rise to a strong attractive central force and a spin-orbit force in the nucleon-nucleon interaction, while the vector meson gives rise to a strong repulsive central force and a spin-orbit force (with the same sign as the spin-orbit force of the scalar meson) [83]. Therefore, the nucleon-nucleon interaction is described by two fields, the baryon-scalar meson field and the baryon-vector meson fields. No charged mesons are included in this parameter set (i.e. the electric properties of the baryons are not considered) and the masses of the proton and neutron are taken to be equal in QHD-I. Hence, in this simple model, the only degrees of freedom introduced are protons, nucleons and mesons and all the hadrons are regarded as point-like particles.

In constructing the Lagrangian density it was assumed that the neutral scalar mesons coupled to the scalar density $\overline{\psi}\psi$ of the baryon field and that the neutral vector mesons coupled to the conserved baryon current $\overline{\psi}\gamma^{\mu}\psi$ [17, 84]. In this context, the interaction part of the Lagrangian density, which incorporate the meson-nucleon coupling constant, can be written as:

$$\mathcal{L}_{\text{int}} = g_{\sigma}\sigma(x)\overline{\psi}\psi - g_{\omega}\omega_{\mu}(x)\overline{\psi}\gamma^{\mu}\psi \,, \tag{1.5}$$

where $x \equiv x^{\mu} \equiv (t, x, y, z)$ and the sign over the fields are arbitrary. Now, adding the interaction part to the free Lagrangian of nucleons and mesons, we obtain the total QHD-I Lagrangian density (in natural units) [17, 84]:

$$\begin{aligned} \mathcal{L}_{\text{N}} &= \bar{\psi}(x)[\gamma_{\mu}\left(i\partial^{\mu} - g_{\omega}\omega^{\mu}(x)\right) - (M - g_{\sigma}\,\sigma(x))]\,\psi(x) \\ &+ \frac{1}{2}(\partial_{\mu}\sigma(x)\partial^{\mu}\sigma(x) - m_{\sigma}^{2}\sigma^{2}(x)) + \frac{1}{2}\,m_{\omega}^{2}\,\omega_{\mu}(x)\omega^{\mu}(x) - \frac{1}{4}F_{\mu\nu}(x)F^{\mu\nu}(x)\,, \end{aligned} \tag{1.6}$$

where

- ω^{μ} denotes the vector meson field,

- σ denotes the scalar meson field,

- m_{σ} and m_{ω} the different meson masses and M denotes the nucleon bare mass,

- g_{σ} and g_{ω} the scalar and vector coupling constants,

- $F_{\mu\nu} = \partial_{\mu}F_{\nu}(x) - \partial_{\nu}F_{\mu}(x)$

The equations of motion can be derived, as usual, from the Euler-Lagrange equation:

$$\frac{\partial\mathcal{L}}{\partial\phi(x)} = \partial_{\mu}\frac{\partial\mathcal{L}}{\partial(\partial_{\mu}\phi(x))}\,, \tag{1.7}$$

Using this equation, we obtain a set of n coupled differential equations of motion for the meson fields and the dirac equation of motion for nucleons (where n is the number of degrees of freedom of the system), given by:

$$\partial_{\mu}\partial^{\mu}\sigma(x) + m_{\sigma}^{2}\sigma(x) = g_{\sigma}\bar{\psi}(x)\psi(x)\,, \tag{1.8}$$

$$\partial_{\mu}F^{\mu\mu} + m_{\omega}^{2}\omega^{\nu}(x) = g_{\omega}\bar{\psi}(x)\gamma^{\mu}\psi(x)\,, \tag{1.9}$$

$$[\gamma_{\mu}(i\partial^{\mu} - g_{\omega k}\omega^{\mu}) - (M - g_{\sigma}\,\sigma(x))]\,\psi(x) = 0\,, \tag{1.10}$$

where scalar (σ) and vector (ω) mesons are coupled respectively with $\bar{\psi}(x)\psi(x)$ and $\bar{\psi}(x)\gamma^\mu\psi(x)$. Furthermore, in the Dirac equation (1.10), the term $(M_k - g_{\sigma k}\,\sigma)$ represents the effective mass of the nucleon due to the attractive interaction of the σ meson field.

At this point, in order to resolve this set of non-linear differential equations, we introduce two approximations in the relativistic mean-field theory.

The first one is known as relativistic mean field approximation (RMF). Here, nucleons (more in general hadrons) behave as noninteracting particles, moving in a mean field generated by mesons fields (in our analyze σ, ω and ρ mesons). The second one is known as no-sea approximation, where we neglect the contribution of the vacuum polarization (Dirac sea) at the mean field level.

These approximations allow us to easily resolve the set of non-linear coupled equations (1.8)–(1.10), since, in the stationary un uniform state, all the time derivatives and all the space vector components of densities and fields vanish (the quantum fluctuation of the mesons fields are removed and we can express them as classical field through their expectation values [17]).

In the relativistic mean-field approximation within QHD, the meson field operators are therefore replaced by their ground state ($|\Psi\rangle$) expectation values, which are classical fields, in the following way [17, 84]:

$$\sigma \to \langle\Psi|\sigma|\Psi\rangle = \sigma\,,$$
$$\omega_\mu \to \langle\Psi|\omega_\mu|\Psi\rangle = \delta_{\mu 0}\omega_0\,. \tag{1.11}$$

For a stationary and uniform system σ and ω_0 will be constants and space-time independent. Furthermore, the spatial components of ω_μ will vanish, since the baryon flux is zero and the system is at rest, whereas, the particle filed operators remain operators. This implies that baryon operators must be evaluated by operating on the ground state. Therefore, they normal ground state expectation values can be written as:

$$\bar{\psi}(x)\psi(x) \to \langle\Phi| : \bar{\psi}(x)\psi(x) : |\Phi\rangle = \langle\bar{\psi}\psi\rangle\,,$$
$$\bar{\psi}(x)\gamma^\mu\psi(x) \to \langle\Phi| : \bar{\psi}(x)\gamma^\mu\psi(x) : |\Phi\rangle = \langle\bar{\psi}\gamma^0\psi\rangle\,, \tag{1.12}$$

where the spatial component vanished due to the hypothesis of stationarity and uniformity of the system.

Therefore, in the RMF approximation, the equation of motion of the meson fields and of the Dirac equation for the nucleons, reduce to:

$$m_\sigma^2\sigma = g_\sigma\langle\bar{\psi}\psi\rangle\,,$$
$$m_\omega^2\omega_0 = g_\omega\langle\bar{\psi}\gamma_0\psi\rangle\,,$$
$$[i\gamma_\mu\partial^\mu - g_\omega\gamma^0\omega_0 - (M - g_\sigma\sigma)]\psi = 0\,, \tag{1.13}$$

where $\langle\bar{\psi}\gamma_0\psi\rangle$ and $\langle\bar{\psi}\psi\rangle$ stays respectively for the vector and scalar baryon density, that, in the statics and uniform limit, are given respectively by the well know equations (see [17]):

$$\rho_B \equiv \langle\bar{\psi}\gamma_0\psi\rangle = 4\int_0^k \frac{d\mathbf{k}}{(2\pi^3)} = \frac{2k^3}{3\pi^2}\,, \tag{1.14}$$

and $(\bar{\psi}\psi)_{\mathbf{k}} = \partial E(k)/\partial m$:

$$\rho_B^S \equiv \langle\bar{\psi}\psi\rangle = \frac{2}{\pi^2}\int_0^k k^2 dk \frac{m - g_\sigma\sigma}{\sqrt{k^2 + (m - g_\sigma\sigma)^2}}\,, \tag{1.15}$$

where $\mathbf{k}$ is the 3-vector momentum of the particle and $e(k) = g_\omega\omega_0 - E(k)$ is the Dirac eigenvalues, with $E(k) = \sqrt{k^2 + (m - g_\sigma\sigma)^2}$.

In the relativistic mean field approximation, the QHD-I Lagrangian density take the form:

$$\mathcal{L}_{\text{RMF}} = \bar{\psi}[i\gamma_\mu\,\partial^\mu - g_\omega\gamma^0\omega^0 - (M - g_\sigma\,\sigma)]\,\psi - \frac{1}{2}m_\sigma^2\sigma^2 + \frac{1}{2}\,m_\omega^2\,\omega_0^2\,. \tag{1.16}$$

From the above Lagrangian, through the use of the energy-momentum tensor, we can obtain the corresponding relativistic equation of state (EOS).

The energy-momentum tensor is given, as usual, by:

$$T^{\mu\nu} = \frac{\partial\mathcal{L}}{\partial(\partial_\mu\phi_\alpha)}\partial^\nu\phi_\alpha - \mathcal{L}\eta^{\mu\nu}\,, \tag{1.17}$$

(where ϕ_α is the generic field operator) that give us:

$$(T^{\mu\nu})_{RMF} = i\overline{\psi}\gamma^\mu\partial_\nu\psi - \eta^{\mu\nu}(-\frac{1}{2}m_\sigma^2\sigma^2 + \frac{1}{2}m_\omega^2\omega_0^2)\,. \tag{1.18}$$

In this context, the energy density (ε) and the pressure (P) for QHD-I Lagrangian density, results:

$$\begin{aligned}
\varepsilon &= \langle T^{00}\rangle \\
&= \langle i\overline{\psi}\gamma_0\partial_0\psi - (-\frac{1}{2}m_\sigma^2\sigma^2 + \frac{1}{2}m_\omega^2\omega_0^2)\rangle \\
&= \langle i\overline{\psi}\gamma_0\partial_0\psi\rangle + \frac{1}{2}m_\sigma^2\sigma^2 - \frac{1}{2}m_\omega^2\omega_0^2\,, \\
P &= \frac{1}{3}\langle T^{ii}\rangle \\
&= \frac{1}{3}\langle i\overline{\psi}\gamma^i\partial_i\psi + (-\frac{1}{2}m_\sigma^2\sigma^2 + \frac{1}{2}m_\omega^2\omega_0^2)\rangle \\
&= \frac{1}{3}\langle i\overline{\psi}\gamma^i\partial_i\psi\rangle - \frac{1}{2}m_\sigma^2\sigma_+^2\frac{1}{2}m_\omega^2\omega_0^2\,, \tag{1.20}
\end{aligned}$$

where the first term in the energy density $\langle i\overline{\psi}\gamma_0\partial_0\psi\rangle$, refers to the contribution of occupied nucleon momentum states, that is given by (see [17]):

$$\begin{aligned}
\langle\overline{\psi}\gamma_0 k_0\psi\rangle &= \frac{2}{\pi^2}\int_0^k k^2 dk\, e(k) \\
&= g_\omega\omega_0\rho + \int_0^k k^2 dk\sqrt{k^2 + (m - g_\sigma\sigma)^2} \\
&= m_\omega^2\omega_0^2 + \frac{2}{\pi^2}\int_0^k k^2 dk\sqrt{k^2 + (m - g_\sigma\sigma)^2}\,. \tag{1.21}
\end{aligned}$$

and $\langle i\overline{\psi}\gamma^i\partial_i\psi\rangle = \partial E(k)/\partial k$ gives:

$$\langle i\overline{\psi}\gamma^i\partial_i\psi\rangle = \frac{2}{\pi^2}\int_0^k k^2 dk \frac{k^4}{\sqrt{k^2 + (m - g_\sigma\sigma)^2}}dk. \qquad (1.22)$$

Therefore, the equation of state take the form:

$$\varepsilon = +\frac{1}{2}m_\sigma^2\sigma^2 + \frac{1}{2}m_\omega^2\omega_0^2 + \frac{\gamma}{2\pi^3}\int_0^{k_f} d\mathbf{k}\sqrt{\mathbf{k}^2 + (M - g_\sigma\sigma)^2}, \qquad (1.23)$$

$$P = -\frac{1}{2}m_\sigma^2\sigma^2 + \frac{1}{2}m_\omega^2\omega_0^2 + \frac{1}{3}(\frac{\gamma}{2\pi^3}\int_0^{k_f} d\mathbf{k}\frac{k^4}{\sqrt{k^2 + (m - g_\sigma\sigma)^2}}), \qquad (1.24)$$

and the RMF equations of motion for the meson fields reduce to:

$$\sigma = \frac{g_\sigma}{m_\sigma^2}\langle\overline{\psi}\psi\rangle = \frac{g_\sigma}{m_\sigma^2}\frac{\gamma}{2\pi^2}\int_0^k k^2 dk \frac{m - g_\sigma\sigma}{\sqrt{k^2 + (m - g_\sigma\sigma)^2}}, \qquad (1.25)$$

$$\omega_0 = \frac{g_\omega}{m_\omega^2}\langle\overline{\psi}\gamma_0\psi\rangle = \frac{g_\omega}{m_\omega^2}\rho_B, \qquad (1.26)$$

where γ is the degenerancy spin factor ($\gamma = 2$ for nucleons).

The coupling constants of QHD-I are fitted to reproduce the proprieties of saturation nuclear matter, in general, $\rho_B = 0.153$ fm^{-3} and binding energy of $B/A = -16.3$ MeV [17]. Unfortunately, this parameterizations produces too high a value of the nuclear matter compressibility (K). For this reason, in 1977 J. Boguta and A. R. Bodmer proposed that self-couplings of the scalar meson field should be included in the Lagrangian density and the coupling constants re-adjusted to reproduce K more accurately [85].
Another implementation of the model is the introduction of the charged (iso-vector) vector rho meson triplet (ρ^0, $\rho^\pm$), that have its source in the isospin current $\overline{\psi}(x)\gamma^\mu\overrightarrow{t}\psi(x)$, where $\overrightarrow{t}$ is the isospin operator of the nucleon. Since protons and neutrons practically only differ in terms of their isospin projections, the rho mesons are included to distinguish between these baryons and to give a better account of the symmetry energy [17]. (As these vector meson are charged, the reaction between a rho meson and a proton will differ from the reaction between a rho meson and a neutron). Therefore, ρ mesons introduce an additional restoring energy that favors isospin symmetry as manifested in the valley of beta stability in nuclear physics. This restoring produces a quadratic term in the deviation from isospin symmetry and so favor symmetric systems. Furthermore, ρ mesons are introduced in a similar fashion as the other mesons in QHD: the free Lagrangian density describing the vector field is included in the QHD Lagrangian density as well as a coupling between the rho meson and the conserved isospin density [17, 84, 86].

1.3   Non-linear walecka type model

Because we are going to investigate a finite temperature and density nuclear matter, we need to a more complex and complete relativistic mean filed model, which include all the baryons octet, mesons degrees of freedom and leptons (if presents). This is particulary valid

	M (MeV)	C	B	S	t_3
p	939	1	1	0	1/2
n	939	0	1	0	-1/2
Λ	1115.70	0	1	-1	0
Σ^+	1189.37	1	1	-1	1
Σ^0	1192.64	0	1	-1	0
Σ^-	1197.45	-1	1	-1	-1
Φ^0	1314.86	1	1	-2	1/2
Φ^-	1321.71	1	1	-2	-1/2

Table 1.1: Baryons masses and quantum numbers (note that the nucleon mass in TM1 is set equal to 938MeV)

	ρ_0 (fm^{-3})	K (MeV)	$\frac{M_N^*}{M_N}$	α_{sym} (MeV)	$\frac{g_{\sigma N}}{m_\sigma}$ (fm)	$\frac{g_{\omega N}}{m_\omega}$ (fm)	$\frac{g_{\rho N}}{m_\rho}$ (fm)	a (fm^{-1})	b	c
GM2	0.153	300	0.78	32.5	3.025	2.195	2.189	0.01656	0.01328	-
GM3	0.153	240	0.78	32.5	3.151	2.195	2.189	0.04121	-0.002442	-
TM1	0.145	281	0.63	36.9	3.871	3.178	2.374	0.00717	0.00006	0.00282

Table 1.2: Proprieties of nuclear matter and nucleon coupling constants of the parameters sets used in the work. The energy per particle is $E/A = 16.3$ MeV, calculated at the saturation density ρ_0 with a compression modulus K and effective mass M_N^* (the nucleon mass M_N is fixed to 939 MeV for $GM2$ and $GM3$, and $M_N = 938$ MeV in the $TM1$ parameters set). The symmetry energy is denoted by a_{sym}.

above the nuclear saturation density, where the presence of many kinds of hadronic degrees of freedom must be taken into account.

In this context, we introduce the hyperon degrees of freedom to the baryon Lagrangian density. Hyperons (Λ, Σ^+, Σ^0, Σ^-, Ξ^-, Ξ^0) are hadrons composed by one or more strange quarks, with different electric charge and strangeness number (see Tab. 1.1). Like the others hadrons, they participate to the nuclear force mediated by the exchange of mesons, but are unstable particles and decay in nucleons plus mesons and leptons (it depends on the kind of hyperon)

In this study, we investigate the nuclear medium in the context of non-linear relativistic Walecka type mean-field models, using the parameter set marked as GM2, GM3 and TM1 of Tab. 1.2. In this context, the nuclear force is mediated by the exchange of virtual isoscalar scalar (σ), isoscalar vector (ω) and isovector vector (ρ) meson fields [87, 86, 85].

The most general QHD-baryons Lagrangian density, that describes the GM2, GM3

and TM1 parameter sets, can be written as:

$$
\begin{aligned}
\mathcal{L}_{\mathrm{B}} \;=\; & \sum_{B} \overline{\psi}_B \left[i\,\gamma_\mu\,\partial^\mu - (M_B - g_{\sigma B}\,\sigma) - g_{\omega B}\,\gamma_\mu\,\omega^\mu - g_{\rho B}\,\gamma_\mu\,\vec{t}\cdot\vec{\rho}^{\,\mu} \right] \psi_B \\
& + \frac{1}{2}(\partial_\mu\sigma\partial^\mu\sigma - m_\sigma^2\sigma^2) - U(\sigma) + \frac{1}{2}\,m_\omega^2\,\omega_\mu\omega^\mu + \frac{1}{4}\,c\,(g_{\omega B}^2\,\omega_\mu\omega^\mu)^2 \\
& + \frac{1}{2}\,m_\rho^2\,\vec{\rho}_\mu\cdot\vec{\rho}^{\,\mu} - \frac{1}{4}F_{\mu\nu}F^{\mu\nu} - \frac{1}{4}\vec{G}_{\mu\nu}\vec{G}^{\mu\nu}\,,
\end{aligned}
\tag{1.27}
$$

where the sum runs over the full baryons octet $(p,\ n,\ \Lambda,\ \Sigma^+,\ \Sigma^0,\ \Sigma^-,\ \Xi^-,\ \Xi^0)$, M_B is the baryons vacuum mass and $\vec{t}$ is the isospin operator which acts on the ith-baryons.

The field strength tensors for the vector mesons are given by the usual expressions $F_{\mu\nu} \equiv \partial_\mu\omega_\nu - \partial_\nu\omega_\mu$, $\vec{G}_{\mu\nu} \equiv \partial_\mu\vec{\rho}_\nu - \partial_\nu\vec{\rho}_\mu$, and $U(\sigma)$ is the nonlinear potential of σ meson

$$
U(\sigma) = \frac{1}{3}a(g_{\sigma N}\sigma)^3 + \frac{1}{4}b(g_{\sigma N}\sigma)^4\,,
\tag{1.28}
$$

introduced by Boguta and Bodmer in order to obtain a reasonable compression modulus for equilibrium normal nuclear matter [88, 85].

For TM1 parameter set, we have also taken in consideration the additional self-interaction ω-meson field, $c(g_{\omega N}^2\omega_\mu\omega^\mu)^2/4$, suggested by Bodmer [89] to get a good agreement with Dirac-Brückner calculations at high density and to achieve a more satisfactory description of the properties of finite nuclei in the mean-field approximation.

As discussed in Section 1.2, in the RMF approach, baryons are considered as Dirac quasi-particles moving in classical meson fields and the field operators are replaced by their expectation values. As a consequence the field equations in a mean field approximation are

$$
(i\gamma_\mu\partial^\mu - M_B^* - g_{\omega B}\gamma^0\omega - g_{\rho B}\gamma^0 t_3\rho)\psi_B = 0\,,
\tag{1.29}
$$

$$
m_\sigma^2\sigma + ag_{\sigma B}^3\sigma^2 + bg_{\sigma N}^4\sigma^3 = \sum_i g_{\sigma i}\rho_i^S\,,
\tag{1.30}
$$

$$
m_\omega^2\omega + cg_{\omega B}^4\omega^3 = \sum_i g_{\omega i}\rho_i^B\,,
\tag{1.31}
$$

$$
m_\rho^2\rho = \sum_i g_{\rho i}t_{3i}\rho_i^B\,,
\tag{1.32}
$$

where $\sigma = \langle\sigma\rangle$, $\omega = \langle\omega^0\rangle$ and $\rho = \langle\rho_3^0\rangle$, are the nonvanishing expectation values of meson fields, the index i runs over the considered baryon particles and the effective mass of the ith baryon is defined as

$$
M_i^* = M_i - g_{\sigma i}\sigma\,.
\tag{1.33}
$$

In Fig. 1.1, we show the behavior of the nucleon effective mass in the three aforementioned models at $T = 0$ MeV and $y = \rho_C/\rho_B = 0.5$. As we can observe, M_N^* is very sensitive to the particular choice of the parameter set of the Lagrangian density. In particular, for $TM1$, we observe a very strong reduction of the nucleon effective mass, also at low baryon density, due to the strong attractive interaction of the σ-fields.
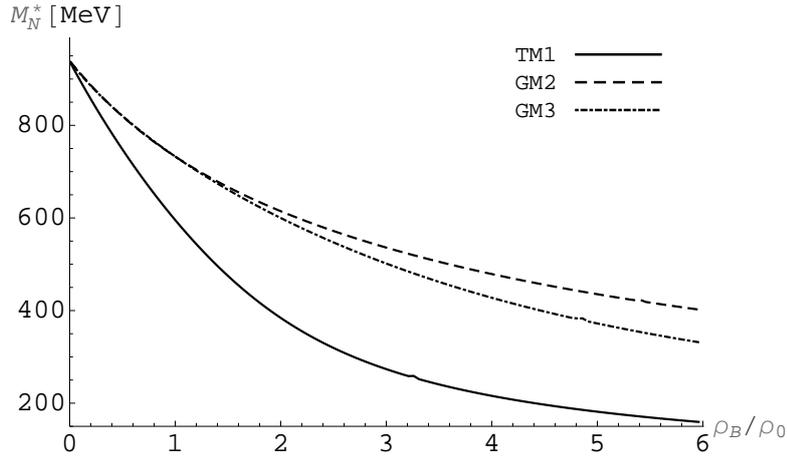
Figure 1.1: Effective nucleon mass at zero temperature and $y = 0.5$ for $GM2$, $GM3$ and $TM1$ parameter set.

The ρ_i^B and ρ_i^S are the baryon density and the baryon scalar density, respectively. They are given by

$$\rho_i^B = \gamma_i \int \frac{\mathrm{d}^3 k}{(2\pi)^3} \left[n_i(k) - \overline{n}_i(k) \right], \tag{1.34}$$

$$\rho_i^S = \gamma_i \int \frac{\mathrm{d}^3 k}{(2\pi)^3} \frac{M_i^*}{E_i^*} \left[n_i(k) + \overline{n}_i(k) \right], \tag{1.35}$$

where $\gamma_i = 2J_i + 1$ is the degeneracy spin factor ($\gamma_i = 2$ for baryons) and $n_i(k)$ and $\overline{n}_i(k)$ are the fermion particle, antiparticle distributions function, given by

$$n_i(k) = \frac{1}{\exp(E_i^*(k) - \mu_i^*)/T + 1}, \tag{1.36}$$

$$\overline{n}_i(k) = \frac{1}{\exp(E_i^*(k) + \mu_i^*)/T + 1}. \tag{1.37}$$

The baryon effective energy is defined as $E_i^*(k) = \sqrt{k^2 + M_i^{*2}}$ and the effective chemical potentials μ_i^* are given in terms of the meson fields as follows

$$\mu_i^* = \mu_i - g_{\omega i}\omega - g_{\rho i}t_{3i}\rho, \tag{1.38}$$

where μ_i are the thermodynamical chemical potentials $\mu_i = \partial\varepsilon/\partial\rho_i$.

The thermodynamical quantities are obtained from the minimization of the baryon grand potential Ω_B. More explicitly, the pressure $P_B = -\Omega_B/V$ and the energy density ε_B
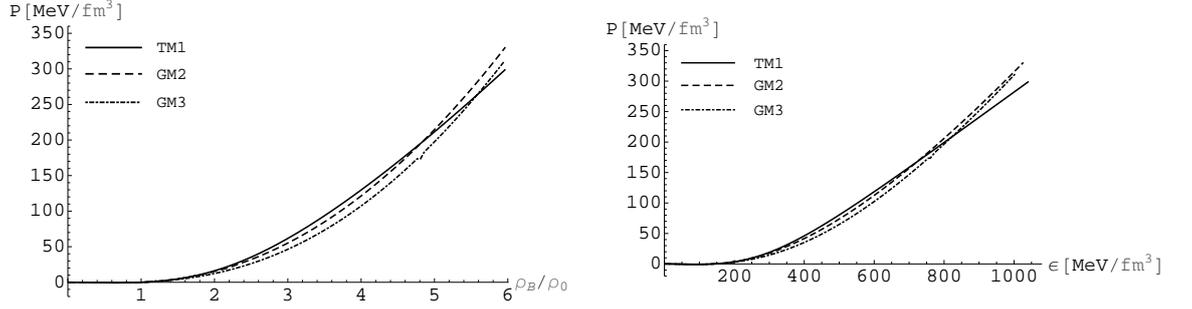
Figure 1.2: Pressure as a function of the baryon density (left panel) and energy density (right panel) at zero temperature and $y = 0.5$, for $GM2$, $GM3$ and $TM1$ parameter set.
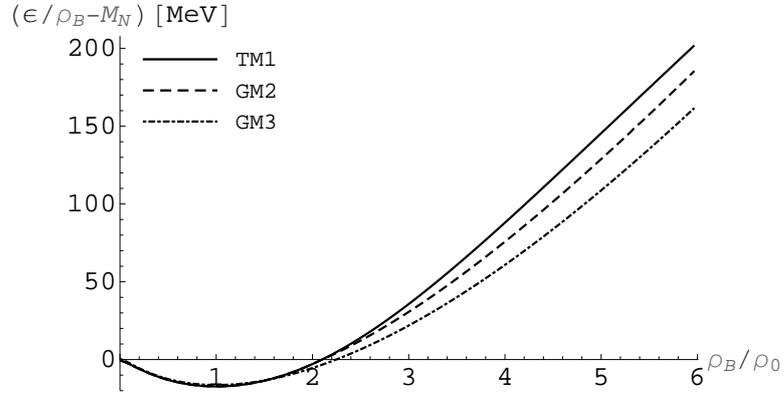
Figure 1.3: Energy per baryon versus baryon density at zero temperature and $y = 0.5$ for $GM2$, $GM3$ and $TM1$ parameter set.

of baryons, can be written as

$$
\begin{aligned}
P_B &= \frac{1}{3} \sum_i \gamma_i \int \frac{\mathrm{d}^3 k}{(2\pi)^3} \frac{k^2}{E_i^*(k)} \left[n_i(k) + \overline{n}_i(k) \right] - \frac{1}{2} m_\sigma^2 \sigma^2 - U(\sigma) \\
&+ \frac{1}{2} m_\omega^2 \omega^2 + \frac{1}{4} c \left(g_{\omega N} \omega \right)^4 + \frac{1}{2} m_\rho^2 \rho^2,
\end{aligned} \tag{1.39}
$$

$$
\begin{aligned}
\varepsilon_B &= \sum_i \gamma_i \int \frac{\mathrm{d}^3 k}{(2\pi)^3} E_i^*(k) \left[n_i(k) + \overline{n}_i(k) \right] + \frac{1}{2} m_\sigma^2 \sigma^2 + U(\sigma) \\
&+ \frac{1}{2} m_\omega^2 \omega^2 + \frac{3}{4} c \left(g_{\omega N} \omega \right)^4 + \frac{1}{2} m_\rho^2 \rho^2 .
\end{aligned} \tag{1.40}
$$

At this regard, in Fig 1.2, we show respectively the baryonic Pressure as a function of the baryon density (left panel) and energy density (right panel) at zero temperature

34

	$x_{\sigma\Delta}$	$x_{\sigma\Sigma}$	$x_{\sigma\Xi}$
GM2	0.606	0.328	0.322
GM3	0.606	0.328	0.322
TM1	0.616	0.447	0.319

Table 1.3: Ratio of the scalar σ-meson coupling constants for hyperons: $x_{\sigma Y} = g_{\sigma Y}/_{\sigma N}$

and $y = 0.5$. As one can easily observe, $TM1$ parameter set make the pressure stiffer in the range of baryon density interesting for the relativistic heavy ion collision experiments ($0 < \rho_B < 4\rho_0$), whereas at very high density, $GM2$ and $GM3$ parameter set make the pressure harder. Note, however, that above $\rho_B > 4\rho_0$, phase transition phenomena in the hot and dense fireball created during the collisions may take place and therefore the system can not be in pure hadronic phase (see Chapter 4).

Finally, in Fig. 1.3, we report the energy per baryon as a function of the baryon density at $T = 0$ MeV and $y = 0.5$. We observe again a remarkable difference in the three parameter set, however, at $\rho_B = \rho_0$, is well visible the minimum of the energy per baryon, which corresponds, for each parameter set to a binding energy of $B.E. = -16.3$ MeV.

The implementation of the model with the inclusion of the full octet of baryons (see Tab. 1.1), comes from the determination of the corresponding meson-hyperon coupling constant that have been fitted to hypernuclar proprieties at the nuclear saturation density. In this context, it is possible to determinate the corresponding isoscalar-vector ($g_{\omega Y}$) and isovector-vector ($g_{\rho Y}$) meson-hyperon coupling constant, using the simple SU(6) quark model [90, 91, 54, 92, 93]. This formalism allow us to obtain the following set of coupling constant:

$$\frac{1}{3}g_{\omega N} = \frac{1}{2}g_{\omega\Lambda} = \frac{1}{2}g_{\omega\Sigma} = g_{\omega\Xi}\,, \tag{1.41}$$

$$g_{\rho N} = \frac{1}{2}g_{\rho\Sigma} = g_{\rho\Xi} \quad g_{\rho\Lambda} = 0\ . \tag{1.42}$$

The scalar σ-meson hyperon coupling constant ($g_{\sigma Y}$), is determined from the analysis of the potential depth of the corresponding hyperon in normal dense matter, obtained in the recent experiments [93, 94, 95, 96]:

$$U_\Lambda^N = -28 MeV, \quad U_\Sigma^N = 30 MeV, \quad U_\Xi^N = -18 MeV\,. \tag{1.43}$$

In this context we obtain the following set of σ-hyperons coupling ratio, expressed as the ratio of the hyperon versus the nucleon sigma-coupling constant $x_{\sigma Y} = g_{\sigma Y}/g_{\sigma N}$. The results are reported in the Tab (1.3) for the different choices of parameters set using in this study. Naturally, hyperons, start to be abundantly produced only at high temperature, therefore at moderate temperature ($T < 50$ MeV) their contribution to the nuclear EOS is negligible.

Finally, in order to obtain a correct description of the nuclear medium at finite temperature and density, we have to require the conservation of three charges: the baryon number

(B), the electric charge (C) and the strangeness number (S). At high temperature, in fact, strangeness production can not be neglected and must be take in consideration. In this context each conserved charge is described by a conjugate chemical potential, therefore the system is described by three independent chemical potentials: μ_B, μ_C and μ_S, respectively the baryon, electric and strange chemical potential.

The chemical potential of a particle of index i can be written as:

$$\mu_i = b_i \mu_B + c_i \mu_C + s_i \mu_S \,, \tag{1.44}$$

where b_i, c_i and s_i are, respectively the baryon, the electric charge and the strangeness quantum number of the particle i-th.

Furthermore, at a given temperature temperature, all the aforementioned equations must be evaluated self-consistently by requiring the conservation of the baryon, electric charge fraction, and strangeness numbers. This implies that, at a given baryon density (ρ_B), a given elctric charge fraction y ($\rho_C = y\rho_B$) and a given strangeness fraction z ($\rho_S = z\rho_B$), the chemical potentials (μ_B, μ_C, μ_S) are determinated by the following set of equations:

$$\rho_B = \sum_i b_i \rho_i(T, \mu_B, \mu_C, \mu_S) \,, \tag{1.45}$$

$$\rho_C = \sum_i c_i \rho_i(T, \mu_B, \mu_C, \mu_S) \,, \tag{1.46}$$

$$\rho_S = \sum_i s_i \rho_i(T, \mu_B, \mu_C, \mu_S) \,, \tag{1.47}$$

where the sum extends over all hadrons that carrying the respective quantum number (b_i, c_i, s_i). Note that the total strangeness fraction of the system is usually set equal to zero ($z = 0$). This is almost always true, but, if the quark-gluon plasma is produced during the relativistic heavy collision, the net strangeness of the hadronic or quark phase may not be conserved, although the total net strangeness for both the phases will be conserved. [90]

1.3.1 Δ-isobars degrees of freedom

Delta baryons are a family of subatomic hadrons constituted by a triplet of quark up and down, in different combination (therefore they do not carrying strangeness). They are present in 4-isobars (Δ^{++}, Δ^{+}, Δ^{0}, Δ^{-}) of electric charge $+2$, $+1$, 0 and -1, with a bare mass close to 1232 MeV and a spin and isospin projection of $3/2$ (all the quarks have the spin axis pointing in the same direction), see Tab. (1.4).

At low energy, they are instable and decay via the strong force generally in nucleons plus pions (it depends by the electric charges of the specific isobars), in a typical life-time of 10^{-24} seconds.

Like the others baryons, Δ's are sensitive to the nuclear interaction, mediated by the exchange of virtual isoscalar scalar (σ), isoscalar vector (ω) and isovector vector (ρ) meson fields.

In regime of finite values of density and temperature, a state of high density resonance matter may be formed and the $\Delta(1232)$-isobar degrees of freedom are expected to play a

	M (MeV)	C	B	S	t_3
Δ^{++}	1232	2	1	0	3/2
Δ^{+}	1232	1	1	0	3/2
Δ^{0}	1232	0	1	0	3/2
Δ^{-}	1232	-1	1	0	3/2

Table 1.4: Δ's masses and quantum numbers.

central role in relativistic heavy ion collisions and in the physics of compact stars [63, 64, 65, 66, 67]. In particular, transport model calculations and experimental results indicate that an excited state of baryonic matter is dominated by the Δ-resonance at the energy from AGS to RHIC [68, 69, 70, 71]. However, the formation of resonances matter contributes essentially to baryon stopping, hadronic flow effects and increase strangeness particles production at higher temperature [97].

The QHD-Lagrangian density concerning the Δ's degrees of freedom can be written as [73]

$$\mathcal{L}_\Delta = \overline{\psi}_{\Delta\,\nu}\,[i\gamma_\mu\partial^\mu - (M_\Delta - g_{\sigma\Delta}\sigma) - g_{\omega\Delta}\gamma_\mu\omega^\mu]\psi_\Delta^\nu\,, \qquad (1.48)$$

where ψ_Δ^ν is the Rarita-Schwinger spinor for Δ-isobars (Δ^{++}, Δ^{+}, Δ^{0}, Δ^{-}). The equation of motion for Δ's and σ, ω and ρ meson fields are obtained, as usual, from the Euler-Lagrange equation (1.3).
The Dirac equation of motion take the form:

$$(i\gamma_\mu\partial^\mu - M_\Delta^* - g_{\omega\Delta}\gamma^0\omega)\psi_\Delta = 0\,, \qquad (1.49)$$

where $M_\Delta^* = M_\Delta - g_{\sigma\Delta}$ is the Δ's effective mass.
In this context, the contribution of the Δ-isobars to σ, ω and ρ meson fields, is obtained by adding to eq.s (1.30)–(1.32), the contribution of Δ-isobars weighted for the corresponding meson-Δ coupling constants. The EOS and the scalar and vector baryon density, are obtained respectively from eq.s (1.34), (1.35) and (1.39), (1.40), weighted for the corresponding degeneracy spin factor $\gamma_\Delta = 2J_\Delta + 1 = 4$.

In this context, it is important to remark that the meson-Δ coupling constants are only known with a certain uncertainty. This suggest us to consider in this work, only the corresponding coupling-constant with the σ and ω meson fields, more of which are explored in the literature [73, 98, 99].
In Chapter 5, we will deeply study the finite temperature and dense nuclear medium in presence of Δ-isobar degrees of freedom, and and we will investigate the possible phase transition from nucleon fluid to resonant-dominant Δ-matter.

1.4 Mesonic degrees of freedom

As known, mesons are a family of subatomic particles composed of a quark and an anti-quark. They are hadrons and therefore sensitive to the strong force mediated by the exchange of

	π	K	η	$\eta^{'}$	K^*	ρ	ω	ϕ
M	140	494	547	958	892	771	782	1020
C	0, ± 1	0, ± 1	0	0	0, ± 1	0, ± 1	0	0
B	0	0	0	0	0	0	0	0
S	0	± 1	0	0	± 1	0	0	0
t_3	0, ± 1	$\pm 1/2$	0	0	$\pm 1/2$	0, ± 1	0	0

Table 1.5: Mesons quantum number and vacuum masses (given in MeV).

virtual isoscalar scalar (σ), isoscalar vector (ω) and isovector vector (ρ) meson fields, like the baryons.

All mesons are unstable, with lifetimes ranging from 10^{-8} second to less than 10^{-22} seconds, in particular charged mesons decay (sometimes through intermediate particles) to form electrons and neutrinos. Uncharged mesons may decay to photons.

Historically, mesons are important because, for example, through the study of the J/ψ decay, it was possible to discover a new quark (charm) and, furthermore, through the study of the kaons, it was possible to demonstrate the violation of the parity during the weak reaction. The CP violation is currently under investigation also in B-mesons (which contain bottom quarks).

Especially at low baryon density and high temperature, their contribution to the total thermodynamical potential (and, consequently, to the other thermodynamical quantities) becomes very important. Furthermore, kaon degrees of freedom (K^+, K^-, K^0, $\overline{K}^0$ and K^{*+}, K^{*-}, K^{*0}, $\overline{K}^{*0}$) carrying also strangeness quantum number and for therefore, they may play a crucial role in the physics of a relativistic heavy ion collision experiments.

For this reason, in this section, we implement the hadronic Lagrangian density introducing the contribution of the mesons degrees of freedom.

1.4.1 Effective relativistic mean field model

Let us now introduce the contribution of the lightest pseudo-scalar (π, K, $\overline{K}$, η, $\eta^{'}$) and vector mesons (ρ, ω, K^*, $\overline{K}^*$, ϕ) to the nuclear equation of state, Tab. (1.5).

It is known that, in many cases, the coupling constants of the mesons with the mesons-fields are only known with a bad approximation. For this reason, in this section, we show an alternative formulation of the problem, that overcome the large uncertainty of the meson-coupling constant present in literature, taking into account of an effective chemical potential depending on the self-consistent interaction between baryons.

From a phenomenological point of view, we can take into account the meson degrees of freedom by adding their one-body contribution to the thermodynamical potential, that is, the contribution of an ideal Bose gas with an effective chemical potential μ_j^*, depending self-consistently from the meson fields [67].

In this way, the hadronic system is still regarded as an ideal gas but here we have a (quasi-free) meson gas with an effective chemical potential that contains the self-consistent interaction of the meson fields.

The value of the meson effective chemical potential μ_j^* is obtained from the "bare" one given in eq. (1.44) and subsequently expressed in terms of the corresponding effective baryon one respecting the strong interaction. More explicitly, for π^+ meson we have $\mu_{\pi+} = \mu_C \equiv \mu_p - \mu_n$, where μ_C is the electric charge chemical potential. Thus, the corresponding effective pion chemical potential can be written as

$$
\begin{aligned}
\mu_{\pi+}^* &\equiv \mu_p^* - \mu_n^* \\
&= \mu_p - \mu_n - 2\,g_{\rho N}\rho\,.
\end{aligned}
\tag{1.50}
$$

where the last equivalence follows from Eq.(1.38). Therefore, the ρ meson field couples to the total isospin density, which receives a contribution from nucleons and pions. Analogously for the kaons, setting $x_{\omega\Lambda} = g_{\omega\Lambda}/g_{\omega N}$, we have:

$$
\begin{aligned}
\mu_{k^+(k^{*+})}^* &\equiv \mu_p^* - \mu_{\Lambda(\Sigma^0)}^* \\
&= \mu_p - \mu_\Lambda - (1 - x_{\omega\Lambda})g_{\omega N}\omega - \frac{1}{2}g_{\rho N}\rho\,, \\
\mu_{k^0(k^{*0})}^* &\equiv \mu_n^* - \mu_{\Lambda(\Sigma^0)}^* \\
&= \mu_n - \mu_\Lambda - (1 - x_{\omega\Lambda})g_{\omega N}\omega + \frac{1}{2}g_{\rho N}\rho\,.
\end{aligned}
$$

$$\tag{1.51}$$
$$\tag{1.52}$$

Other strangeless neutral mesons have a vanishing chemical potential.

Their one-body contribution to the thermodynamical quantities can then be easily found. In particular, the pressure P_M, the energy density ε_M and the particle density ρ_j^M of the j-the meson are:

$$
P_M = \frac{1}{3}\sum_j \gamma_j \int \frac{\mathrm{d}^3k}{(2\pi)^3}\,\frac{k^2}{E_j^*(k)}\,g_j(k)\,,
\tag{1.53}
$$

$$
\varepsilon_M = \sum_j \gamma_j \int \frac{\mathrm{d}^3k}{(2\pi)^3}\,E_j^*(k)\,g_j(k)\,,
\tag{1.54}
$$

$$
\rho_j^M = \gamma_j \int \frac{\mathrm{d}^3k}{(2\pi)^3}\,g_j(k)\,,
\tag{1.55}
$$

where the sun runs over all meson particles and $\gamma_j = 2J_j + 1$ is the degeneracy spin factor of the j-th meson (γ=1 for pseudoscalar meson and $\gamma = 3$ for vector ones). Note that the contribution of the particles and anti-particles is take separately, in particular in the boson particle distribution $g_j(k)$ the contribution of anti-boson is obtained by substituting $\mu_j^* \to -\mu_j^*$ in the boson particles distribution function:

$$
g_j(k) = \frac{1}{exp[(E_j(k) - \mu_j^*)/T - 1]}\,,
\tag{1.56}
$$

where $E_j(k) = \sqrt{k^2 - m_j^2}$ and m_j is the bar mass of the j-th meson.

In presence of mesons it is also important take in consideration the possible onset of Bose condensation. In particular, if $|\mu_j^*| \le m_j$ the condensation may take place. However, in the range of temperatures and baryon densities explored in this thesis, such condition is never reached.

1.4.2 Chiral models

In this investigation we also analyze the mesonic contribution to the nuclear equation of state, following the classical approach, that incorporate the meson degrees of freedom to the hadronic lagrangian density through a direct coupling of the mesons to the mesons fields.

In this context, we concentrate our analysis in particular on the lightest pseudo-scalar K mesons (K^+ and K^-). This is because we are particular interested in the study of the strangeness production at high temperature and baryon density, where the contribution of the lightest strange mesons may play an important rule (see Tab. 1.5).

In this context, the Kaon Lagrangian density can be written in terms of minimal coupling scheme, as follow [40, 44, 45, 100]

$$\mathcal{L}_K = D_\mu^* \Phi^* D^\mu \Phi - m_K^{*2} \Phi^* \Phi \,, \tag{1.57}$$

where $D_\mu = \partial_\mu + i g_{\omega K} \omega_\mu + i g_{\rho K} \tau_{3K} \rho_\mu$ is the covariant derivative of the meson field, $m_K^* = m_K - g_{\sigma K} \sigma$ is the effective kaon mass and τ_{3K} is the third component of the isospin operator.

In order to obtain the correspondent meson-kaon vector coupling constant, we use the well known formalism obtained through the quark model and isospin counting rules and we obtain $g_{\omega K} = g_{\omega N}/3$ and $g_{\rho K} = g_{\rho N}$. The scalar $g_{\sigma K}$ coupling constant, can be determined from the study of the real part of the anti-kaon optical potential, at the saturation nuclear density, in a symmetric nuclear matter, by setting $U_{K^-} = -g_{\sigma K}\sigma - g_{\omega K}\omega$.

In this investigation we set the anti-kaon optical potential equal to $U_{K^-} = -50$ MeV, -100 MeV and -160 MeV, based on recent theoretical calculations and experimental measurements [40, 41, 43, 44, 45, 46, 47, 48, 101]. For these values of the anti-kaon potential depth, we obtain the following kaon optical potentials ($U_{K^+} = -g_{\sigma K}\sigma + g_{\omega K}\omega$, where the sign $+$ in the ω-field, is due to the G-parity): $U_{K^+} = 47$ MeV, -3 MeV and -63 MeV, respectively for $U_{K^-} = -50$ MeV, -100 MeV and -160 MeV, at the saturation nuclear density. In this approach we neglect the contribution of the neutral kaons (K^0 and $\overline{K}^0$) because of the large uncertainty in literature on their coupling constants with the meson fields.

The kaon-field equations are obtained in the usual way, from the minimization of the corresponding kaons thermodynamic potential Ω_K, with respect to the σ, ω and ρ meson field. In the relativistic mean field approximation, the Euler-Lagrangian equation (1.3) gives:

$$m_\sigma^2 \sigma = g_{\sigma K} \left(\rho_K^S + \rho_K^c \right) , \tag{1.58}$$

$$m_\omega^2 \omega = g_{\omega K} \, \rho_K \,, \tag{1.59}$$

$$m_\rho^2 \rho = g_{\rho K} \left(\rho_{K^+} - \rho_{K^-} \right) , \tag{1.60}$$

as for baryons, $\sigma = \langle \sigma \rangle$, $\omega = \langle \omega^0 \rangle$ and $\rho = \langle \rho_3^0 \rangle$ are the nonvanishing expectation values of mesons fields. Furthermore the kaon contribution to the mesons fields must be added to that of the baryon component of the field equation of motions, given in eq.s (1.30) and (1.31)–(1.32).

In this context, the kaons vector and scalar density (ρ_K and ρ_K^S), assume the form

$$\rho_K = 2\xi^2(\mu_K - X_0) + \int \frac{d^3p}{(2\pi)^3} \left[n_K(p) - \overline{n}_K(p) \right], \tag{1.61}$$

$$\rho_K^S = \int \frac{d^3p}{(2\pi)^3} \frac{m_K^*}{\sqrt{p^2 + m_K^{*2}}} \left[n_K(p) + \overline{n}_K(p) \right], \tag{1.62}$$

where we set $\mu_K = \mu_{K^+}$ (given in eq. 1.44), $X_0 = g_{\omega K}\omega_0 + g_{\rho K}\rho_0$ and ξ is the order parameter, obtained from the minimization of the thermodynamical potential Ω_K (naturally for $\xi = 0$ we have no condensation). The corresponding boson particle, anti-particle (K^+, K^-) distribution function are given by

$$n_K(p) = \frac{1}{\exp[(\omega^+(p) - \mu_K)/T] - 1}, \tag{1.63}$$

$$\overline{n}_K(p) = \frac{1}{\exp[(\omega^-(p) + \mu_K)/T] - 1}, \tag{1.64}$$

where $\omega^\pm(p) = \sqrt{p^2 + m_K^*} \pm g_{\omega K}\omega_0 + g_{\rho K}\tau_{3K}\rho_0$ stays respectively for kaons and anti-kaons effective energy and the sign ($\pm g_{\omega K}\omega_0$) is due to the G-parity.

The kaon vector density in Eq.(1.61), can be viewed therefore as the sum of a "condensate" and a "thermal" contribution:

$$\rho_K = \rho_K^c(\xi) + \rho_K^T(T). \tag{1.65}$$

The total hadronic pressure and energy density, are given naturally as the sum of the baryons plus the kaons component, where P_K and ε_K are given respectively by:

$$P_K = \xi^2[(\mu_K - X_0)^2 - m_K^{*2}] - T \int \frac{d^3p}{(2\pi)^3} \{ \ln[1 - e^{-\beta(\omega^+ - \mu_K)}]$$
$$+ \ln[1 - e^{-\beta(\omega^- + \mu_K)}] \}, \tag{1.66}$$

$$\varepsilon_K = \xi^2[m_K^{*2} + \mu_K^2 - X_0^2] + \int \frac{d^3p}{(2\pi)^3} [\omega^+ n_K(p) + \omega^- \overline{n}_K(p)]. \tag{1.67}$$

Finally, we would like to point out that the condition for the onset of the kaon condensation, is given by [100]

$$\xi[\mu_K - \omega^+(0)][\mu_K + \omega^-(0)] = 0, \tag{1.68}$$

therefore, for a s-wave condensation at $p = 0$, we obtain, respectively, $\mu_{K^+} = \omega^+$ for K^+ and $\mu_{K^-} = \omega^-$ for K^- (naturally when the condensate is not present, $\xi = 0$).

1.5   Strangeness production at finite temperature and baryon density

We would like to present now, a detailed discussion of the strangeness production at finite temperature and baryon density, by means of the effective relativistic mean field model 1.4.1

and the comparison of the obtained results with that of the chiral formulation exposed in Section 1.4.2.

In this context, we are particularly interested in the study of the kaon and anti-kaon production, in the regime of relativistic heavy ion collision experiments as well as in compact stars (hyperons degrees of freedom are include in the hadronic Lagrangian density following the prescription of Section 1.3).

This study, may help us to well determinate the real part of the anti-kaon optical potential, currently affected by big uncertainties, due to the difficulty of finding out its value from the experimental results at the nuclear saturation density. As partial discussed in the introduction, a stronger attractive potential depth should in fact favor the formation of the condensation, but, on the other hand, a stiffer or softer equation of state (EOS) should help or not the condensation itself. At this regard, the analysis of kaonic atom data leads to the real part of anti-kaon optical potential close to $U_{K^-} = -180 \pm 20$ MeV at the saturation nuclear matter density [40, 41, 42, 43, 44, 45]. Contrariwise, chiral-models and coupled-channel G-matrix theory, seem to suggest a strength of the optical potential close to $U_{K^-} = -(50 \div 80)$ MeV [46, 47, 48]. These uncertainties in the estimation of the anti-kaon potential depth, imply some difficulties in the calculation of the effective kaon mass in-medium. Moreover, different mean field models predict negative or imaginary effective kaon mass at sufficiently large values of the σ-meson field, responsible of the medium range attraction [44, 45, 54]. At this regard, the future CBM (Compressed Baryonic Matter) experiment of FAIR (Facility of Antiproton and Ion Research) at GSI Darmstadt, will be of great importance to create compressed baryonic matter with a high net baryon density and finite temperature [55, 56, 57, 58] and make possible an accurate analysis of the proprieties of kaons and, more in general, of the strangeness production at high baryon density.

Here, we investigate the strangeness production at finite isospin density ($y = 0.4$) and zero net strangeness ($z = 0$), using the effective relativistic mean field model and the chiral one.

In particular, we focused our analyze in the range of temperature and baryon density reachable in high energy heavy ion collisions with particular attention to the physical conditions relevant for the future CBM experiment at FAIR. At this stage, the possible formation of a mixed phase or deconfinement phase transition to a quark-gluon plasma is not take in consideration. Whereas our attention is pointed in exploring the strangeness production of a hadronic system and the possible onset of the kaon condensation for the two aforementioned models. In this context, other strangeless mesons are not considered in our analysis, because they do not sensibly affect the strangeness production but they contribute mainly to the total pressure and energy density.

This study is based on the results obtained in [102, 103, 104]

1.5.1 Hadronic equation of state and main results

The analyze is performed in the framework of relativistic mean field theory. In particular, the nuclear medium is investigated at finite temperature and baryon density, by requiring the conservation of the baryon number (B), electric charge (C) and strangeness number (S). In this context the meson-nucleon couplings constant ($g_{\sigma N}$, $g_{\omega N}$, $g_{\rho N}$) are fixed to reproduce

the parameters set marked as GM3 of Tab. 1.2.

Due to the high temperature and high baryon density achieved by the system, the hadronic Lagrangian density take the form:

$$\mathcal{L}_H = \mathcal{L}_B + \mathcal{L}_K \, , \tag{1.69}$$

where $\mathcal{L}_B$ stands for the full octet of baryons (p, n, Λ, Σ^+, Σ^0, Σ^-, Ξ^-, Ξ^0) eq. (1.27) and $\mathcal{L}_K$ corresponds to the kaon meson degrees of freedom (K^+, K^-) eq. (1.57).

As already discussed in the previous section, especially due to the large uncertainties in the measure of the anti-kaon optical potential, here we presents a comparative study of the strangeness production in hadronic matter, comparing the results obtained through the effective relativistic mean field model, exposed in section 1.4.1, with that of the chiral one, obtained through a direct coupling of the kaons with the meson fields, widely exposed in section 1.4.2.

The baryon scalar density, the vector density and the EOS are obtained following the eq.s (1.34), (1.35) and (1.39)–(1.40) whereas the kaons, anti-kaons scalar and vector density and the corresponding EOS are obtained respectively the eq.s (1.61), (1.62) and (1.66)–(1.67). In the effective relativistic mean field model, the vector density and the EOS are instead given by eq.s (1.55) and (1.53)–(1.54).
Naturally, the total pressure and energy density, are given by the sum of the baryons and the mesons component, calculated in one of the two aforementioned approaches .

1.5.2 Kaons to anti-kaons ratio.

To start this numerical investigation, we report in Fig. 1.4, the kaon to anti-kaon ratio K^+/K^- as a function of baryon density and of the temperature, for different values of the anti-kaon optical potential. As expected, the ratio results to be very sensitive to the choices of the anti-kaon potential depth. At fixed temperature and by increasing the baryon density, we observe a continuous growing in the K^+/K^- ratio for moderate values of U_{K^-}, whereas in presence of a strong attractive potential, the ratio decreases after reaching the nuclear saturation density, mainly due to the strong reduction of the kaon effective mass.

In this context it is interesting to observe that the results obtained in the minimal coupling scheme for a moderate potential depth ($U_{K^-} = -50$ MeV), as suggested by recent self-consistent calculations based on chiral Lagrangian [47, 48] and coupled-channel G-matrix theory [46], are very close to those of the effective relativistic mean field model. Contrariwise, in absence of kaon interaction (dot dashed line) and especially at higher baryon density, we observe a strong increase in the K^+/K^- ratio. This effect is mainly due to the absence of an effective kaon mass and chemical potential. In Fig. 1.5, we show the variation of the kaon to anti-kaon ratio as a function of the temperature at a fixed baryon density $\rho_B = \rho_0$, where ρ_0 is the nuclear saturation density. It is possible to observe again a good correspondence between the two approaches for a moderate value of the anti-kaon optical potential. In presence of a free kaons gas, there is a strong enhancement in the K^+/K^-, due to the absence of the σ and ω fields self-interaction. The contribution of ρ-meson field appears to be instead negligible for this choice of parameter set ($y = 0.4$) and especially at higher temperature, where anti-kaons are abundantly produced and the K^+/K^- rapidly decreases.
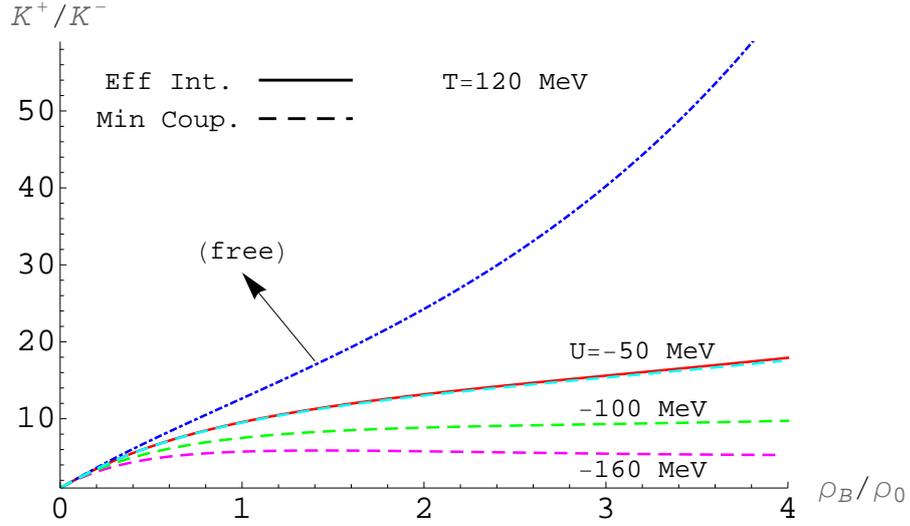
Figure 1.4: Kaon to anti-kaon ratio as a function of baryon density at a fixed temperature $T = 120$ MeV. The solid lines correspond to the results obtained in the effective relativistic mean field model, the dashed lines correspond to different values of anti-kaon optical potential and the dot-dashed lines to a non-interacting free kaon gas.
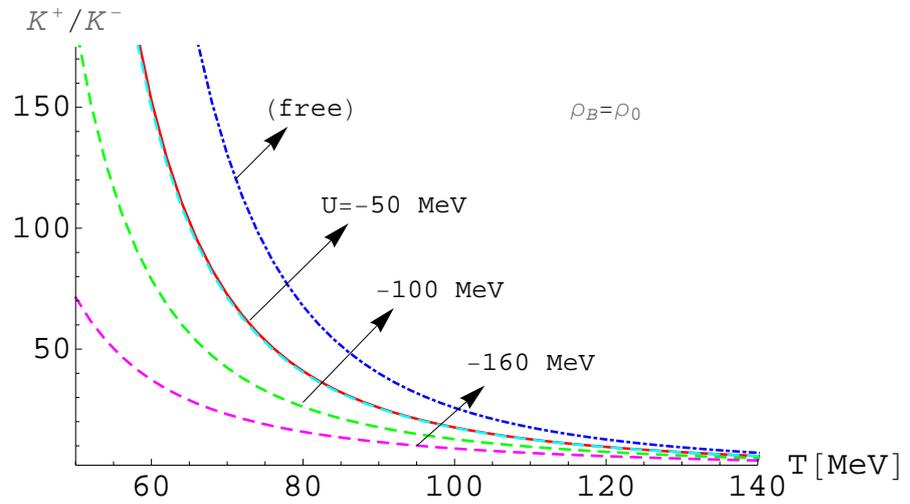
Figure 1.5: The same of Fig. 1.4 as a function of temperature at a baryon density fixed to the nuclear ρ_0.
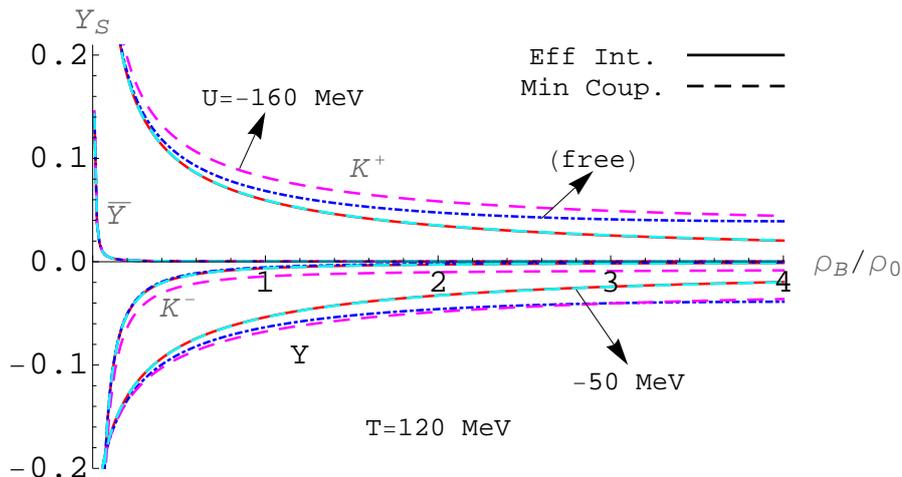
Figure 1.6: Strangeness concentration as a function of baryon density at a fixed temperature $T = 120$ MeV. The solid lines correspond to the results obtained in the effective relativistic mean field model, the dashed lines correspond to different values of anti-kaon optical potential and the dot-dashed lines to a free kaon gas.

Such a sensible difference in the kaon to anti-kaon ratio can be considered as a relevant feature for the determination of the real part of the anti-kaon optical potential, in the future relativistic heavy ion collision experiments at high baryon density.

1.5.3 Strangeness concentration and kaons condensation.

To better clarifies the role played by strange particles in the nuclear medium, we report in Fig. 1.6, the strangeness concentration Y_S of kaons (K^+) and anti-kaons (K^-), hyperons (Y) and anti-hyperons ($\overline{Y}$) as a function of the baryon density. The total strangeness is fixed to zero. As expected, almost all the strangeness fraction is carried by kaons and hyperons, whereas K^- and anti-hyperons play a marginal role, contributing only at low baryon density and high temperatures.

   The results obtained through the relativistic mean field model, are in very good agreement with the minimal coupling scheme, when we set $U_{K^-} = -50$ MeV. In absence of kaon interaction (free kaon gas, dot dashed lines), at low baryon density, the kaon strangeness concentration is close to that of the relativistic mean field model, whereas, at higher ρ_B it converges to that of the effective minimal coupling scheme obtained for $U_{K^-} = -160$ MeV. Instead, anti-kaons strangeness fraction do not show an appreciable variation in absence of meson-field interaction.

   In the following figure 1.7, we show the strangeness dependence of the system at the nuclear saturation density ρ_0 for a wide range of temperatures. As one can see, the strangeness concentration is practically negligible below $T = 60$ MeV. Strange particles start to be abundantly produced above $T = 80$ MeV and the corresponding anti-particles are produced at higher temperatures. The free kaon gas case is also reported. In this
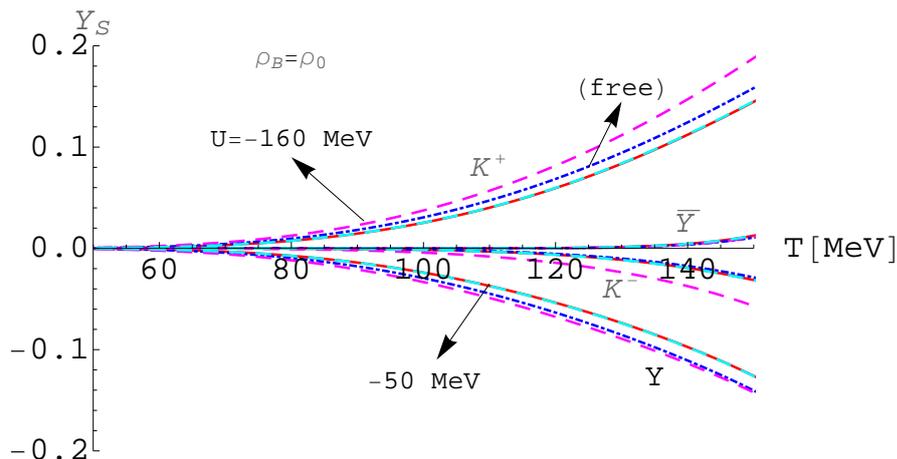
Figure 1.7: The same of Fig. 1.6 as a function of temperature at a fixed baryon density $\rho_B = \rho_0$.

context, it is relevant to note that, for a choice of $U_{K^-} = -50$ MeV, the results obtained in the minimal coupling scheme are very close to those of the relativistic mean field one, because in this case the effective kaon mass is very close to the bare one. At the increasing of the anti-kaon optical potential, the effective kaon mass rapidly decreases, deviating from the behavior of the relativistic mean field model.

Before concluding, we would like to present a brief analyze of the condition for the onset of the kaon condensation, for a wide range of temperatures and baryon densities, in the two aforementioned models, considering $U_{K^-} = -50$ and -160 MeV. At this purpose, in Fig. 1.8 , we report the threshold condition for the onset of the kaon and anti-kaon condensation ($\omega^+ = \mu_{K^+}$ for K^+ and $\omega^- = \mu_{K^-}$ for K^-) at $p = 0$ (s-wave condensation) as a function of baryon density and at the lower temperature at which strange particles start to be produced ($T = 80$ MeV). As one can easily observe, the kaon/anti-kaon chemical potential $\mu_{K^\pm}$ is always lower than the corresponding kaon/anti-kaon threshold energy $\omega^\pm$, therefore the condition for the onset of the condensation is never reached. However, it is interesting to note that, for $U_{K^-} = -160$ MeV, μ_{K^+} approaches ω^+, but they do not come close enough to allow the formation of the condensation. Note also that for $U_{K^-} = -50$ MeV, the minimal coupling curves are perfectly overlapping to that of the effective relativistic one. In absence of the kaon interaction, the effective kaon energy is obviously constant and equal to the kaon mass ($\omega^\pm = m_K$). The chemical potential is close to that of the minimal coupling scheme for $U_{K^-} = -160$ MeV, hence also in this case the threshold condition for the onset of the condensation is never reached.

Analogously, in Fig. 1.9, we show the variation of the kaon and anti-kaon effective energy and chemical potential for a very wide range of temperatures at the maximum baryon density explored in this work ($\rho_B = 4\rho_0$). It is interesting to observe that both kaon and anti-kaon effective energies seem to be very little affected by variation of the temperature, contrariwise kaon and anti-kaon chemical potentials show a little increase at higher temper-

46
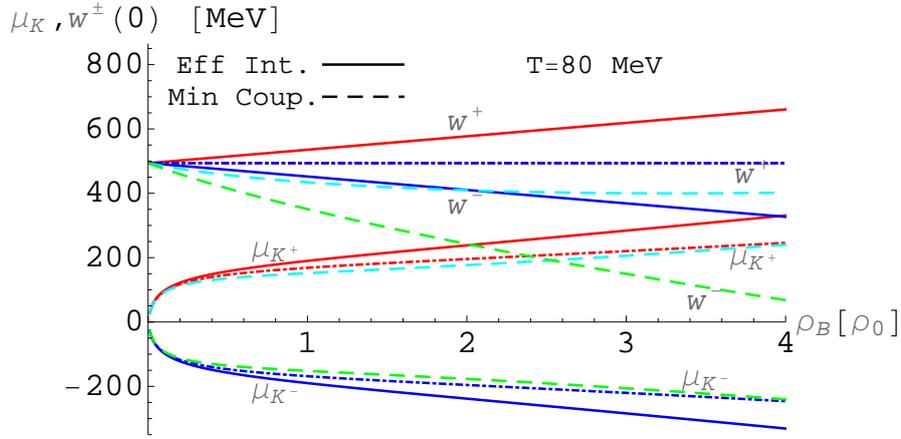
Figure 1.8: Kaon and anti-kaon effective energy $\omega^\pm(p=0)$ and chemical potential as a function of baryon density at $T = 80$ MeV, for free kaons gas (dot-dashed lines), in the effective relativistic mean field model (solid lines) and in the minimal coupling scheme (dashed lines) for $U_{K^-} = -160$ and -50 MeV.
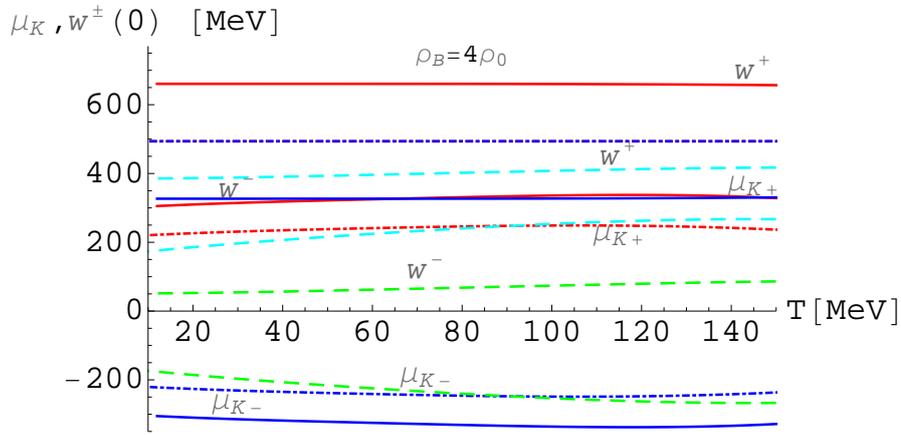
Figure 1.9: The same of Fig. 1.8 as a function of the temperature at $\rho_B = 4\rho_0$.

ature (such a feature persists also by increasing the isospin asymmetry y). This behavior seems to suggest that in relativistic heavy ion collision kaons can never reach the threshold condition for the onset of the condensation. Such a result appears to be in agreement with the predictions of very recent transport models [53]. The situation is of course different in systems like neutron stars, where the total strangeness is not conserved and the kaon condensation can take place [49, 50, 51, 40].

1.5.4 General consideration

In conclusion, the results obtained in the relativistic mean-field model and in the chiral one, are in good agreement when we choice a moderate value of the anti-kaon optical potential ($U_{K^-} = -50$ MeV), as suggested by recent self-consistent calculation based on chiral Lagrangian and G-matrix theory [46, 47, 48]. In this condition, the kaon to anti-kaon ratio and the strangeness fraction become very close to those of the effective relativistic mean field model. Contrariwise, when we take in consideration a stronger potential depth (e.g. $U_{K^-} = -160$ MeV), the results appear to be significantly different, mainly due to the strong variation in the kaon effective mass in the meson-exchange model.
Furthermore, in absence of kaon in-medium interaction, the kaon to anti-kaon ratio rapidly diverges by the results obtained in the meson exchange and the relativistic mean field model, mainly due to the absence of the contribution of the σ and ω field into the kaon mass and chemical potential. The kaon strangeness concentration is also sensibly modified taking a behavior intermediate between that of the relativistic mean field model, at low baryon density and the minimal coupling scheme at $U_K = -160$ MeV, for higher values of ρ_B. Whereas anti-kaons strangeness fraction do not show an appreciable variation in absence of meson-field interaction. The strong difference in the kaon to anti-kaon ratio, could therefore be considered as a relevant feature in the determination of the real part of the anti-kaon optical potential, especially in relativistic heavy ion collisions at high baryon density [55, 57, 58].

Finally, we have also analyzed the possible onset of the kaon condensation in regime of density and temperature reachable in relativistic heavy ion collisions. We have found that the kaons chemical potential is always less then the corresponding kaon threshold energy $\omega^{\pm}$). This matter of fact seems to suggest, in agreement with the results obtained within modern transport codes [53], that kaon condensation does not take place at any temperature and density in those systems in rapid evolution, like the relativistic heavy ion collision, where the zero net strangeness condition is conserved.

1.6 Quark-gluon plasma equation of state

In the last years, there was an increasing theoretical and experimental evidences that, during the condition reached in a relativistic heavy ion experiment, baryons are forced to stay so close one to another that they would overlap. Therefore, at large densities or high temperature, constituent quarks are shared by neighboring baryons and should eventually become mobile over a distance larger than the typical size of one baryon. This means that quarks become deconfined and the real degrees of freedom of strongly interacting matter instead of baryons.

Unfortunately it is not possible to directly study the QGP state, due to the rapid time evolution ($\approx 10^{-22}$ sec) of the fireball and the consequent rehadronization process, but it is possible to make some prediction about its proprieties through some physical observable, such as for example the strangelet production (the s-$\bar{s}$ separation mechanism in the hadron and in the quark phase during the phase transition) and the enhancement of strange particle production during the rehadronization [105, 106].

Furthermore, from a theoretical point of view, lattice calculation predict a critical phase transition from hadronic matter to quark-gluon plasma (QGP) at temperature T_c of about 170 MeV, corresponding to a critical energy density $\varepsilon_c \approx 1$ GeV/fm^3 [107]. At finite baryon chemical potential a rapid-cross over of the thermodynamics observable around a quasi-critical temperature and a first order phase transition is excepted.

In our investigation, we analyze the quark-gluon plasma (QGP) equation of state through the well know and simple MIT-Bag model.

The relative Lagrangian density can been written as:

$$ L_{\text{Mit}} \quad = \quad \sum_q \bar{\psi}_q [i\gamma_\mu \, \partial^\mu - m_q] \, \psi_q - B \,, \tag{1.70} $$

where q is the quark flavor (u, d, s), m_q is the quark vacuum mass ($m_u = m_d = 0$ MeV and $m_s = 150$ MeV) and B is the bag pressure.

In this context, all the non-perturbative effects are simulated by the bag constant B which represents the pressure of the vacuum. Furthermore, it is well known using the simplest version of the MIT bag model, at moderate temperatures the deconfinement transition takes place at very large densities if the bag pressure B is fixed to reproduce the critical temperature computed in lattice QCD. On the other hand there are strong theoretical indications that at moderate and large densities (and not too large temperatures) diquark condensates can form, whose effect can be approximately taken into account by reducing the value of the effective bag constant [108].

A phenomenological approach can therefore be based on a bag constant depending on the baryon chemical potential, as proposed in Ref [109]. We have adopted a parametrization of the form

$$ B_{\text{eff}} = \frac{B_0 - B_\infty}{1 + e^{\frac{\mu_B - \mu_0}{a}}} + B_\infty \,, \tag{1.71} $$

where we have set $B_0^{1/4} = 254$ MeV (bag constant at vanishing μ_B), $B_\infty^{1/4} = 160$ MeV (bag constant at very large μ_B), $\mu_0 = 600$ MeV and $a = 320$ MeV. The above values have been obtained by requiring that, at vanishing chemical potential, the critical temperature is about 170 MeV, as suggested by lattice calculations [107], while the other constraint is the requirement that the mixed phase starts forming at a density slightly exceeding $3\,\rho_0$ (see Fig. 1.10) for a temperature of the order of 100 MeV (as suggested by hydrodynamical calculations [110]).

Following this line, the pressure, energy density and baryon number density for a

relativistic Fermi gas of quarks can be written, respectively, as [111]

$$P \quad = \frac{\gamma_f}{3} \sum_f \int_0^\infty \frac{\mathrm{d}^3 k}{(2\pi)^3} \frac{k^2}{e_f} \left[n_f(k) + \overline{n}_f(k) \right] - B_{\text{eff}} \, , \tag{1.72}$$

$$\varepsilon \quad = \gamma_f \sum_f \int_0^\infty \frac{\mathrm{d}^3 k}{(2\pi)^3} \, e_f \left[n_f(k) + \overline{n}_f(k) \right] + B_{\text{eff}} \, , \tag{1.73}$$

$$\rho \quad = \frac{\gamma_f}{3} \sum_f \int_0^\infty \frac{\mathrm{d}^3 k}{(2\pi)^3} \left[n_f(k) - \overline{n}_f(k) \right] , \tag{1.74}$$

where the quark degeneracy factor for each flavor $(f = u, d, s)$ is $\gamma_f = 6$ and $n_f(k)$, $\overline{n}_f(k)$ are the particle and antiparticle quark distributions function:

$$n_i(k) = \frac{1}{\exp(E_f(k) - \mu_f)/T + 1} \, , \tag{1.75}$$

$$\overline{n}_i(k) = \frac{1}{\exp(E_f(k) + \mu_f)/T + 1} \, , \tag{1.76}$$

where $E_f(k) = \sqrt{k_f^2 + m_f^2}$ and μ_f is the quark chemical potential, given by eq. (1.44).

Let us remark that, in this investigation, light quarks (u, d) are considered as massless particles, while for strange quarks $(s, \bar{s})$ we consider a finite mass of $m_s = 150 MeV$.

Similar expressions for the pressure and the energy density can be written for gluons, treating them as a massless Bose gas with zero chemical potential. Explicitly, we can calculate the P_g and energy density ε_g for gluons as

$$P_g \quad = \frac{\gamma_g}{3} \int_0^\infty \frac{\mathrm{d}^3 k}{(2\pi)^3} \frac{k}{\exp(E_f(k) - \mu_f)/T - 1} \, , \tag{1.77}$$

$$\varepsilon_g \quad = 3 \, P_g \, , \tag{1.78}$$

with the gluon degeneracy factor $\gamma_g = 16$.

In the Fig. 1.10, we report the pressure of the system as a function of the baryon density at different temperatures using the $GM3$ parameter set for the hadronic phase and the simple MIT Bag model with two quarks flavors and $B^{1/4} = 190$ MeV, for the quarks phase. Gluons are also taken in consideration through Eq.s (1.77) and (1.78).

Although the simplest version of the MIT bag model considered in this example, appears to be not fully appropriate to describe the nuclear medium, especially at high temperature and density, due to the absence of a Bag parametrization of the form of Eq. (1.71), we can anyhow observe the dependence of the QGP deconfinement phase transition from the temperature of the system. For example, at $T = 130$ MeV, the QGP phase is present around $\rho_B = 1.4\rho_0$, whereas, at lower temperature, the deconfinement phase transition to QGP is achieved at very high baryon density. At zero baryon density the deconfinement phase transition is expected to exist only at higher temperature $(T_c \approx 170$ MeV), or alternatively, in the inner core of compact object, such as for example neutron stars, the condition can be reached also at $T = 0$ MeV, due to the high baryon density present in its core.
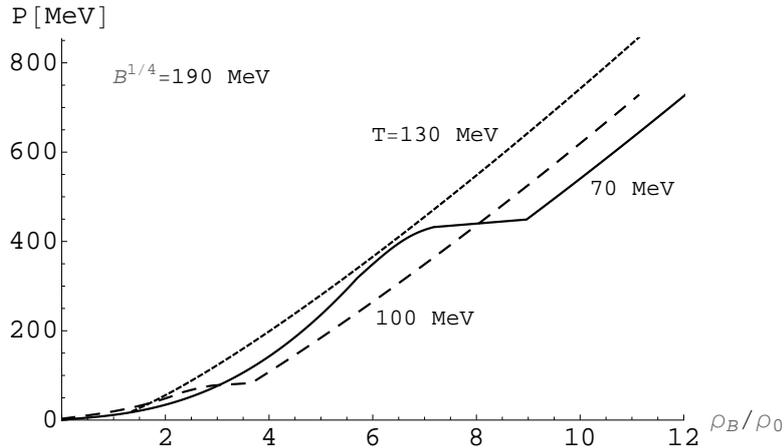
Figure 1.10: Pressure as a function of the baryon density at $y = 0.5$ for $GM3$ parameter set and MIT-Bag model with two quarks flavors and $B^{1/4} = 190$ MeV.

Furthermore, since one has to employ the fermion (boson) distributions, the results are not analytical, even in the massless quark approximation. Hence a numerical evaluations of the integrals in Eq.s (1.72)–(1.74) and (1.77) must be performed.

1.7   Major conclusions

In this chapter, we have presented a detailed discussion of the Lagrangian formalism in the context of relativistic mean-field model, where the nuclear force is mediated by the exchange of virtual isoscalar-scalar (σ), isoscalar-vector (ω) and isovector-vector (ρ) meson fields.
In this context, we have developed and implemented the nuclear EOS at finite temperature and baryon density, in the framework of non-linear relativistic Walecka type models. Furthermore, we have introduce the meson degrees of freedom through an effective formulation where the effective chemical potential depends on the self-consistent interaction between baryons (section 1.4.1). In this context, we have also introduced and analyzed the mesons contribution to the hadronic Lagrangian density, through a more traditional approach, in which the kaons are direct coupled with the meson fields.
We have also analyzed the strangeness production at finite temperature and baryon density, comparing the results obtained in the effective relativistic formulation of section 1.4.1 with that of the minimal coupling scheme of section 1.4.2. We have found a good correspondence between the two models for a moderate attractive value of the anti-kaon optical potential ($U_{K^-} = -50$ MeV). Furthermore, in agreement with the results obtained within modern transport codes [53], we have found that kaon condensation does not take place at any temperature and density in those systems in rapid evolution, like the relativistic heavy ion collision, where the zero net strangeness condition is conserved.
Finally, we have introduced the MIT Lagrangian density, in order to treat the QGP phase transition during the relativistic heavy ions collision experiments.

51

In this context, we have proposed two simply phenomenological approaches, one with a constant Bag, and another one based on a bag constant depending on the baryon chemical potential, as proposed in Ref [109].

The hadronic Lagrangian density and the MIT Bag model, will be used in the next Chapters in order to obtain the EOS and the thermodynamical proprieties of high compressed nuclear matter experiments, in a range of temperatures and baryon densities relevant in the future CBM (compressed baryonic matter) experiment of the FAIR (Facility of Antiproton and Ion Research) project at GSI Darmstadt [55, 58, 57]. However, in this direction, interesting results have already been obtained at low energy at the CERN Super Proton Collider (SPS) and are foreseen at a low-energy [112, 113, 114]. Finally, we will explore the mechanical and thermodynamical structure of proto-neutronstars, under β-stability condition in Chapter 3.

Chapter 2

Nonextensive statistical mechanics

In this chapter, we present the most important features of the so called nonextensive statistical mechanics, that is an implementation of the common Boltzmann-Gibbs statistics and it can be considered as an appropriate basis to deal with physical phenomena where strong dynamical correlations, long-range interactions and microscopic memory effects take place.

2.1 Introduction

As known, one of the major challenges in the modern physics is the determination of the physical proprieties and of the equation of state (EOS) of a strongly interacting systems at high temperature and finite baryon density.

In this context, the physics of relativistic heavy ion collisions, where the matter can reaches a value of few times the nuclear saturation density, is a goldmine of problems in statistical mechanics and thermodynamics due to a large average number of particles involved and possible phase transition phenomena in the hot and dense fireball created during the collisions [1].

For example, although in principle the process of deconfinement phase transition and the equation of state of quark-gluon matter can be described by quantum chromodynamics, in the last years, there is an increasing evidence that, in energy density range reached in relativistic heavy-ion collisions, non-perturbative effects in the complex theory of QCD are not negligible [107]. For this reason, the generated QGP immediately after the collision, does not at all resemble a quasi-ideal gas of quarks and gluons presenting strongly dynamical correlations, including long-range interactions [1, 115, 18, 2, 19].

In this context, the nonextensive statistical mechanics, proposed firstly by Tsallis, appears as a natural candidate in order to investigate physical phenomena where strong dynamical correlations, long-range interactions and microscopic memory effects take place [20, 21, 22, 25]. A considerable variety of physical applications involve a quantitative agreement between experimental data and theoretical models based on Tsallis thermostatistics. The existence of nonextensive statistical effects, therefore, should strongly affects the finite temperature and density nuclear EOS [116, 117, 27]. In fact, by varying temperature and density, the EOS reflects in terms of the macroscopic thermodynamical variables the micro-

scopic interactions of the different phases of nuclear matter.

Furthermore, under the phase transition, long range correlation and fluctuation in the temperature and in the others thermodynamical variables can be important and, in this situation, standard statistics constitute only a very strong approximation for the system.

2.2 Nonextensive statistical mechanics

Here, we present a brief discussion of the main features of the nonextensive mechanics. The importance of develop a phenomenological new and powerful statistical approach to the thermodynamics, is of great importance in order to obtain a connection between variables such as for example the temperature, pressure, energy of the system and the macroscopic world. This is particularly valid under the extreme condition reached during the relativistic heavy ion collision experiments or in the inner core of dense and hot compact objects, where strongly dynamical correlations, including long-range interactions, may take place.

In this context, from a theoretical point of view, it is important to resume firstly the basic properties of the Boltzmann-Gibbs (BG) formulation of statistical mechanics, that provide a magnificent tool in order to treat a very different kinds of physical phenomenons.

The basis of the BG statistics, is the following expression of the entropy:

$$S_{BG} \equiv -k \sum_{i=1}^{W} p_i \ln p_i \,, \tag{2.1}$$

with

$$\sum_{i=1}^{W} p_i = 1 \,, \tag{2.2}$$

where p_i is the probability associated with the ith microscopic state of the system, and k is Boltzmann constant. In the particular case of equiprobability, i.e., $p_i = 1/W$ $(\forall i)$, Eq. (1) yields the celebrated *Boltzmann principle*:

$$S_{BG} = k \ln W \,. \tag{2.3}$$

From now on, and without loss of generality, we shall take k equal to unity.

In presence of continuous variables, BG entropy could be written as

$$S_{BG} \equiv -\int dx \, p(x) \ln p(x) \quad (x \in R^d), \tag{2.4}$$

with

$$\int dx \, p(x) = 1 \,. \tag{2.5}$$

In particular, for a quantum system, BG statistics take the form:

$$S_{BG} \equiv -Tr \rho \ln \rho \,, \tag{2.6}$$

with

$$Tr\rho = 1 \; , \qquad (2.7)$$

ρ being the density operator or matrix. When the $W \times W$ matrix ρ is diagonalized, it shows the set $\{p_i\}$ in its diagonal.

Although of its tremendous power and usefulness, the BG concepts and statistical mechanics appear to be not universally applicable. Indeed, there is a plethora of natural and artificial systems (see, for instance, [21] and references therein) for which they do not provide the adequate mathematical frame for handling physically relevant quantities. This fact started being explicitly recognized at least as early as in 1902 by Gibbs himself, where he addresses anomalies related to systems such as gravitation. A formalism becomes therefore desirable which would address such anomalous systems. A vast class of them (although surely not *all* of them) appears to be adequately discussed within a generalization of the BG theory, frequently referred to as *nonextensive statistical mechanics*. This theory was first introduced by Tsallis, in 1988 [118] and then refined in 1991 [119] and 1998 [120]. It is based on the following generalization of S_{BG}:

$$S_q \equiv \frac{1 - \sum_{i=1}^{W} p_i^q}{q-1} \quad (q \in R;\; S_1 = S_{BG}) \; . \qquad (2.8)$$

Expressions (2.4) and (2.6) are respectively generalized into

$$S_q \equiv \frac{1 - \int dx\, [p(x)]^q}{q-1} \; , \qquad (2.9)$$

and

$$S_q \equiv \frac{1 - Tr\, \rho^q}{q-1} \qquad (2.10)$$

In this context, through eq. (9), the equiprobability condition (i.e., $p_i = 1/W$, $\forall i$), yields

$$S_q = \ln_q W \; , \qquad (2.11)$$

with the *q-logarithm* function defined as [20, 22]

$$\ln_q x \equiv \frac{x^{1-q} - 1}{1-q} \quad (x \in R;\; x > 0;\; \ln_1 x = \ln x) \, , \qquad (2.12)$$

and its inverse function (defined as *q-exponential*), given by:

$$e_q(x) \equiv [1 + (1-q)x]^{1/(1-q)} \; . \qquad (2.13)$$

The generalized entropy has, therefore, the usual properties of positivity, equiprobability, concavity and irreversibility and preserves the whole mathematical structure of thermodynamics (Legendre transformations). The real parameter q determines the degree of

non-additivity exhibited by the entropy form (2.9) and in the limit $q \rightarrow 1$, becomes additive and reduces to the standard Boltzmann-Gibbs entropy.

To better clarify this aspect and have a complete formulation of the nonextensive statistical mechanics, we have to optimize the S_q (given in eq. (2.8)), introducing the concept of energy in the aforementioned formalism. In this context, the best way to do so, is using the so called canonical ensamble, where the system is typically described by a quantum Hamiltonian, and it is characterized by the spectrum of energies $\{E_i\}$ ($i = 1, 2, ..., W$) defined as the eigenvalues associated with the Hamiltonian and its boundary conditions.

Here, the *internal energy* of the nonextensive system is given, in analogy to that of the Gibbs formalism ($\sum_{i=1}^{W} p_i E_i = U_{BG}$), by:

$$\frac{\sum_{i=1}^{W} p_i^q E_i}{\sum_{i=1}^{W} p_i^q} = U_q \,, \tag{2.14}$$

or equivalently: ($\sum_{i=1}^{W} p_i^q (E_i - U_q) = 0$).

The functional take instead the form:

$$\Phi_q \equiv S_q + \alpha \Big[\sum_{i=1}^{W} p_i - 1 \Big] - \beta \Big[\sum_{i=1}^{W} p_i^q (E_i - U_q) \Big] \,, \tag{2.15}$$

where α and β are the Lagrange parameters (their signs have been chosen using the standard notation) and the extremizing condition $\delta \Phi_q / \delta p_j = 0$ yields

$$p_j = \left(\frac{q}{\alpha} \right)^{1/(1-q)} e_q^{-\beta(E_j - U_q)} \quad (j = 1, 2, ..., W) \,. \tag{2.16}$$

In this way, from the condition of eq. (2.2), we can eliminate the parameter α and therefore find the generalized weight:

$$p_i = \frac{e_q^{-\beta(E_i - U_q)}}{Z_q} \quad (i = 1, 2, ..., W) \,, \tag{2.17}$$

where $\beta = 1/T$ and the q-generalized partition function is defined as follows:

$$Z_q(\beta) \equiv \sum_{j=1}^{W} e_q^{-\beta(E_j - U_q)} \,. \tag{2.18}$$

This probability distribution corresponds to a *maximum (minimum)* of S_q for $q > 0$ ($q < 0$). For $q = 0$, the entropy is constant, namely $S_0 = W - 1$, and the distribution is given by $p_i = [1 - \beta(E_i - U_0)] / \sum_{j=1}^{W} [1 - \beta(E_j - U_0)]$. Moreover, for $q < 1$, the q-exponential function presents a natural high-energy *cutoff*, hence the states for which $[1 - \beta(E_i - U_0)] < 0$ do not contribute.

A fundamental feature of Tsallis generalized thermostatics, is the concept of non-additivity of the entropy (2.8). In fact, if we have two statistically independent subsystems A e B, described, respectively, by individual probability density $f^{(A)}$ and $f^{(B)}$ and we call

$f^{(A+B)}(\mathbf{x}_A, \mathbf{x}_B) = f^{(A)}(\mathbf{x}_A) f^{(B)}(\mathbf{x}_B)$ the joint probability density of a composite system $A + B$, the nonadditive (nonextensive) character of S_q is summarized in the relation [22]

$$S_q[f^{(A+B)}] = \quad S_q[f^{(A)}] + S_q[f^{(B)}])$$
$$+ (1-q) \, S_q[f^{(A)}] \, S_q[f^{(B)}] \,. \qquad (2.19)$$

In the limit $q \to 1$, the above equation reduces to the well-known additivity (extensivity) relation of the Boltzmann-Gibbs logarithmic entropy. Here, the word nonextensive should be associated with the fact that the total energy of long-range-interacting mechanical systems is nonextensive, in contrast with the case of short-range-interacting systems, whose total energy is extensive in the thermodynamical sense [22].

The second crucial assumption on nonextensive statistics is the introduction of the q-mean value (or escort mean value) of a physical observable $A(\mathbf{x})$ [118, 20, 21, 22]:

$$\langle A \rangle_q = \frac{\int A(\mathbf{x}) \, [f(\mathbf{x})]^q d\Omega}{\int [f(\mathbf{x})]^q d\Omega} \,. \qquad (2.20)$$

The probability distribution can be obtained maximizing the measure S_q under appropriate constraints related to the previous q-mean value definition. In this context, we want to remark that the Tsallis classical distribution can be seen as a superposition of Boltzmann distributions with different temperature which have a mean value corresponding to the temperature appearing in the Tsallis distribution. The nonextensive q parameter is related to the fluctuation in the temperature and describes the spread around the average value of the Boltzmann temperature [121]. Unfortunately, in many occasion, is not possible to calculate the value of the non extensive q parameter a priori, especially due to the unknown or extremely complex microscopic dynamics of the systems. In this cases, q can be obtained through the fitting of experimental data.

Following the above prescriptions, it is possible to obtain the associate quantum mean occupation number of particles species i in a grand canonical ensemble. For a dilute gas of particles and for small deviations from the standard statistics ($q \approx 1$), it can be written as [122, 123]

$$n_i = \frac{1}{\tilde{e}_q(\beta(E_i - \mu_i)) \pm 1} \,, \qquad (2.21)$$

where $\beta = 1/T$, the sign (± 1) stays for fermions and bosons respectively, and $\tilde{e}_q(x)$ is the q-exponential function given in the eq. (2.13). At this regards, let us remember that, with this prescription, when $q < 1$, the above distribution has a natural high-energy cutoff, which implies that the energy tail is depleted, therefore we have to require that the solution satisfy the condition of $[1 + (1-q)x] \geq 0$. Contrariwise, when q is greater than 1, the cutoff is absent and the energy tail of the particle distribution (for fermions and bosons) is enhanced.

For this reason, we found more suitable to adopt a different prescription, based on the so called mirror reflection and proposed by Wilk (for details see Ref [33] and reference therein).
In this context the high energy cutoff is absente and the solution are given respectively by:

for $q > 1$

$$\tilde{e}_q(x) = \begin{cases} [1 + (q-1)x]^{1/(q-1)} & \text{if } x > 0; \\ [1 + (1-q)x]^{1/(1-q)} & \text{if } x \leq 0, \end{cases} \qquad (2.22)$$

and, for $q < 1$,

$$\tilde{e}_q(x) = \begin{cases} [1 + (q-1)x]^{1/(q-1)} & \text{if } x \leq 0; \\ [1 + (1-q)x]^{1/(1-q)} & \text{if } x > 0 \end{cases} . \qquad (2.23)$$

where $x = \beta(E - \mu)$ and eq. (2.23), is obtained using the mirror reflection of equation (2.22). Naturally, for $q \to 1$ the above quantum distribution reduces to the standard Fermi-Dirac and Bose-Einstein distribution. Let us observe that, nonextensive statistical effects vanishes approaching to zero temperature. On the other hand, the nonextensive statistics entails a sensible difference on the power-law particle distribution shape in the high energy region with respect to the standard statistics. For this reason, nonextensive effects is expected to play an important role in the finite temperature and high baryon density PNS evolution, as well will show in Chapter 3. In our numerical investigation, we limit ourself to consider only small fluctuations from $q = 1$ and observe the variation in the thermodynamical quantities of the system.

2.3   Nonextesive equation of state

As partially discussed in the previous sections, in presence of high density and high temperature nuclear medium, nonextensive effects may play an important role in the physics of the relativistic heavy ion collision and may alter sensibly the thermodynamical quantities.
In this context, as said in in the Introduction and in Section. 2.1, the nonextensive statistical mechanics, proposed firstly by Tsallis, can be considered as an appropriate basis to deal with physical phenomena where strong dynamical correlations, long-range interactions and microscopic memory effects take place [20, 118, 21, 22, 25]. In particular, in the last years, there was a growing interest into high energy physics applications of nonextensive statistics and several authors have outlined the possibility that experimental observations in relativistic heavy ion collisions can reflect nonextensive statistical behaviors [23, 24, 25, 26, 27, 28, 28, 29, 30, 31, 32, 33, 35, 34, 36, 37].
Unfortunately, the extraction of experimental information about the EOS of matter at large densities and temperatures at intermediate and high energy heavy-ion collisions is very complicated and can be realized only indirectly by comparing the experimental data with different theoretical models, such as, for example, fluid-dynamical models [124]. Related to this aspect, it is relevant to observe that a relativistic kinetic nonextensive theory [125] and a nonextensive version of a hydrodynamic model for multiparticle production processes have been proposed [126]. Very recently, nonextensive statistical effects on the hadronic EOS have been investigated by means of a Walecka type relativistic mean field model [123]. Furthermore, a nonextensive version of Nambu-Jona-Lasinio model [33] and the effects on color superconducting phase for two quark flavors due to a change to Tsallis statistics have been studied [30].

In this section, we implement the nuclear equation of state, introduced in the Chapter 1, in the context of nonextensive statistical mechanics and we show the most important mathematical and physical consequences of this formalism.

2.3.1 Nonextesive hadronic equation of state

In the framework of nonextensive statistical mechanics, the hadronic Lagrangian density of eq. (1.27) is not changed, but, as reported in the section 2.2, the baryon density (ρ_i^B), the scalar density (ρ_i^S), the pressure (P_B) and the energy density (ε_B) are strongly modified.
In fact, by varying temperature and density, the EOS reflects in terms of the macroscopic thermodynamical variables the microscopic interactions of the different phases of nuclear matter.

Using the formalism introduced in the previous section, and in particular the eq.s (2.21)–(2.22) and (2.23), in the hypothesis of $q > 1$ and $\beta(E_i^*(k) - |\mu_i^*|) > 0$, the baryon and scalar density (eq.s (1.34) and (1.35)) assume the form:

$$\rho_i^B = \gamma_i \int \frac{\mathrm{d}^3 k}{(2\pi)^3} [n_i(k) - \overline{n}_i(k)] , \tag{2.24}$$

$$\rho_i^S = \gamma_i \int \frac{\mathrm{d}^3 k}{(2\pi)^3} \frac{M_i^*}{E_i^*} [n_i^q(k) + \overline{n}_i^q(k)] . \tag{2.25}$$

where q is the nonextensive parameter and $n_i(k)$ and $\overline{n}_i(k)$ are the q-deformed particles, anti-particles distribution function:

$$n_i(k) = \frac{1}{[1 + (q-1)\,\beta(E_i^*(k) - \mu_i^*)]^{1/(q-1)} + 1} , \tag{2.26}$$

$$\overline{n}_i(k) = \frac{1}{[1 + (q-1)\,\beta(E_i^*(k) + \mu_i^*)]^{1/(q-1)} + 1} . \tag{2.27}$$

In this context, the baryon effective mass $(M_i^* = M_i - g_{\sigma i}\sigma)$ is also modified by the presence of nonextensive effects, due to the variation in ρ_i^S, that acts on the scalar meson field σ.
The equation of motion of the meson fields (1.30)–(1.31) and (1.55), are in fact sensibly to the presence of nonextensive effect, due to their coupling with the baryon and scalar density. Therefore, even in presence of small deviation from the standard BG statistics, the baryons-fields interaction is sensibly altered and this reflects on the macroscopic proprieties of the system.

Following this formalism, the pressure P_B and the energy density ε_B given in eq. (1.39) and (1.40), become:

$$\begin{aligned} P_B &= \frac{1}{3}\sum_i \gamma_i \int \frac{\mathrm{d}^3 k}{(2\pi)^3} \frac{k^2}{E_i^\star(k)} [n_i^q(k) + \overline{n}_i^q(k)] - \frac{1}{2}\,m_\sigma^2\,\sigma^2 - U(\sigma) + \frac{1}{2}\,m_\omega^2\,\omega^2 \\ &+ \frac{1}{4}\,c\,(g_{\omega N}\,\omega)^4 + \frac{1}{2}\,m_\rho^2\,\rho^2 , \end{aligned} \tag{2.28}$$

$$\begin{aligned} \varepsilon_B &= \sum_i \gamma_i \int \frac{\mathrm{d}^3 k}{(2\pi)^3} E_i^\star(k) [n_i^q(k) + \overline{n}_i^q(k)] + \frac{1}{2}\,m_\sigma^2\,\sigma^2 + U(\sigma) + \frac{1}{2}\,m_\omega^2\,\omega^2 \\ &+ \frac{3}{4}\,c\,(g_{\omega N}\,\omega)^4 + \frac{1}{2}\,m_\rho^2\,\rho^2 . \end{aligned} \tag{2.29}$$
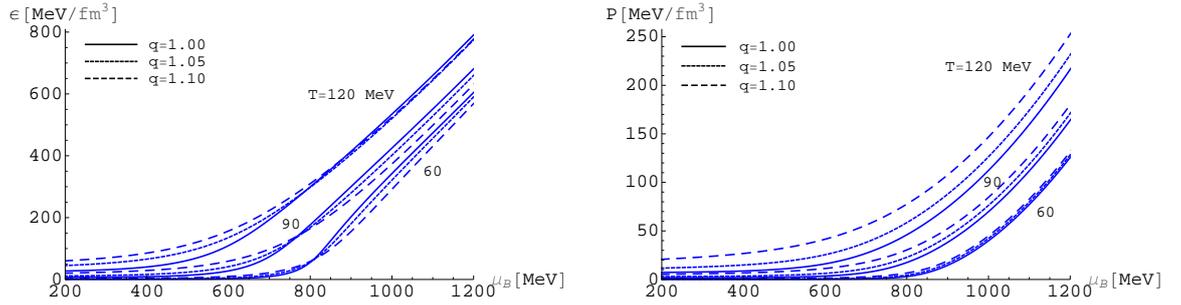
Figure 2.1: Energy density (left panel) and pressure (right panel) versus baryon chemical potential for different values of temperature and q.

Naturally, all the above equation must be solved in a self-consistent way. Hence, the presence of nonextensive statistical effects influences the many-body interaction mediated by the meson fields.

As an example, in Fig. 2.1, we report the hadronic pressure and energy density as a function of the baryon chemical potential μ_B at different values of the nonextensive parameter at $y = 0.4$. The different behavior of P and ε reflects essentially the nonlinear combinations of the meson fields and the different functions under integration in Eq.s (2.28) and (2.29). Concerning the pressure, we show that it becomes stiffer by increasing the non-extensive q parameter. On the other hand, the behavior of the energy density presents features very similar to the σ field one. At low μ_B, nonextensive effects make the energy density greater with respect to the standard case. At medium-high μ_B, the standard ($q = 1$) component of the energy density becomes dominant, this effect is essentially due to the reduction of the σ field for $q > 1$. The intersection point depends, naturally, on the physical parameters of the system.

Finally, let us note that, under the presence of nonextensive effects, the mesonic EOS changes in a phenomenological similar way to that of the baryons ones.

For example, in the effective relativistic mean-field formulation, the pressure (P_M), the energy density (ε_M) and the mesons density (ρ_j^M) of eq.s (1.53) and (1.54)–(1.55) , becomes

$$P_M = \frac{1}{3} \sum_j \gamma_j \int \frac{\mathrm{d}^3 k}{(2\pi)^3} \frac{k^2}{E_j^*(k)} g_j^q(k) \,, \tag{2.30}$$

$$\varepsilon_M = \sum_j \gamma_j \int \frac{\mathrm{d}^3 k}{(2\pi)^3} E_j^*(k) \, g_j^q(k) \,, \tag{2.31}$$

$$\rho_j^M = \gamma_j \int \frac{\mathrm{d}^3 k}{(2\pi)^3} g_j(k) \,, \tag{2.32}$$

where $g_j^q(k)$ is the q-deformed boson distribution function, given in eq. (2.21). Again, if we

choice a value of $q > 1$ and $x = \beta(E - \mu^*) > 0$ we obtain:

$$g_j(k) = \frac{1}{[1 + (q-1)\,\beta(E_j(k) - \mu_j^*)]^{1/(q-1)} + 1}\,. \qquad (2.33)$$

The corresponding anti-boson distribution function is naturally given by substituting $(\mu^* \to -\mu^*)$. Similar expressions for the Chiral model.

2.3.2   Nonextesive MIT-Bag model

As mentioned in the introduction, the process of deconfinement phase transition and the equation of state of quark-gluon matter can in principle be described by quantum chromodynamics. However, in energy density range reached in relativistic heavy-ion collisions, non-perturbative effects in the complex theory of QCD are not negligible [107]. For this reason, the generated QGP in the early stages of the collisions does not at all resemble a quasi-ideal gas of quarks and gluons because strongly dynamical correlations are present, including long-range interactions [1, 115, 18, 127, 19]. In the absence of a converging method to approach QCD at finite density, one often turns to (effective) model investigations [128, 129, 130, 131]. At this regards, a non extensive formulation of the quark-gluon plasma equation of state, seems to be an appropriate basis in order to deal such physical phenomenons otherwise difficult tractable using the standard BG formulation of statistical mechanics.

In the framework of nonextensive effects, in analogy to the results obtained for the nonextensive hadronic EOS, the MIT-Bag Lagrangian density does not change, but following the equations (2.21)–(2.22) and (2.23), the quark and anti-quark distribution function of eq.s (1.75)–(1.76), for $q > 1$ and $\beta(E_i^*(k) - |\mu_i^*|) > 0$, become:

$$n_f(k) = \frac{1}{[1 + (q-1)(E_f(k) - \mu_f)/T]^{1/(q-1)} + 1}\,, \qquad (2.34)$$

$$\overline{n}_f(k) = \frac{1}{[1 + (q-1)(E_f(k) + \mu_f)/T]^{1/(q-1)} + 1}\,, \qquad (2.35)$$

therefore, the pressure (P), the energy density (ε) and the baryon density (ρ), assume the form:

$$P = \frac{\gamma_f}{3} \sum_f \int_0^\infty \frac{\mathrm{d}^3 k}{(2\pi)^3} \frac{k^2}{e_f} \left[n_f^q(k) + \overline{n}_f^q(k)\right] - B_{\mathrm{eff}}\,, \qquad (2.36)$$

$$\varepsilon = \gamma_f \sum_f \int_0^\infty \frac{\mathrm{d}^3 k}{(2\pi)^3} \, e_f \left[n_f^q(k) + \overline{n}_f^q(k)\right] + B_{\mathrm{eff}}\,, \qquad (2.37)$$

$$\rho = \frac{\gamma_f}{3} \sum_f \int_0^\infty \frac{\mathrm{d}^3 k}{(2\pi)^3} \left[n_f(k) - \overline{n}_f(k)\right]\,, \qquad (2.38)$$

where, again, the sum runs over the doublet $(f = u, d)$ or the triplet of quarks $(f = u, d, s)$, $\gamma_f = 6$ is the quark degeneracy spin factor and B_{eff} is the bag factor given in eq. (1.73). Note that the effective Bag parametrization used here, is also sensibly to the presence of
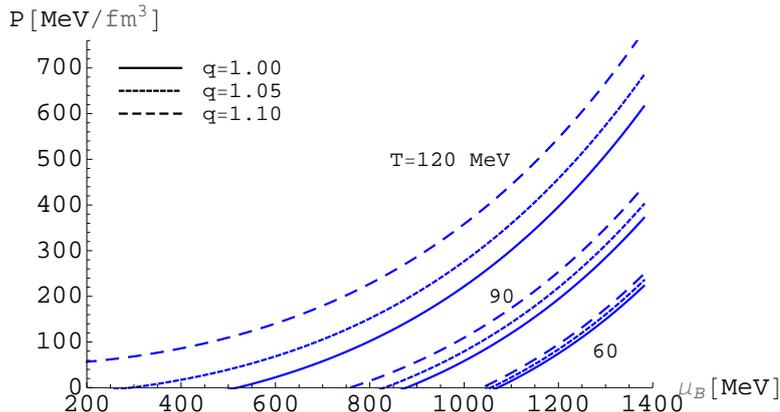
Figure 2.2: Pressure of the quark gluon phase as a function of baryon chemical potential for different values of temperature and q.

nonextensive effects depending on the baryon chemical potential μ_B. This dependence does not take place if we use a constant value of the vacuum pressure B.

Similar expression can be written for gluons. Explicitly the nonextensive pressure P_g and energy density ε_g for the q-deformed Bose gas gives:

$$P_g \;\; = \frac{\gamma_g}{3} \int_0^\infty \frac{\mathrm{d}^3 k}{(2\pi)^3} \, \frac{k}{[1 + (q-1)\,k/T]^{q/(q-1)} - 1} \,, \tag{2.39}$$

$$\varepsilon_g \;\; = 3\,P_g \,, \tag{2.40}$$

with the gluon degeneracy factor $\gamma_g = 16$.

In Fig. 2.2, we report an example of the relevance of the non extensive effects on the QGP equation of state. As in the case of hadronic phase, the pressure is significantly increased even for small deviations from standard statistics. Here we show the total pressure as a function of the baryon chemical potential for massless quarks and gluons, for different values of q and at fixed value of $y = 0.4$. The bag constant is set equal to $B^{1/4}=190$ MeV. Let us note that, since one has to employ the fermion (boson) nonextensive distributions, the results are not analytical, even in the massless quark approximation. Hence a numerical evaluations of the integrals in Eq.s (2.36)–(2.38) and (2.39) must be performed.

2.4   Major conclusions

In this Chapter we have presented the most important features of the so called nonextensive statistical mechanics and we have shown the relevance of implement the nuclear EOS in the framework of nonextensive statistical mechanics, in particular in systems where strong dynamical correlations, long-range interactions and microscopic memory effects may take place [20, 21, 22, 25].
In this context, in Fig.s 2.1 and 2.2, we have reported same preliminary examples, of how

the presence of non extensive effects, may alter the hadronic and QGP equation of state, even in presence of small deviation of standard BG statistics.

This formalism will be amply used in Chapters 3 and 4, where we will analyze, respectively, the mechanical and thermodynamical proprieties of protoneutron stars and the deconfinement phase transition from hadron matter to quark-gluon plasma, at finite temperature and baryon density, comparing the results obtained through the standard BG statistics with that of the nonextensive case.

Chapter 3

Nonextensive statistical effects in protoneutron stars.

In this Chapter, we want to present a study of the bulk proprieties of protoneutron stars in the framework of nonextensive statistics. In this context an accurate analysis of the beta-stable EOS in presence and in absence of trapped neutrino, both for nucleonic and hyperonic protoneutron stars, will be made.

3.1 Introduction

As known from the literature, a protoneutron star (PNS) is born immediately after the gravitational collapse of a massive star ($M \approx 10 \div 20\ M_\odot$). During the first seconds of its evolution a PNS is a very hot, lepton rich and beta-stable object, with a temperature of a few tens of MeV and a lepton concentration typical of the pre-supernova matter [132]. Nearly all of its binding energy is in the form of neutrinos trapped inside the stellar structure. In particular, neutrinos at the star core are basically of the ν_e type and have a typically energy of about $E_\nu \approx 200 \div 300$ MeV [133]. Shortly after the PNS formation, during the cooling, neutrinos escape through the star structure and bring out in few seconds nearly all of its binding energy. The total luminosity of this process depends from several factors, the most important are the total mass of the compact object and the neutrino opacity. During this process, called Kelvin-Helmholtz epoch, the PNS evolves in a quasi hydrostatic equilibrium, from a lepton rich and hot object to a cold neutrino-free compact star [134]. From a measure of neutrinos luminosity and average energy, which are the most important astrophysical observable in the study of the stellar structure, it is in principle possible to deduce the total binding energy and, therefore, the total baryonic mass of the star [135]. However, neutrinos are not only important probes in the study of newborn PNS, but have also relevant consequences on the chemical composition and in the maximum mass of the compact object. The presence of neutrinos in fact alters significantly the chemical composition of the star, varying the formation threshold of different particle species (in general the appearance of non-leptonic negative particles is delayed when neutrinos are present). The changes in the maximum mass, due to neutrinos trapping, are normally greater than those due to finite

temperature effects [133, 134, 135, 136].

From a more theoretical point of view, it appears evident that the knowledge of the nuclear EOS plays a crucial role in the determination of the structure and in the evolution of the PNS [137, 138, 108, 139]. The processes related to strong interaction should in principle be described by quantum chromodynamics. However, in the energy density range reached in the compact stars, strongly non-perturbative effects in the complex theory of QCD are not negligible. The central core of a compact star does not at all resemble a quasi-ideal gas of hadrons because strongly dynamical correlations are present, including long-range interactions [140, 141, 142]. In the absence of a converging method to approach QCD at finite density one often turns to (effective and phenomenological) model investigations.

In this sense, as exposed in Chapter 2, nonextensive statistical mechanics seems to be the natural candidate in order to deal such physical phenomenons. In fact, as remarked in Chapter 4, the existence of nonextensive effects, strongly affects the finite temperature and density nuclear EOS. In this direction, especially in the last years, several authors have outlined the relevance of nonextensive statistical mechanics effects in high energy physics and astrophysical problems [143, 144, 145, 146, 23, 121, 26, 147, 148, 149, 24, 127, 111, 125, 150, 151, 28, 152, 153, 154, 155, 156].

From a phenomenological point of view, this Chapter is based on the investigate of the relevance of nonextensive statistical effects on the main physical properties of PNS and their related astrophysical implications. At this scope, we are going to explore different stages of the PNS evolution, where nonextensive effects are expected to play an important role. The first stage corresponds to an entropy per baryon equal to one, in which neutrinos are trapped and strongly influence the chemical composition of the PNS. After a short time, of about $10 \div 15$ s, the temperature of the PNS fast rises up until it reaches a value of $T \simeq 45 \div 80$ MeV, it depends again on the chemical composition [157]. This stage is called deleptonization era and corresponds to the maximum heating and entropy per baryon ($s = 2$). This is the phase, at high temperature and high baryon density, in which the presence of nonextensive effects may alter more sensibly the thermodynamical and mechanical proprieties of the PNS. In this numerical investigation will be take in consideration only an hadronic composition of the PNS, without considering the possible formation of a mixed hadron-quark phase region or a quark core inside it. This choice is principally due to the fact that the presence of trapped neutrinos delays the on-set of strange particles and also possible formation of quark matter [133, 134]. As a consequence, the appearance of a mixed phase or a quark core could be shifted at the end, or nearly at the end of the deleptonization era [158].

This chapter is based on the results obtained in [35].

3.2   Nonextensive hadronic equation of state and beta-stability condition

The equation of state and the structure of the PNS is analyzed through the relativistic mean field theory, in the framework of nonextensive statistical mechanics. In this context we adopt the Wilk prescription, exposed in section 2.2 and the analysis is performed both for a super-extensive ($q > 1$) eq.(2.22) and for a sub-extensive ($q < 1$) eq. (2.23) case.

As reported in section 2.2, the use of the Wilk prescription, avoid the high energy cutoff present in the Tsallis distribution, when $q < 1$.

In this context, before starting to analyze the PNS structure, it is important establish the chemical composition of the compact object. This is possible knowing that, the concentrations of the different constituents in the stellar interior are determined by the requirements of electric charge neutrality and equilibrium under weak interaction processes (chemical equilibrium), strange number is not conserved:

$$B_1 \to B_2 + l + \bar{\nu}_l, \quad B_2 + l \to B_1 + \nu_l, \tag{3.1}$$

where B_1 and B_2 are baryons, l are leptons and ν_l ($\bar{\nu}_l$) are the associate neutrinos (anti-neutrinos).

At this point it is important to underline that, because in the first stages of PNS evolution neutrinos are trapped inside the stellar structure, the lepton number per baryon Y_L of each lepton flavor must be conserved on dynamical scales [133, 135, 136]. Therefore, in this analysis, the conservation of the lepton number is obtained by imposing the following condition:

$$Y_L = Y_l + Y_{\nu_l} = (\rho_l + \rho_{\nu_l})/\rho_B, \tag{3.2}$$

where ρ_l, ρ_{ν_l} and ρ_B are the lepton, neutrino and baryon number densities, respectively (electrons and muons flavors).

At this regard, recent gravitational collapse calculations of the core of massive stars, indicate that, at the onset of trapping, the electron lepton fraction is close to $Y_{L_e} = Y_e + Y_{\nu_e} = 0.4$. In addition, as the trapping in supernova occurs when the collapsing core reaches densities where no muons exist, we can impose $Y_{L_\mu} = Y_\mu + Y_{\nu_\mu} = 0$. For this reason, because we are particularly interested in the first stages of PNS evolution, when the stellar temperature is particularly high and nonextensive effects are expected to alter more sensibly the thermodynamical and mechanical proprieties of the PNS, we can neglet in this numerical calculation the contribution of muons. Therefore, the leptonic component of the PNS, reduces to electrons and electronic neutrinos (anti-neutrinos) only.

For matter where nucleons and hyperons are the relevant hadronic degrees of freedom, the chemical equilibrium conditions can be explicitly written as

$$\mu_\Lambda = \mu_{\Sigma^0} = \mu_{\Xi^0} = \mu_n, \tag{3.3}$$

$$\mu_{\Sigma^-} = \mu_{\Xi^-} = \mu_n + \mu_e, \tag{3.4}$$

$$\mu_p = \mu_{\Sigma^+} = \mu_n - \mu_e; \tag{3.5}$$

$$\rho_p + \rho_{\Sigma^+} - \rho_{\Sigma^-} - \rho_{\Xi^-} - \rho_e = 0, \tag{3.6}$$

where the lepton chemical potential is determined as usual by eq. (1.44). This guaranties the β-stability condition.

Furthermore, in case of trapped neutrinos, the new equalities are obtained by the replacement of $\mu_e \to \mu_e - \mu_{\nu_e}$. The total entropy per baryon is calculated using $s = (S_B + S_l)/(T\rho_B)$, where $S_B = P_B + \varepsilon_B - \sum_{i=B} \mu_i \rho_i$ and $S_l = P_l + \varepsilon_l - \sum_{i=l} \mu_i \rho_i$, and the sums are extended over all the baryons and leptons species.

The total Lagrangian can therefore be written as:

$$
\begin{aligned}
\mathcal{L}_{tot} &= \mathcal{L}_B + \mathcal{L}_l \\
&= \sum_B \bar{\psi}_B [i\gamma_\mu \partial^\mu - (M_B - g_{\sigma B}\sigma) - g_{\omega B}\gamma_\mu \omega^\mu - g_{\rho B}\gamma^\mu \vec{\tau} \cdot \vec{\rho}_\mu] \psi_B \\
&+ \frac{1}{2}(\partial_\mu \sigma \partial^\mu \sigma - m_\sigma^2 \sigma^2) - U(\sigma) + \frac{1}{2}m_\omega^2 \omega_\mu \omega^\mu + \frac{1}{2}m_\rho^2 \vec{\rho}_\mu \cdot \vec{\rho}^{\,\mu} \\
&- \frac{1}{4}F_{\mu\nu}F^{\mu\nu} - \frac{1}{4}\vec{G}_{\mu\nu}\vec{G}^{\mu\nu} + \sum_l \bar{\psi}_l [i\gamma_\mu \partial^\mu - m_l] \psi_l \,,
\end{aligned}
\tag{3.7}
$$

where $\mathcal{L}_B$ stands for the full octet of baryons (p, n, Λ, Σ^+, Σ^0, Σ^-, Ξ^-, Ξ^0) eq. 1.27 and $\mathcal{L}_l$ corresponds to the leptons degrees of freedom (e^-, ν_e and $\bar{\nu}_e$).

The β-stable EOS and the scalar and vector baryon density are given as usual by the set of eq.s (2.24), (2.25) and (2.29)–(2.28).

Finally the leptonic contribution to the stellar EOS are calculated using the expressions for non-interacting relativistic fermions, which are well known from the literatures.

Once the composition of β-stable matter is determined, we can compute the total energy density and the total pressure as follow: $\varepsilon = \varepsilon_B + \varepsilon_l$ and $P = P_B + P_l$.

Here and in the following, we focus our investigation on considering the so-called GM3 parameter set of Tab. 1.2 (even if comparable results can be obtained in other parameter sets). The implementation of hyperon degrees of freedom comes from determination of the corresponding meson-hyperon coupling constants that have been fitted to hypernuclear properties and their specific values for the GM3 parameter set, as explained in section 1.3.

3.3   Protoneutron star structure

The stable configuration of a relativistic and non-rotating protoneutron star can be obtained from the well-known hydrostatic equilibrium equations of Tolman, Oppenheimer, and Volkov (Shapiro and Teukolsky 1983) for the pressure P and the enclosed mass m, it takes the form:

$$
\frac{dP(r)}{dr} = -\frac{Gm(r)\varepsilon(r)}{r^2}\frac{[1 + \frac{P(r)}{\varepsilon(r)}][1 + \frac{4\pi r^3 P(r)}{m(r)}]}{1 - \frac{2Gm(r)}{r}} \,,
\tag{3.8}
$$

$$
\frac{dm(r)}{dr} = 4\pi r^2 \varepsilon(r) \,,
\tag{3.9}
$$

once the EOS $P(\varepsilon)$ is specified, being ε the total energy density (G is the gravitational constant). For a chosen central value of the energy density, the numerical integration of eq.s (3.8) and (3.9) provides the mass-radius relation.

Furthermore, in this analyze, the protoneutron star crust is not taken in consideration, due to its negligible influence on the main mechanical and thermodynamical properties of the compact object.

An important annotation regards the concept of stellar mass. In fact, the mass of the totality of the particles in a star is called baryon mass (M_B). Anyway, we generally call stellar mass, what is in reality the gravitational mass of the star M_G, hereafter M. The

difference between the gravitational mass and the baryon mass is in general negative and it is called binding energy of the star ($B.E.$). Normally, the gravitational binding is of the order of 100 MeV per nucleon in star near the mass limit, about 10 times bigger then the corresponding binding energy by strong force in nuclei.

3.4   Thermodynamical and mechanical proprieties of PNS

As briefly mentioned in the section 3.1, this analysis focus on the relevance of possible nonextensive statistical effects during the first PNS evolution phases. We can ideally divide the evolution into three phases. The first, at the beginning, in which neutrinos are trapped and the entropy per baryon is assumed fixed to $s = 1$ and $Y_L = 0.4$. A second phase, after about $10 \div 15$ sec, which corresponds to the maximum heating of the star and neutrinos are free ($s = 2, Y_{\nu_e} = 0$). Finally, a third phase of cold-catalyzed PNS ($s = 0, Y_{\nu_e} = 0$) [157, 159, 160], where T$\to$ 0 MeV. Regarding the relevance of nonextensive statistical effects, the most important phase corresponds to the maximum heating, in which the presence of nonextensive statistical effects may play a crucial role in the determination of the PNS chemical composition and related thermodynamical proprieties. In this work we limit ourselves to consider only a small variations from the standard statistics (from $q = 0.97$ to $q = 1.03$).

3.4.1   PNS EOS and thermodynamical proprieties

In Fig. 3.1, we show the temperature as a function of the baryon density (in units of the saturation nuclear density $\rho_0 = 0.153$ fm^{-3}) and for different values of the nonextensive parameter, in absence (np) and in presence (npH) of hyperons. We limit our analysis in the first two phases: in the left panel, the first leptonic rich state ($s = 1, Y_L = 0.4$) and, in the right panel, the maximum heating phase ($s = 2, Y_{\nu_e} = 0$). Indeed in the cold-catalyzed phase ($s = 0, Y_{\nu_e} = 0$), the temperature is very low (fews MeV), and nonextensive statistical effects may be neglected. In both previous cases, we observe a reduction in temperature in presence of a sub-extensive statistics ($q < 1$) and a general increase for $q > 1$. This effect is more remarkable when hyperons are present and for higher values of entropy for baryon. For example, in the maximum heating phase, in presence of hyperons and for $q = 1$, the temperature is about $T \cong 37$ MeV at baryon density $\rho_B = 5\rho_0$, whereas, for $q = 1.03$ and $q = 0.97$, it is approximately equal to $T \cong 51$ MeV and $T \cong 21$ MeV, respectively. Note also that, when hyperons are present, for $s = 1$ and $Y_L = 0.4$, the system evolves in a quasi isothermal configuration above $\rho_B = 2.5 \div 3\,\rho_0$. The different behavior in the stellar temperature have important consequences in the PNS evolution and in its particles concentration. Finite temperature properties of matter at high density influence the diffusion of neutrinos, being the neutrino mean free paths strongly temperature dependent [135, 159]. In particular, neutrino opacity is very sensitive to the inner temperature (in general proportional to T^2) and, therefore, this would affect sensibly the cooling of the PNS, making it longer when $q > 1$, and shorter when $q < 1$. This matter of fact could have important consequences on the neutrino luminosity, because its drop is associated with the end of this cooling process [134]. Consequently, an alteration in the Kelvin-Helmholtz
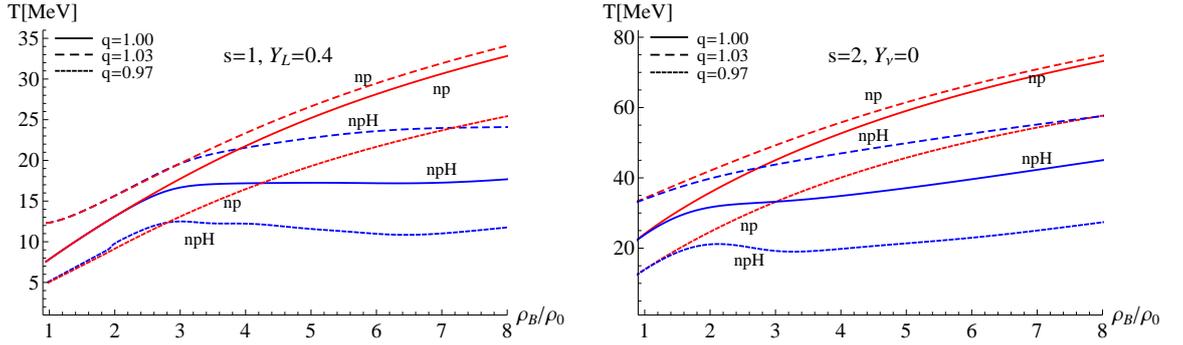
Figure 3.1: Temperature as a function of the baryon density (in units of the saturation nuclear density ρ_0) for different values of q, entropy per baryon and neutrino fraction (left panel: $s = 1, Y_L = 0.4$ and right panel: $s = 2, Y_{\nu_e} = 0$). The labels np and npH stand for nucleons and nucleons plus hyperons.

epoch, that does not correspond to the predict direct or modified URCA process, could be an indication of nonextensive statistical effects.

In Fig. 3.2, is reported the dependence of the pressure from the baryon density, for different values of q, in the initial phase: $s = 1, Y_L = 0.4$ (left panel) and in the maximum heating phase: $s = 2$ and $Y_{\nu_e} = 0$ (right panel). With the appearance of hyperons, around $\rho_B = 3\,\rho_0$, we have a general softening of the EOS. However, due to the low temperature achieved in this phase (see Fig. 3.1), nonextensive statistical effects do not change significantly the total pressure of the PNS. The situation is somewhat different when we analyze the maximum heating phase. In such a condition, the temperature is higher and nonextensive statistical effects are more relevant, especially when hyperons are present.

As it is well known, the softening of the EOS, due to the appearance of additional fermionic degrees of freedom in the form of hyperons, leads to higher central densities. This matter of fact is, however, influenced from the presence of nonextensive statistical effects. To better focalized this aspect, in Fig. 3.3, is plotted the central baryon density ρ_c in the PNS core corresponding to a total baryon mass M_B (in units of the solar mass $M_\odot$). The case $q > 1$ ($q < 1$) implies a general reduction (increase) of the central density at fixed total baryon mass. This effect is emphasized in the maximum heating condition (right panel). In particular, for $q > 1$ and until $M_B \approx 1.7\,M_\odot$, the central densities of hyperons stars (npH) are lower than the ones corresponding to the standard ($q = 1$) nucleons-only stars (np). This feature, together the variation of the temperature, can be very relevant in the determination of the specific heat of the stellar matter and, as a consequence, on the neutrino diffusion [135].

3.4.2 PNS chemical composition

In addition to the considerations of section 3.4.1, we want now study the chemical composition of the PNS. Firs off all, we investigate the lepton chemical potentials in different PNS
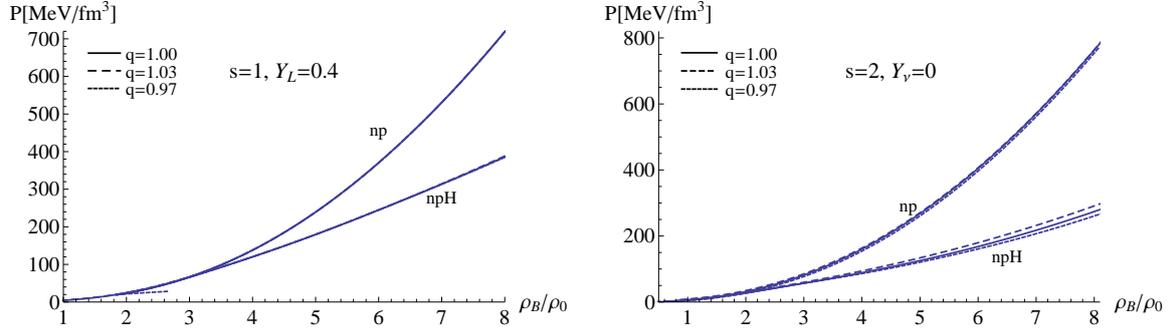
Figure 3.2: Total pressure as a function of baryon density (in units of the saturation nuclear density) for different values of q in the lepton rich case: $s = 1$ and $Y_L = 0.4$ (left panel) and in the maximum heating phase: $s = 2$ and $Y_{\nu_e} = 0$ (right panel). The labels np and npH stand for nucleons and nucleons plus hyperons matter, respectively.
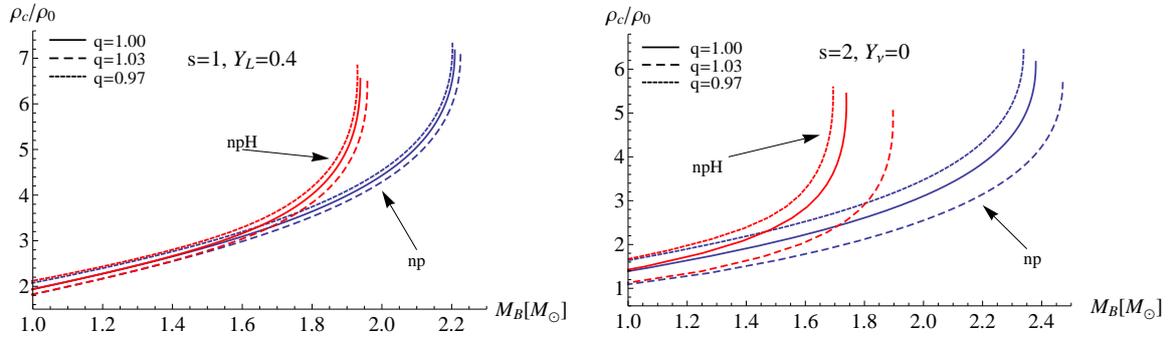
Figure 3.3: Central baryon density ρ_c (in units of the saturation nuclear density) corresponding to a total stellar baryon mass M_B in the lepton rich phase (left panel) and in the maximum heating phase (right panel). The labels np and npH stand for nucleons and nucleons plus hyperons matter, respectively.
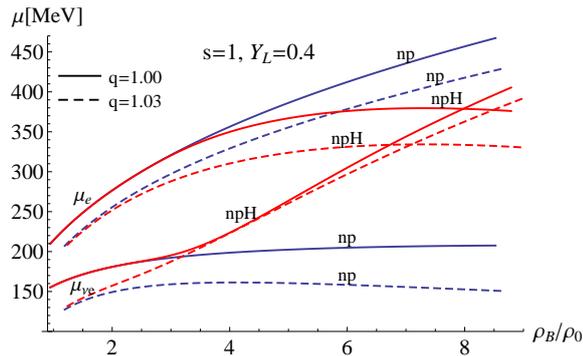
Figure 3.4: Lepton chemical potentials in lepton rich matter as a function of the baryon density (in units of the nuclear saturation density). The labels np and npH stand for nucleons and nucleons plus hyperons matter, respectively.

conditions, because they strongly influence the deleptonization process [135, 136]. At this scope, in Fig. 3.4, we show the lepton chemical potentials in lepton rich matter ($s = 1$ and $Y_L = 0.4$) in absence (np) and in presence (npH) of hyperon degrees of freedom (higher curves for the electron chemical potential μ_e and lower curves for the neutrino chemical potential μ_{ν_e}). For clarify, we report only the case $q > 1$ compared to the standard ($q = 1$) results. It is interesting to observe that for a nucleons-only EOS, super-extensive statistical effects imply a general reduction of the electron and neutrino chemical potentials respect to the standard case. Otherwise, in presence of hyperons, a sensible reduction of the electron chemical potential is not accompanied by a reduction of the neutrino chemical potential which retains very similar values to the standard case at high baryon density. Such a feature could have important consequence on the diffusion of the electron neutrinos inside the PNS.

Moreover, the neutrino mean free paths and the matter specific heat depend sensitively on the composition; under degenerate conditions even modest changes to the composition significantly alter the neutrino scattering and absorbtion mean free paths. It is, therefore, relevant to investigate how nonextensive statistical mechanics influences particle compositions in different PNS epochs. In Fig. 3.5, we report the particle concentrations for $s = 1$ and $Y_L = 0.4$ in absence (left panel) and in presence (right panel) of hyperons for different values of q. It is well known that the presence of trapped neutrinos significantly alter the protons and the electrons abundance and strongly influence the threshold of hyperons formation [133, 135, 136]. In absence of hyperons, nonextensive statistical effects do not play a significantly role, in fact the particle concentrations are almost the same. The situation changes when we include hyperon degrees of freedom. The presence of sub-extensive effects ($q < 1$) slightly lowers the neutrinos concentration, while increases the neutrons and the electrons ones. Moreover, hyperons start later and their concentration are in general decreased, excepted for the Λ particles ratio, which becomes greater after $\rho_B > 4\,\rho_0$ respect to the standard case. Otherwise, in case of super-extensive statistical effects ($q > 1$), we can observe a general reduction in the neutrons and the electrons fractions and a small increase
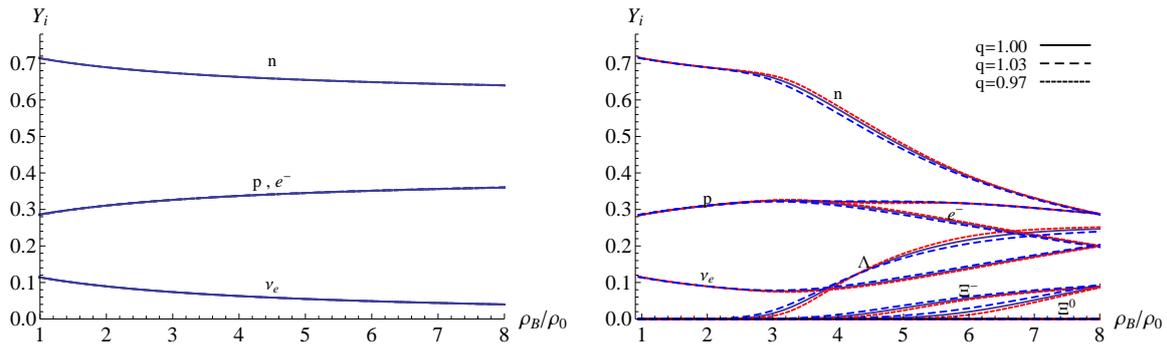
Figure 3.5: Particle concentrations Y_i without (left panel) and with hyperons (right panel) as a function of the baryon density for $s = 1$ and $Y_L = 0.4$.

of the neutrinos and the hyperons concentrations, with important effects on the softening of the EOS.

In the Fig. 3.6, particle concentrations for the maximum heating phase ($s = 2$, $Y_{\nu_e} = 0$) are reported. In this condition, due to the higher temperature achieved in the stellar matter, nonextensive statistical effects become more relevant and, consequently, particle concentrations change significantly. When $q < 1$, we observe a reduction in the protons and the electrons concentrations and an increase of the neutrons fraction. Whereas, in the super-extensive case ($q > 1$), we have a lower neutrons fraction and an increase of the protons and electrons concentrations. When hyperons are included, Fig. 3.6, right panel, we have two main consequences. Firstly, with the absence of neutrinos, the hyperons on-set is shifted at low baryon densities, below $2\rho_0$. Secondly, as a consequence, the electrons and the protons concentrations decrease sensibly with respect to the initial lepton-rich regime ($s = 1, Y_L = 0.4$). Therefore, the absence of neutrinos in the stellar matter implies a strong softening of the EOS. In presence of sub-extensive statistics ($q < 1$), hyperons start later with respect to the standard case ($q = 1$), and have in general a bigger concentration at high baryon density. The other way round takes place for super-extensive statistics ($q > 1$).

Finally, to better understand the role of nonextensive statistical effects on hyperons formation in the PNS core, in Fig. 3.7, we report the total hyperons concentration (strangeness per baryon) as a function of the stellar baryon mass (in units of $M_\odot$) in the lepton rich (left panel) and in the maximum heating (right panel) epoch. Although, for $q > 1$, hyperons are present at lower baryon densities with respect to the standard case ($q = 1$) and a greater hyperons concentration at lower baryon masses is present, we have a significant reduction at higher baryon masses, especially in case of the maximum heating condition. For $q < 1$, we have instead the opposite effect: a reduction of the hyperons fraction at low baryon masses and an enhancement at high baryon masses. These features, principally due to the behavior of Λ particles concentration as a function of the baryon density (see Fig.s 3.5 and 3.6), could imply relevant phenomenological consequences on the evolution of the PNS. In fact, it is known that hyperons significantly increase the neutrino scattering and absorption cross
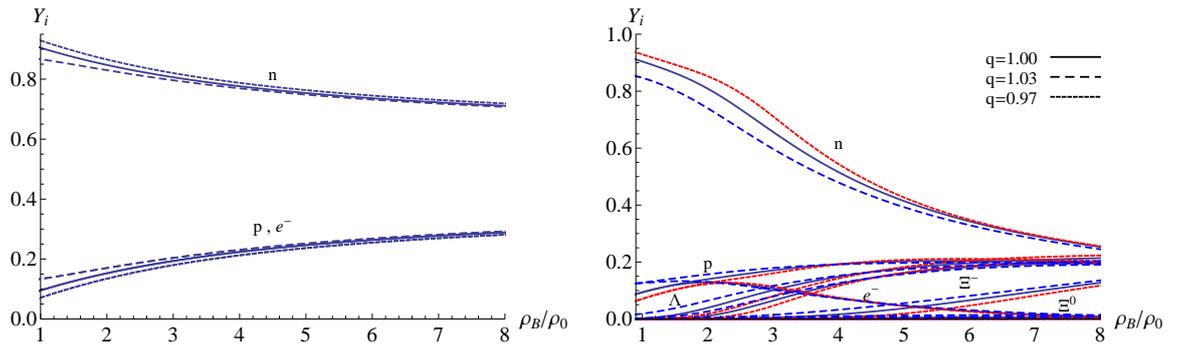
Figure 3.6: The same of Fig. 3.5 for the maximum heating phase ($s = 2$ and $Y_{\nu_e} = 0$).
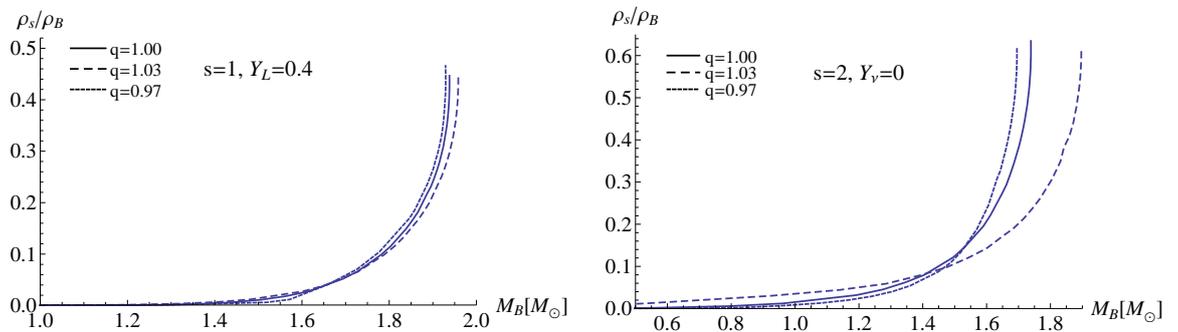
Figure 3.7: Hyperons concentration ρ_s/ρ_B (strangeness per baryon) as a function of the baryon mass M_B in the lepton rich (left panel) and in the maximum heating phase (right panel).

sections [135]. Furthermore, the central densities of hyperons stars become progressively larger than that of purely nucleon stars and the evolution timescale of hyperons stars results to be slightly larger because of the smaller mean free path of hyperonic matter. Larger central densities and higher electron neutrino energies, reached in hyperonic PNS, increase the neutrino opacity, temporarily reducing the loss of neutrinos from the stellar core and allow to sustain a higher luminosity at late times.

3.4.3   M-R relation and PNS structure

Let us now discuss the most important changes in the mechanical proprieties of the PNS in presence of nonextensive effects, during the first phases of its evolution.

At this regards, in the Table 3.1, we report the maximum gravitational (baryonic) masses (in units of $M_\odot$) and the corresponding values of radius and central baryon density, for different
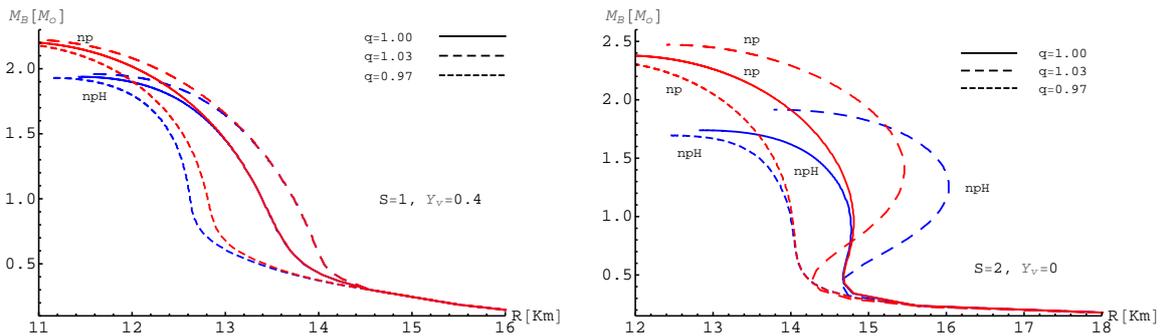
Figure 3.8: Stellar baryon mass M_B (in units of solar mass $M_\odot$) as a function of the central baryon density (in units of ρ_0), for different values of q, for nucleons and hyperons stars. In the left and right panel, we report respectively the lepton rich and the maximum heating phase.

PNS configurations. We have taken in consideration different values of the nonextensive q-parameter, entropy per baryon and leptons concentration, in absence (np) and in presence (npH) of hyperons.

As we have already remarked, nonextensive statistical effects result to be most relevant when hyperons are present and the maximum heating phase is achieved ($s = 2$, $Y_{\nu_e} = 0$). In fact, when the entropy per baryon is equal to one and the matter is lepton rich, the difference in the maximum mass is very small both with and without hyperons. Moreover, immediately after the deleptonization, nonextensive statistical effects become more important, especially in presence of hyperons. The maximum mass is in general decreased when we consider a sub-extensive statistics ($q < 1$), and increased when $q > 1$.

This behavior, appear much more evident in Fig. 3.8, where we have analyzed the mass-radius relation, for different values of nonextensive parameter and different chemical composition of PNS. Here, we can observe the role played by the nonextensive effects on the stellar structure. In particular, in presence of sub-extensive statistics, we observe a remarkable reduction of the stellar radius and consequently, an increase of the central baryon density, as already reported in Fig. 3.3 and in Tab. 3.1. Contrariwise, in presence of super-extensive effects, we observe a general softening of the EOS and a consequently increase of the PNS radius.

Furthermore, in the presence of hyperons, when the stellar core contains non-leptonic negative charges, the maximum masses of neutrino-trapped stars result to be significantly larger than for low temperatures and for lepton poor matter. Hence, there exists a window of initial masses for which the star becomes unstable to gravitational collapse during deleptonization and a black hole can take place [133, 135, 136]. We can see that the formation of such a metastable phase strongly depends on the presence of nonextensive statistical effects and the window of metastability grows with the value of the nonextensive index q. In particular, for $q > 1$, we still have a very large value of the maximum baryonic mass in

Table 3.1: Maximum gravitational (baryonic) masses $M_{\max}$ (in units of $M_\odot$) and corresponding values of radius R and central baryon density ρ_c in absence (np) and in presence (npH) of hyperons for different values of the nonextensive parameter q. The results are reported for different values of entropy per baryon and leptons concentration. For completeness, the values for the cold-catalyzed phase ($s = 0, Y_{\nu_e} = 0$) for $q = 1$ are also reported (nonextensive statistical mechanics does not play any role in this last regime).

	np		npH	
q	$s = 1, Y_L = 0.4$	$s = 2, Y_{\nu_e} = 0$	$s = 1, Y_L = 0.4$	$s = 2, Y_{\nu_e} = 0$
0.97	$M_{\max} = 1.96\,(2.20)$ R=10.52 km $\rho_c = 7.33\,\rho_0$	$M_{\max} = 2.06\,(2.34)$ R=11.37 km $\rho_c = 6.50\,\rho_0$	$M_{\max} = 1.75\,(1.93)$ R=11.11 km $\rho_c = 6.84\,\rho_0$	$M_{\max} = 1.55\,(1.69)$ R=12.39 km $\rho_c = 5.59\,\rho_0$
1.00	$M_{\max} = 1.97\,(2.21)$ R=10.69 km $\rho_c = 7.23\,\rho_0$	$M_{\max} = 2.09\,(2.38)$ R=11.80 km $\rho_c = 6.17\,\rho_0$	$M_{\max} = 1.76\,(1.94)$ R=11.41 km $\rho_c = 6.62\,\rho_0$	$M_{\max} = 1.59\,(1.74)$ R=12.75 km $\rho_c = 5.44\,\rho_0$
1.03	$M_{\max} = 1.98\,(2.23)$ R=10.81 km $\rho_c = 7.15\,\rho_0$	$M_{\max} = 2.15\,(2.47)$ R=12.39 km $\rho_c = 5.75\,\rho_0$	$M_{\max} = 1.78\,(1.96)$ R=11.56 km $\rho_c = 6.51\,\rho_0$	$M_{\max} = 1.71\,(1.90)$ R=13.34 km $\rho_c = 5.05\,\rho_0$
	$s = 0, Y_{\nu_e} = 0$		$s = 0, Y_{\nu_e} = 0$	
1.00	$M_{\max} = 2.05\,(2.39)$ R=11.11 km $\rho_c = 6.91\,\rho_0$		$M_{\max} = 1.57\,(1.76)$ R=12.35 km $\rho_c = 5.66\,\rho_0$	

the maximum heating phase ($s = 2$, $Y_{\nu_e} = 0$), significantly larger than the one in the cold catalyzed condition (where nonextensive statistical effects do not play any role). Therefore, for nucleons-only stars, a black hole could form only after the core bounce, because the maximum mass supported by neutrino-free stars is bigger than that supported for neutrino-rich case. Whereas, in presence of hyperons, a black hole can take place also after the deleptonization era because of the realization of a metastable phase, which becomes more relevant in presence of super-extensive statistical effects.

3.5 Major conclusions

In this Chapter we have investigated the physical properties of the PNS in the framework of a relativistic mean field theory based on nonextensive statistical mechanics, characterized by power-law quantum distributions. In this context we have studied the finite temperature EOS in β-stable matter in absence and in presence of hyperons and trapped neutrinos. From a phenomenological point of view, we have considered the nonextensive index q as a free parameter, even if, in principle, it should depend on the physical conditions inside the PNS, on the fluctuation of the temperature and be related to microscopic quantities (such as, for example, the mean interparticle interaction length). In this context, let us remember that, in the diffusional approximation, a value $q \neq 1$ implies the presence of an anomalous diffusion among the constituent particles (the mean square displacement obeys to a power-law behavior $< x^2 > \propto t^\alpha$ with $\alpha \neq 1$).

We have shown that nonextensive statistical effects could play a crucial role in the structure and in the evolution of the PNS also for small deviations from the standard Boltzmann-Gibbs statistics. As expected, nonextensive statistical effects result to be particularly important during the maximum heating phase ($s = 2, Y_{\nu_e} = 0$), while become less relevant during the initial lepton rich state ($s = 1, Y_L = 0.4$) and negligible in the cold catalyzed phase ($s = 0, Y_{\nu_e} = 0$), due to the low temperatures achieved.

We have studied the relevance of nonextensive statistical effects: i) in the temperature behavior as a function of the baryon density, ii) in the softening of the EOS and, consequently, in the central baryon densities reached in the PNS core at fixed baryon mass, iii) in the lepton chemical potentials, iv) in the particle concentrations, in the hyperons formation and in the strangeness per baryon at fixed total baryon mass, v) in the maximum gravitational and baryonic masses. Such a variation of physical quantities, respect to the standard case, can imply important consequences on the determination of the matter specific heat, on the neutrino mean free path inside the stellar core and, consequently, in the neutrino opacity and luminosity.

We have considered both cases of sub-extensive ($q < 1$) and super-extensive ($q > 1$) statistical effects which entail a sensible difference on the power-law particle distribution in the high energy region. When the entropic q parameter is smaller than one, the energy tail of the particle distribution is depleted, otherwise, when q is greater than one, the energy tail is enhanced. In the PNS context, the physical meaning of the difference between a sub-extensive or a super-extensive statistical behavior is reflected in different and well distinguishable phenomenological PNS properties. For $q < 1$, we have a reduction in temperature at fixed baryon density with respect to the standard case ($q = 1$). Especially in the maximum heating phase, the EOS becomes slightly softer and higher central baryon densities at fixed total baryon mass are reached, influencing the neutrino diffusion during the deleptonization process. In the case of sub-extensive effects, hyperons start later but have a bigger concentration at high baryon density, allowing to sustain a higher neutrino luminosity at late times. The other way round takes place in the case of $q > 1$. We have an increase of the temperature as a function of the baryon density and lower central densities at fixed baryon mass are reached. The hyperons on-set is shifted at lower baryon densities and a greater hyperons concentration at low baryon masses is present. On the other hand,

a significant reduction of the hyperons concentration at high stellar masses take place, contributing to a lower luminosity at late times. Moreover, we have shown that, in presence of super-extensive statistical effects and hyperon degrees of freedom, it is favored the realization of a metastable phase, with an enhancement of a possible black hole formation after the deleptonization era.

Chapter 4

Nonextensive statistical effects and strangeness production in hot and dense nuclear medium.

In this Chapter we are planning to investigate the deconfinement phase transition from hadron matter to quark-gluon plasma, at finite temperature and baryon density, through effective models (nonextensive statistical mechanics and effective relativistic mean field model).

4.1 Introduction

As we have pointed out in the previous Chapters, relativistic heavy-ion collisions provide the unique possibility to explore in laboratory nuclear matter under extreme regimes in which the baryon density can reach values of a few times the saturation nuclear density and/or high temperatures. In these conditions, phase transition phenomena in the hot and dense fireball created during the collisions can take place [1]. Various results from QCD inspired models indicate that, increasing the baryon chemical potential in the phase diagram, a region of non-singular but rapid cross-over of thermodynamic observable around a quasi-critical temperature, leads to a critical endpoint (CEP), beyond which the system shows a first order phase transition from confined to deconfined matter (second order by Ehrenfest definition and therefore continuous). The existence or exclusion of a CEP has not yet been confirmed by QCD lattice simulations. Actually, there are some extrapolation techniques to finite chemical potentials, although the precise location of the CEP is still a matter of debate [161, 162]. Such a CEP can be in principle detected in future high-energy compressed nuclear matter experiments such as FAIR at GSI in Darmstadt [55] and NICA at JINR in Dubna [163]. In this direction interesting results have been obtained at low SPS energy and are foreseen at a low-energy scan at RHIC [112, 113, 114].
Therefore, although in principle the process of deconfinement and the equation of state (EOS) of hot and dense nuclear matter can be described by QCD, such a theory is highly nonperturbative in the energy density range involved in relativistic heavy-ion collisions. The generated quark-gluon plasma (QGP) in the early stages of the collisions does not at all

resemble a quasi-ideal gas of quarks and gluons because strongly dynamical correlations are present, including long-range interactions [18, 2, 164]. Therefore, the implementation of the nuclear EOS through effective models is of great importance in order to take in consideration such phenomenons.

For this reason, in this Chapter, we will investigate the deconfinement phase transition from hadrons to QGP in the framework of nonextensive statistical mechanics, exposed in the Chapter 2.
In this context, we investigate two different scenarios. In the first one, we explore the situation realized in heavy-ion collision experiments at not too high energy, where finite temperature and high compressed baryon density are generated. Under this condition, a large fraction of strangeness cannot be produced and, therefore, we will limit ourselves to study the deconfinement transition from hadronic matter to up and down quark matter [165, 166, 167]. We expect that, in the range of temperature and density considered, the presence of strange particles does not significantly affect the main conclusions regarding the relevance of nonextensive statistical effects to the nuclear EOS.
In the second scenario, we investigate the nuclear equation of state at higher temperature and finite baryon density. In this situation the strangeness production can not be neglected and strange particles are expected to play an important role in the physics of the system.
For this reason, in order to have a complete description of the degrees of freedom of the nuclear medium at this energy, we implement the nuclear EOS including all the baryons octet and the lightest scalar and vector mesons, through the effective formulation exposed in Section. 1.4.1.

This chapter is based on the results obtained in [34, 36, 168, 169].

4.2   Gibbs formalism

As briefly mentioned in the Introduction, with increasing the baryon chemical potential, the phase diagram is characterized by a rapid crossover of thermodynamic observable around a quasi-critical temperature with a CEP, beyond which the system shows a first order phase transition from confined to deconfined matter. Since it occurs over a very narrow range of temperatures, for several practical purposes the transition can still be considered of first order. Indeed, the lattice data with 2 or 3 dynamical flavors, are not precise enough to unambiguously disentangle the difference between the two situations. Moreover, the aim of this study is to show the relevance of nonextensive statistical effects in a finite range of temperature and baryon density relevant for compressed baryonic matter experiments rather than the ultrarelativistic regime at vanishing baryon chemical potential. Thus, by considering the deconfinement transition at finite density, a mixed phase can be formed, which is typically described using two separate equations of state: one for the hadronic phase and another one for the quark-gluon phase (as reported respectively in the paragraphs 2.3.1 and 2.3.2). In order to study the phase transition from hadronic matter to QGP, we apply the Gibbs conditions to systems with more than one conserved charge, by requiring the global conservation of the baryon number (B), electric charge (C) and zero net strangeness (S).

The structure of the mixed phase is therefore obtained by imposing the following conditions

$$\mu_B^{(H)} = \mu_B^{(Q)}, \quad \mu_C^{(H)} = \mu_C^{(Q)}, \quad \mu_S^{(H)} = \mu_S^{(Q)}, \tag{4.1}$$

$$P^{(H)}(T, \mu_B, \mu_C, \mu_S) = P^{(Q)}(T, \mu_B, \mu_C, \mu_S), \tag{4.2}$$

$$\rho_B = (1 - \chi)\rho_B^H(T, \mu_B, \mu_C, \mu_S) + \chi\rho_B^Q(T, \mu_B, \mu_C, \mu_S), \tag{4.3}$$

$$\rho_C = (1 - \chi)\rho_C^H(T, \mu_B, \mu_C, \mu_S) + \chi\rho_C^Q(T, \mu_B, \mu_C, \mu_S), \tag{4.4}$$

$$\rho_S = (1 - \chi)\rho_S^H(T, \mu_B, \mu_C, \mu_S) + \chi\rho_S^Q(T, \mu_B, \mu_C, \mu_S), \tag{4.5}$$

where $\rho_B^{H(Q)}$, $\rho_C^{H(Q)}$ and $\rho_S^{H(Q)}$ are, respectively, the baryon, the electric charge and the strange densities in the hadronic (H) and in the quark (Q) phase and $\chi = V^Q/V$ is the fraction volume of quark-gluon matter in the mixed phase.

Whereas, the energy density of the hadrons and quarks during the mixed phase is given by:

$$\varepsilon = (1 - \chi)\varepsilon^H(T, \mu_B, \mu_C, \mu_S) + \chi\varepsilon^Q(T, \mu_B, \mu_C, \mu_S). \tag{4.6}$$

In this context it is important to note that the pressure, during the mixed phase, is not generally constant. This is because it depends from the energy density through the relationship $P = -\partial E/\partial V$ and therefore, due to the non linearity of ε, the pressure normally varies during the phase transition.
Therefore, at fixed T and μ_B, the charge μ_C and strangeness μ_S chemical potentials are obtained by fixing the total electric charge y (for example, $y = 0.4$ for lead-lead heavy ion collisions) and the total strangeness neutrality by the conditions ($\rho_C = y\rho_B$ and $\rho_S = 0$)

Another important aspect it that the presence of more than one conserved charge implies a global and not local charge conservation, therefore the charge densities ρ_B, ρ_C and ρ_S are fixed only as long as the system remains in one of the two pure phases. In the mixed phase, the charge concentration in each of the regions of one phase or the other may be different. As we will see, this feature plays a crucial role on the strangeness production during the mixed phase of hadron and quark-gluon matter.

Concluding, deconfinement phase transition (transition to quark-gluon plasma phase) is a finite-temperature transition (crossover in the most recent terminology) from a multi-scale confinement phase to an ordered phase. There is no agreement yet if the deconfinement is true phase transition or a smooth crossover. Ordered (free) behavior is reached only at asymptotically large temperatures.

4.3 Nonextensive statistical effects in the hadron to quark gluon plasma phase transition

In the first part of this analyze, we study the deconfinement phase transition from hadron matter to quark-gluon plasma at not to high energy.
Under this condition, a large fraction of strangeness cannot be produced and, therefore, we will limit ourselves to study the deconfinement transition from hadronic matter to up

and down quark matter [165, 166, 167]. In this context we study how nonextensive statistical effects influence, from a phenomenological point of view, the nuclear EOS and, as a consequence, the relative phase transition at finite temperature and density reachable in high-energy heavy-ion collisions.

We expect that, in the range of temperature and density considered in this analyze, the presence of strange particles does not significantly affect the main conclusions regarding the relevance of nonextensive statistical effects to the nuclear EOS.

Under this assumption, the system is described by two independent conserved charges (B and C) and therefore the Gibbs construction is obtained without requiring the conservation of the strangeness.

Furthermore, due to the not so high temperature achieved in the system and because here we are only interested in exploring the influence of the nonextensive statistical effects on the nuclear EOS and in particular in the variation of the first critical density, we can avoid the use of the Bag parametrization of eq. (1.73) and we can set the vacuum pressure at constant value ($B^{1/4} = 190 MeV$).

In the second part of this analyze, we will consider a more energetic event, where strange particles are abundantly produced. In this context, we implement the hadronic EOS including all the baryon octet, Δ-isobars degrees of freedom and the lightest pseudo-scalar (π, K, $\overline{K}$, η, $\eta^{'}$) and vector mesons (ρ, ω, K^*, $\overline{K}^{*}$, ϕ), through the effective formulation exposed in (1.4.1). Furthermore, the MIT-Bag model is implemented including the strange quark flavor and, due to the high energy and temperature achieved during the relativistic heavy ion collision, we adopt the Bag parametrization exposed in eq. (1.73).

Before starting this analyze, we would like to remember that, in the mixed phase, due to the high dimensionality of the system (two or three conserved charges) the concentration in each of the regions of one phase or the other may be different. Their values are restricted only by the conservation of the total charge numbers and strangeness (normally set equal to zero). The essential point is that conservation laws in chemical thermodynamics are global, not local.

4.4   Two quark flavors

In this section, we analyze the relativistic equation of state in the framework of nonextensive statistical effects, using the GM2 parameter set of Tab. 1.2 and the hadronic Lagrangian density of eq. (1.27).

In this context, due to the range of temperatures and baryon density considered in this analyze, the only degrees of freedom relevant for the system are nucleons, quarks up and down and pions, introduced through the effective formulation exposed in section (1.4.1).

The hadronic Lagrangian density assume the form:

$$\mathcal{L}_{QHD} = \mathcal{L}_{\mathcal{N}} + \mathcal{L}_{\text{qfm}} \, , \tag{4.7}$$

where $\mathcal{L}_{\text{qfm}}$ is related to a (quasi) free gas of pions with an effective chemical potential given by eq. (1.50). Hence, the equation of motion for pions are given by eq.s (2.30)–(2.31) and (2.32).
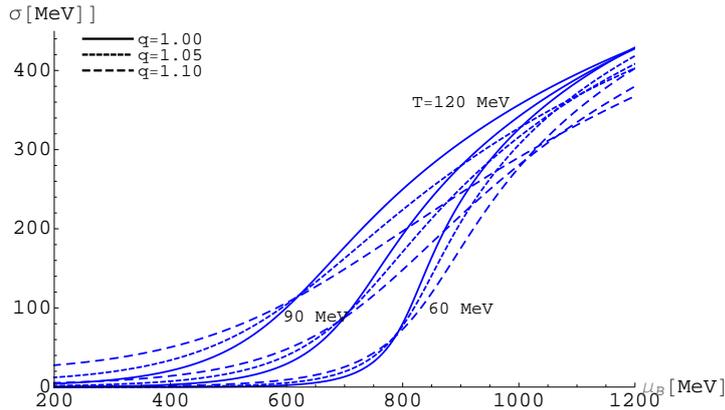
Figure 4.1: The σ meson field as a function of baryon chemical potential for different values of temperature (in units of MeV) and q.

Furthermore, the equation of motion, the scalar and vector baryon density for the hadronic phase are given, respectively, by the set of eq.s (2.24)–(2.25) and (2.28)–(2.29). Naturally for $q \to 1$ and/or low temperature, the $q-$deformed quantum distribution function (eq.s (2.26) and (2.27)), reduces to the standard and well known Fermi-Dirac and Bose-Einstein distribution function (eq.s 1.34 and 1.35).

The nonextensive EOS and vector density for the quark phase, are instead given by eq.s (2.36)–(2.37) and (2.38). Gluons are also take in consideration, following the eq.s (2.39) and (2.40).

The corresponding extensive equations for hadrons, pions and quarks are given in Chapter 1.

4.4.1 Nonextensive meson fields

Let us start our numerical investigation by considering the behavior of σ, ω and ρ meson fields at a fixed value $y = 0.4$, for different values of temperature and nonextensive parameter q. Because meson fields have their source in the baryon and scalar density, which are very sensible to the behavior of the mean occupation number, all meson fields appear to be significantly changed in presence of nonextensive effects.

In Fig.s 4.1, 4.2 and 4.3 we show, respectively, the σ, ω and ρ meson field as a function of the baryon chemical potential μ_B. It is interesting to observe that at lower μ_B, in presence of nonextensive effects, the value of the meson fields are significantly increased for all values of temperature respect to the standard case, the other way round happens for σ at higher μ_B. This important feature is due to the fact that, as already remarked in Section 2.2, for $q > 1$ and fixed baryon density (or μ_B), the (normalized) mean occupation function is enhanced at high values of its argument and depressed at low values. Being the argument of the mean occupation function $x_i = \beta(E_i^* - \mu_i^*)$, in the integration over momentum (energy), at lower μ_B (corresponding to lower values of the effective particle chemical potential μ_i^*) the enhanced Tsallis high energy tail weighs much more that at higher μ_B where depressed
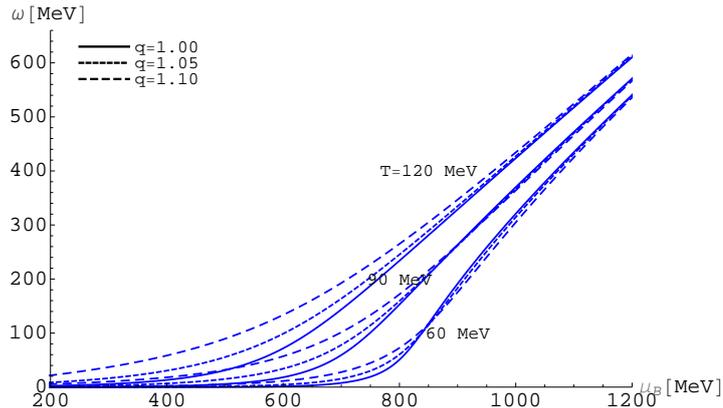
Figure 4.2: The ω meson field as a function of the baryon chemical potential for different values of temperature and q.

low energy effects prevail and the mean occupation number results to be bigger for the standard Fermi-Dirac statistics. Concerning the antiparticle contribution, the argument of $\overline{n}_i$ is $\overline{x}_i = \beta(E_i^* + \mu_i^*)$ and the Tsallis enhancement at high energy tail is favored also at higher μ_B. At the same time, higher temperatures (where antiparticle contribution are more relevant) reduce the value of the argument of n_i and $\overline{n}_i$, favoring the extensive distribution. These effects are much more evident for the scalar density ρ^S (self-consistently related to the σ meson field) where appears $(n_i)^q$ and particle and antiparticle contributions are summed. The same effect involves also the nucleon effective mass $M^* = M - g_\sigma \sigma$, which becomes, respect to the standard case, smaller for lower values of μ_B and bigger for higher values, with very relevant consequences for the hadronic EOS [1].

The situation is different for ω, because it has its source in the baryon density ρ_B where appears n_i and particle and antiparticle contributions are subtracted Fig. 4.2. At lower temperatures ($T = 60$ MeV), antiparticle contributions are negligible and we have a behavior similar (although less evident) to the σ field. At higher temperatures ($T = 120$ MeV), the contributions of antiparticle increase and nonextensive effects vanish at higher μ_B. Finally, in Fig. 4.3, we report the behavior of the ρ meson field which depends from the isospin density (let us remember that we have fixed $y = 0.4$). Similar arguments as done for the ω meson applies also in this case. The valuable increasing of its absolute value, also for weakly asymmetric nuclear matter, makes ρ meson very relevant in the hadronic EOS, especially at not too large μ_B.

4.4.2 Nonextensive EOS and phase diagram

As reported in the Fig.s (2.1) and (2.2) of Chapter 2, even for small deviation from the standard BG statistics, we can observe a strong enhancement in the hadronic and quark

---

[1]In Ref. [123], the nucleon effective mass as a function of temperature always diminishes respect to standard statistics, this behavior is a consequence of the fact that it is plotted only at $\rho_B = 0$.
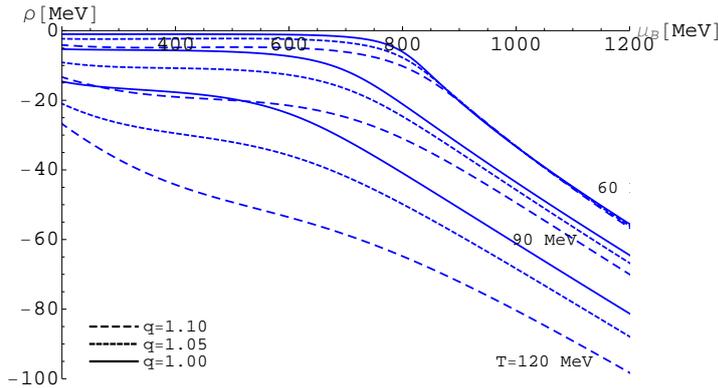
Figure 4.3: The ρ meson field as a function of baryon chemical potential for different values of temperature and q.
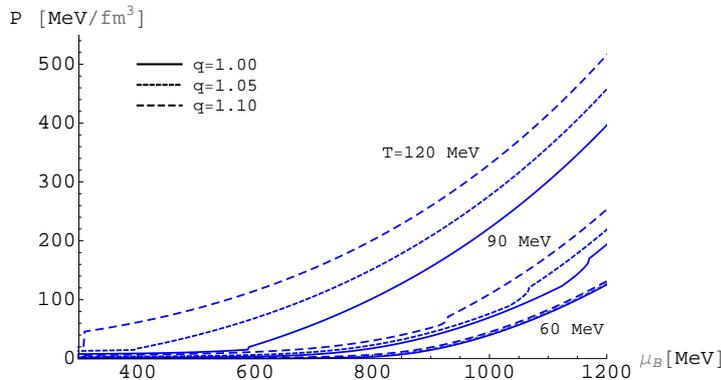
Figure 4.4: Pressure versus baryon chemical potential in the mixed phase for different values of temperature and q.

pressure, for moderate values of temperature and also at low μ_B.

The increasing of the pressure is an important factor in order to achieve the condition of deconfinement phase transition from hadronic matter to QGP. In this context, we e are particularly interested in the lower baryon density (baryon chemical potential) border, i.e. the first critical transition density ρ^I_{cr} (μ^I_{cr}), in order to check the possibility of reaching such conditions in a transient state during a heavy-ion collision at relativistic energies. We do that using the Gibbs formalism exposed in section 4.2 (naturally the strangeness number is set equal to zero).

At this regards, in Fig. 4.4, we report the pressure as a function of baryon chemical potential for different values of nonextensive q parameter and temperatures, for $y = 0.4$ and $B^{1/4} = 190$ MeV. It is well evident that, in presence of nonextensive effects, the onset of the mixed phase region is strongly anticipated, this effect is more evident at the increasing of the temperature. Therefore, in presence of nonextensive effects, the values of the critical

85
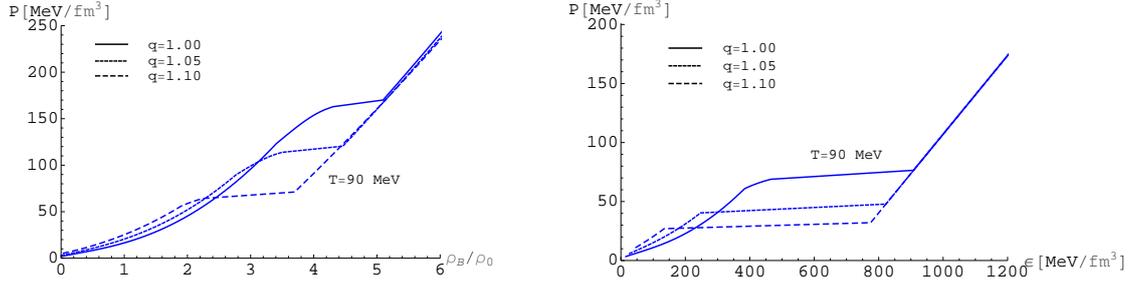
Figure 4.5: Pressure as a function of baryon density (left panel) and energy density (right panel) in the mixed phase for different values of q. The temperature is fixed at $T = 90$ MeV.

densities result to be sensibly reduced with respect to the standard case. This matter of fact is more evident in Fig. 4.5, where we report the pressure at $T = 90$ MeV as a function of baryon density (in units of nuclear saturation density $\rho_0 = 0.153$ fm^{-3}) (left panel) and energy density (right panel). It is interesting to observe that pressure as a function of baryon density (or energy density) is stiffer in the pure hadronic phase for $q > 1$ but appears a strong softening in the mixed phase. This feature results in significant changes in the incompressibility and may be particularly important in identifying the presence of nonextensive effects in high energy heavy ion collisions experiments. Related to this aspect, let us observe that possible indirect indications of a significative softening of the EOS at the energies reached at AGS have been discussed several times in the literature [124, 109, 170, 171, 172].

Related to this aspect, in Fig. 4.6, we would like to show the relative phase diagram from nuclear matter to QGP, in the $T - \rho_B$ plane, for different values of q. The curves labeled with ρ_{cr}^I and ρ_{cr}^{II} represent, respectively, the beginning and the end of the mixed phase. For $q > 1$, both the first and the second critical densities are sensibly reduced, even if the shape of the mixed phase is approximately the same. Furthermore, let us remember that, although an effective bag parametrization is necessary to treat more energetic heavy ion collision, where high temperature condition is reached, here we are only interested in the exploring the effects of nonextensive effects on the nuclear EOS. Therefore, in this simple study we limit our investigation to a restricted range of temperature and baryon density, particular relevant for high energy compressed nuclear matter experiments.

Finally in left and in the right panel of Fig. 4.7, we show respectively the variation of the first critical baryon density as a function of the Bag constant and of the temperature, for different values of q. Obviously, by increasing the bag constant we have a corresponding increase of ρ_{cr}^I. However, this effect depends on the temperature and the nonextensive parameter q. In fact, as appears in the right panel of Fig. 4.7, for $T = 60 MeV$ we can see only a little reduction in the first critical density also for large deviations from the standard statistics; on the other hand, the reduction becomes more pronounced at larger temperatures
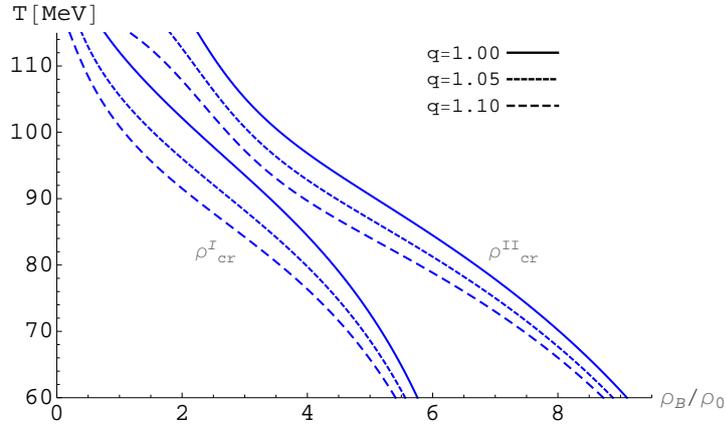
Figure 4.6: Phase diagram $T - \rho_B$ for different values of q. The curves labeled with ρ_{cr}^I and ρ_{cr}^{II} indicate, respectively, the beginning and the end of the mixed phase.
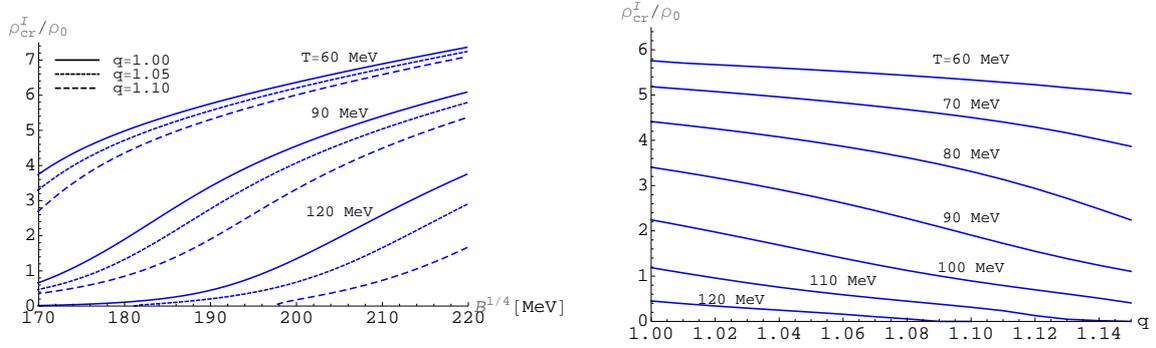
Figure 4.7: Variation of the first transition baryon density as a function of the bag constant (left panel) and nonextensive index q (right panel) for different temperatures.

$T = 60$ MeV	$\rho_{\rm cr}^{I}/\rho_0$	$\rho_{\rm cr}^{II}/\rho_0$	$\mu_{\rm cr}^{I}$ [MeV]	$\mu_{\rm cr}^{II}$ [MeV]
$q = 1.00$	5.75	9.10	1503	1569
$q = 1.05$	5.56	8.88	1472	1537
$q = 1.10$	5.33	8.65	1437	1502
$T = 90$ MeV	$\rho_{\rm cr}^{I}/\rho_0$	$\rho_{\rm cr}^{II}/\rho_0$	$\mu_{\rm cr}^{I}$ [MeV]	$\mu_{\rm cr}^{II}$ [MeV]
$q = 1.00$	3.41	5.09	1123	1170
$q = 1.05$	2.77	4.46	1034	1068
$q = 1.10$	1.91	3.69	916	927
$T = 120$ MeV	$\rho_{\rm cr}^{I}/\rho_0$	$\rho_{\rm cr}^{II}/\rho_0$	$\mu_{\rm cr}^{I}$ [MeV]	$\mu_{\rm cr}^{II}$ [MeV]
$q = 1.00$	0.45	1.93	588	616
$q = 1.05$	0.20	1.33	383	396
$q = 1.10$	0.08	0.71	184	201

Table 4.1: Critical baryon densities and baryon chemical potentials at the beginning (index I) and at the end (index II) of the mixed phase for different values of temperature and nonextensive parameter q.

We conclude this section presenting in Table 4.1, the critical baryon density and baryon chemical potential at the beginning (index I) and at the end of the mixed phase (index II) for different values of temperature and q.

The performed analyze confirm the fact that, in presence of nonextensive effects, the nuclear EOS are strongly modified and the condition for the deconfinement phase transition is also strongly varied. In fact, by varying temperature and density, the EOS reflects in terms of the macroscopic thermodynamical variables the microscopic interactions of the different phases of nuclear matter. In particular, although pressure as a function of baryon density is stiffer in the hadronic phase, we show that a strong softening in the mixed phase takes place in the presence of nonextensive statistics. Such behavior implies an abrupt variation in the incompressibility and could be considered as a signal of nonextensive statistical effects in high-energy heavy-ion collisions.

These facts confirm the importance of consider the possible onset of nonextensive statistical effects (as for eg. long range color interaction, memory effects and strong dynamical correlations) during relativistic heavy ion collision experiments.

4.5 Three quark flavors

We are now ready to extend our numerical investigation to more energetic relativistic heavy ion collision experiments. In particular, we are interested in exploring higher degrees of freedom of the system. For this reason, we include in our numerical investigation all the baryons octet (n, p, Λ, Σ^+, Σ^0, Σ^-, Ξ^-, Ξ^0), Δ-isobar degrees of freedom (Δ^{++}, Δ^+, Δ^0, Δ^-), and the lightest pseudo-scalar (π, K, $\overline{K}$, η, $\eta^{'}$) and vector mesons (ρ, ω, K^*, $\overline{K}^*$, ϕ), through the effective mean field model exposed in section 1.4.1.

In this context, due to the high temperature achieved during the phase transition from had-

rons to QGP, we use the Bag parametrization of eq. (1.73). Furthermore, the system is now described by three independent conserved charges (B, C, S). Therefore, the thermodynamical equilibrium and the mixed phase, are obtained by imposing the condition of eq.s (4.1), (4.2), (4.3), (4.4), (4.5).

The analyze is performed using the parameter set marked as GM3 of Tab. 1.2 , hence the hadronic Lagrangian density can be written as:

$$\mathcal{L}_{\mathcal{QHD}} = \mathcal{L}_B + \mathcal{L}_\Delta + \mathcal{L}_{\text{qfm}}, \tag{4.8}$$

where $\mathcal{L}_{\text{B}}$ is related to the baryons octet eq. (1.27), $\mathcal{L}_\Delta$ is relative to Δ-isobars degrees of freedom eq. (1.48) and $\mathcal{L}_{\text{qfm}}$ is related to a (quasi) free mesons gas with an effective chemical potential given by eq. (1.50).

The nonextensive equation of motion, the scalar and vector baryon density for baryons and Δ's, are given by the set of eq.s (2.24)–(2.25) and (2.28)–(2.29), naturally weighed for the corresponding degeneracy spin factor $\gamma_i = 2J_i + 1$ ($\gamma_{octet} = 2$ and $\gamma_\Delta = 4$). Furthermore, in the effective relativistic mean field models, the equation of motion for mesons are given, as usual, by the set of eq.s (2.30)–(2.31) and (2.32). Finally, as for the case of two flavors, the nonextensive quark EOS and the quark density are given by the set of equations (2.36)–(2.37) and (2.38). Gluons are also take in consideration, following the eq.s (2.39) and (2.40). The corresponding extensive equations are given in sections (1.3, 1.4.1 and 1.6).

4.5.1 Nonextensive EOS and phase diagram

Let us start our numerical investigation by reporting in figure 4.8 the variation of the pressure as a function of baryon density (in units of nuclear saturation density $\rho_0 = 0.153$ fm^{-3}), at $T = 120$ MeV and for different values of q. Here and in the following we fix the value $y = 0.4$. In presence of nonextensive statistical effects the pressure results to be considerably increased even for small deviation from the Boltzmann-Gibbs statistics. It is interesting to observe that the pressure presents a strong softening in the mixed phase even if the Gibbs conditions on the phase transition are applied. At this temperature, such a behavior results to be more pronounced by increasing the value of the nonextensive entropic parameter q with a larger range of baryon density involved in the mixed phase region. This matter of fact, already present in absence of strange particle degrees of freedom (section 4.4, figure 4.5), implies an abrupt variation in the incompressibility and results much more evident here due to the additional strangeness conservation constraint. In this context let us observe that indirect indications of a remarkable softening of the EOS at energies reached at AGS have been already outlined [124].

In figure 4.9, we report the phase diagram in the $T - \rho_B$ plane for different values of the nonextensive parameter q. The curves labeled with ρ_{cr}^I and ρ_{cr}^{II} denote, respectively, the beginning and the end of the mixed phase. In presence of nonextensive statistical effects the phase diagram results significantly modified and a remarkable lowering of the critical maximum temperature at vanishing baryon density ρ_B is present. This result is in according to previous investigations where, by fitting the experimental observable at $q > 1$,
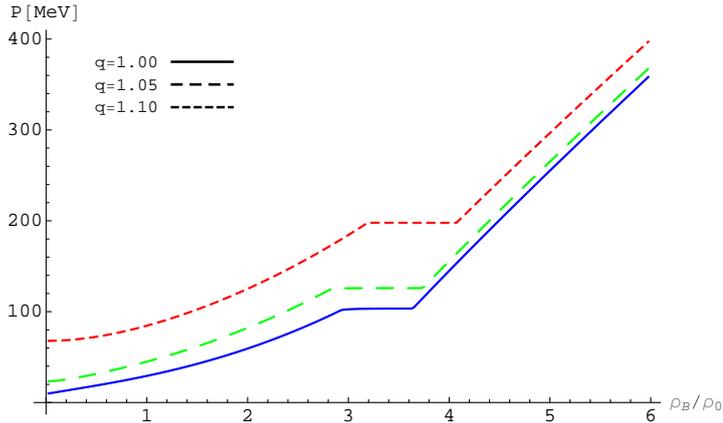
Figure 4.8: Pressure as a function of baryon density (in units of the nuclear saturation density ρ_0) at $T = 120$ MeV and for different values of nonextensive parameter q.

the temperature (or slope) parameter T is usually less that the one obtained in the standard Boltzmann-Gibbs statistics ($q = 1$) [151, 28, 27, 26].

4.5.2 Particle concentration and strangeness fraction

Let us now explore in more detail the particle concentrations for different values of the nonextensive parameter q. In figure 4.10, we report the most relevant net particle ratios ($Y_i = \rho_i/\rho_B$) as a function of baryon density at T=120 MeV. In presence of nonextensive statistical effects (right panel), the net particle concentrations are sensibly modified even for small deviations from the standard statistics. In particular, we observe in the hadronic phase a strong reduction of the neutron and proton fractions and a considerable increase in the hyperon and in the meson concentrations, also at moderate baryon densities.

To better understand the relevance of the nonextensive statistical effects in presence of strange matter, we show in figure 4.11 the strangeness fraction Y_S for baryons (B), mesons (M), strange quarks (s) and their antiparticles as a function of baryon density at a fixed temperature of T=120 MeV. For $q = 1$ (left panel), in the hadronic phase ($\chi = 0$), the total strangeness is carried almost completely by mesons (kaons, mainly K^+ and K^0) and baryons (hyperons), although at low baryon density anti-mesons $\overline{M}$ (anti-kaons, mainly K^- and $\overline{K}^0$) bring a non-negligible fraction of strangeness. At the beginning of the mixed phase ($\rho_B \approx 3\,\rho_0$) the onset of s and $\bar{s}$ quarks rapidly dominates the strangeness ratio and the contribution of the other particle fractions becomes gradually less relevant.

In presence of nonextensive statistical effects (right panel) the situation is quite different. Here we observe a strong enhancement in all strange-particle concentrations and, in particular, the contribution of anti-baryons $\overline{B}$ (anti-hyperons) becomes relevant and comparable to anti-mesons and baryons.

This behavior is also evident in figure 4.12, where the strangeness fractions in the hadron and in the mixed phase as a function of the temperature at $\rho = 3\,\rho_0$ are shown
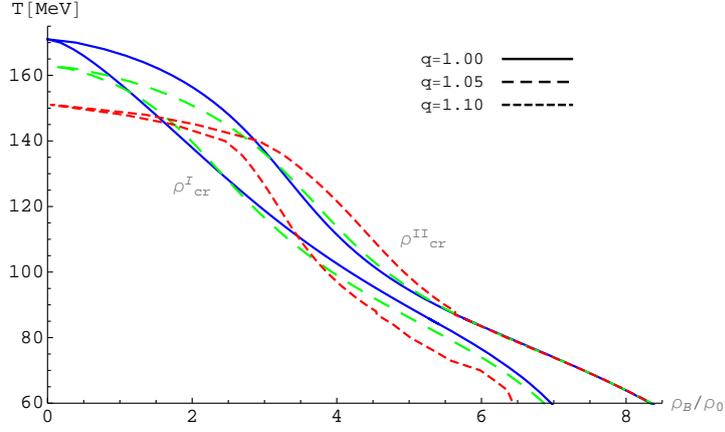
Figure 4.9: Phase diagram in the $T - \rho_B$ plane for different values of q.
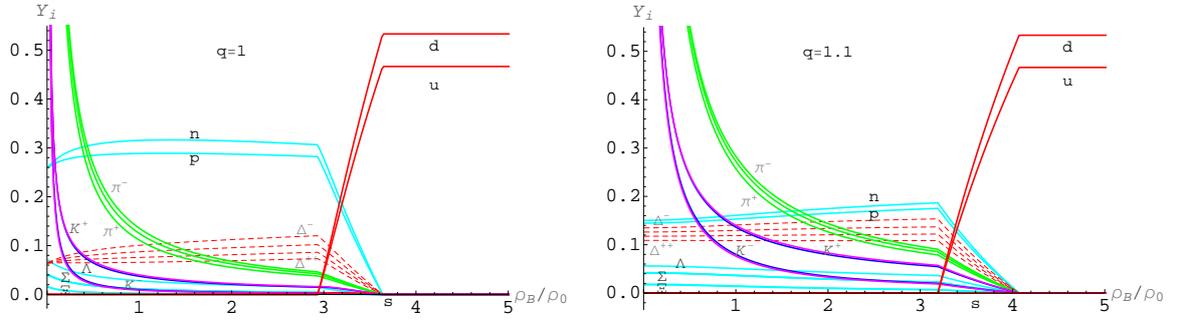
Figure 4.10: Particles concentration as a function of baryon density at $T = 120$ MeV and for $q = 1$ (left panel) and $q = 1.1$ (right panel).
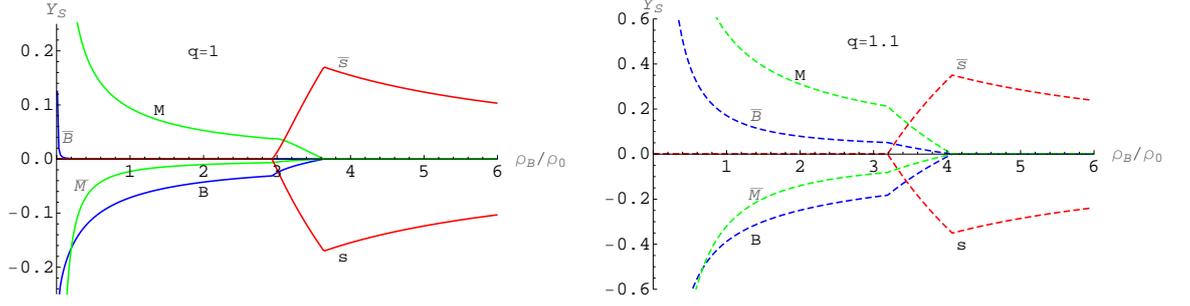
Figure 4.11: Strangeness fractions of baryons (B), mesons (M), strange quarks (s) and their antiparticles as a function of baryon density in the pure hadronic phase, mixed phase and quark phase at T=120 MeV for $q = 1$ (left panel) and $q = 1.1$ (right panel).
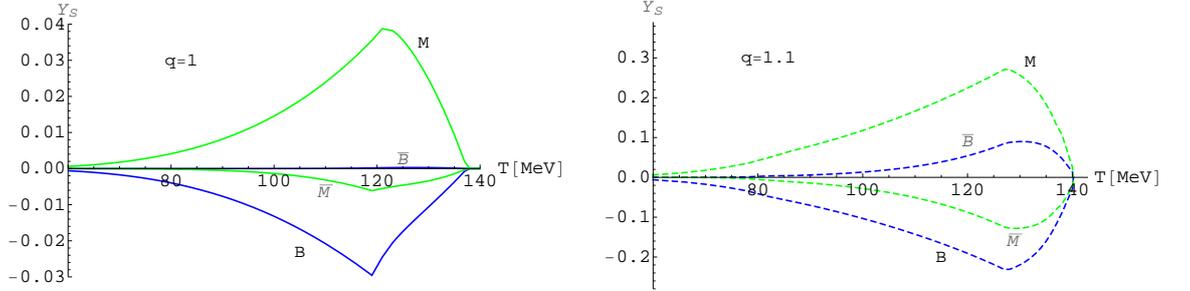
Figure 4.12: Strangeness fractions as a function of temperature in the pure hadronic and mixed phase at $\rho_B = 3\,\rho_0$ for $q = 1$ (left panel) and $q = 1.1$ (right panel).

(quark phase is not reported in this figure). As expected, by increasing the temperature all the strange particle densities are sensibly enhanced. Furthermore, in both panels we observe a peak at the end of the hadronic phase and a rapid decrease at the beginning of the mixed phase, due to the onset of the strange quarks.

At this regard, in figure 4.13, we show the variation of the baryon chemical potential μ_B (left panel) and the strangeness chemical potential μ_S (right panel) as a function of temperature at fixed $\rho_B = \rho_0$ and for different values of q. As expected, for a multicomposed strange hadronic matter, μ_S is positive and decreased with T at a fixed ρ_B. It is interesting to observe the different behavior of μ_S at lower and higher temperatures in the presence ($q \neq 1$) and in absence ($q = 1$) of nonextensive statistical effects.

The strong enhancement of the strange hadrons, in presence of nonextensive statistical effects, is a direct consequence of the normalized mean occupation function n_i because, for
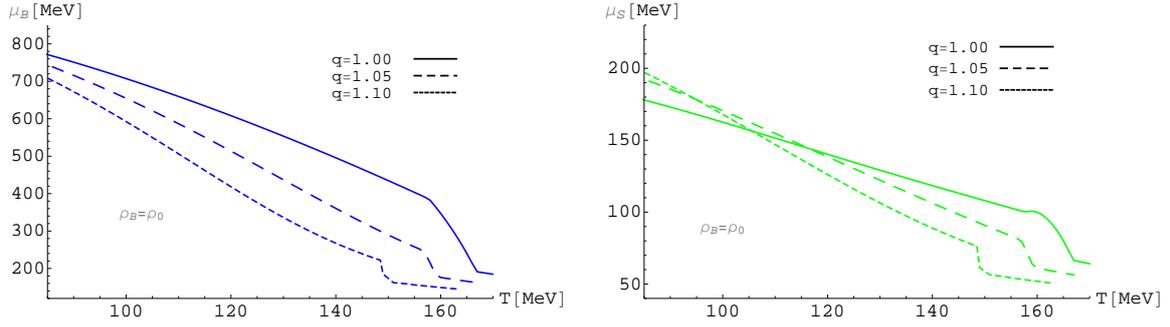
Figure 4.13: Variations of the baryon chemical potential μ_B (left panel) and the strangeness chemical potential μ_S (right panel) as a function of temperature at $\rho_B = \rho_0$ and for different values of q.

$q > 1$ and fixed baryon density (or μ_B), it is enhanced at high values of its argument and depressed at low values. In particular, as reported in the previous section 4.4.1, the argument of the mean occupation function $x_i = \beta(E_i^* - \mu_i^*)$, in the integration over momentum (energy), at lower μ_B (corresponding to lower values of μ_i^*) the enhanced nonextensive high energy tail weighs much more that at higher μ_B where depressed low energy effects prevail and the mean occupation number results to be bigger for the standard Fermi-Dirac statistics. Concerning the antiparticle contribution, the argument of $\overline{n}_i$ is $\overline{x}_i = \beta(E_i^* + \mu_i^*)$ and the nonextensive enhancement at high energy tail is favored also at higher μ_B. As a consequence, the formation of antiparticles, as well as strange particles, results to be enhanced in presence of nonextensive statistical effects. At the same time, higher temperatures reduce the value of the argument of n_i and $\overline{n}_i$, reducing the effect of the nonextensive distribution function.

These properties change significantly the behavior of the σ meson field and, therefore, the effective baryon mass which is related by the relation: $M_i^* = M_i - g_{\sigma i}\sigma$. In fact, for $q > 1$, M_i^* becomes smaller at low baryon density (and higher temperature) and bigger at finite densities $\rho_B \geq 0.2\,\rho_0$ (and lower temperature) [173]. This effect appears to be much more significant as a percentage for lighter baryons, therefore, at finite baryon densities, the nucleons effective mass is enhanced compared to the standard case ($q = 1$) with a percentage significantly greater than the hyperons effective masses. This matter of fact favors the formation of hyperons compared to that of nucleons at a fixed baryon density and in presence of nonextensive statistical effects. Moreover, being the strangeness number globally conserved, an increase of hyperon particles implies, in the pure hadron phase, a corresponding increase of strange meson particles in order to satisfy the condition of zero net strangeness.

93

4.5.3 Quark anti-quark strangeness ratio

At the scope of better focalize the role of nonextensive statistical effects in the strangeness production during the mixed phase, in figure 4.14, we report the strange to anti-strange quark ratio $\rho_s/\rho_{\bar{s}}$ as a function of the baryon density, at different values of the volume fraction of quark matter χ in the quark-gluon phase along the phase transition, i.e., for a continuously varying temperature. In this context, let us point out again that, due to the Gibbs conditions, into the mixed phase, the net strangeness in each separate phase need not vanish although the total net strangeness is zero. This matter of fact is evident in figure 4.14. In the left panel ($q = 1$), especially at the beginning of the mixed phase ($\chi = 0.1$), there is a remarkable excess of quark s with respect to $\bar{s}$, with a maximum value around $\rho_B \approx 3\,\rho_0$. This means that in absence of nonextensive statistical effects, during the phase transition, there is a large antistrangeness ($\bar{s}$) content in the hadron phase while quark-gluon plasma retains a large net strangeness (s) excess. This distillation mechanism, already known in literature, may result in "strangelet" formation, i.e. metastable droplets of strange-quark matter, which could imply a unique signature for quark-gluon plasma formation in relativistic heavy-ion collisions [105, 106].

In presence of the nonextensive statistical effects (right panel), there is a very different behavior with a ratio $\rho_s/\rho_{\bar{s}}$ slightly less than one at lower baryon density ($\rho_B < 2\,\rho_0$), whereas the other way round occurs at higher ρ_B with a comparable behavior to the $q = 1$ case but with an excess of s quarks less pronounced. Similar behavior can be observed in figure 4.15, where the same ratio as a function of the temperature is also reported. Of course, at fixed χ, low temperatures imply high densities and viceversa.

As previous discussed, this behavior is a consequence of the power-law behavior of the mean occupational distribution for $q > 1$: the formation of antihyperons and kaons (mainly K^+, K^0) turns out to be disadvantaged at low baryon density and very high temperature and, viceversa, favored at high baryon density and low/intermediate temperature, compared to the standard case ($q = 1$). Although particles with strangeness and antistrangeness content are strongly enhanced in presence of nonextensive statistics, the ratio strangeness/antistrangeness results depleted due to an enhancement of antiparticles production at finite temperature.

4.5.4 Strangeness mesons production

In agreement with the previous results, in figure 4.16, we report the K^+/K^- ratio in the hadronic phase as a function of baryon density at $T = 120$ MeV (left panel) and as a function of temperature at $\rho_B = 3\,\rho_0$ (right panel). For $q = 1$ and fixed temperature, the K^+/K^- ratio increases with continuity by increasing the baryon density until it reaches the first critical density around ($\rho_B \approx 3\,\rho_0$), after that a strong enhancement of the ratio occurs in the mixed phase region. This a consequence of the antistrangeness ($\bar{s}$) excess in the hadronic phase at the beginning of the mixed phase. For the same reason the K^+/K^- ratio decreases by increasing the temperature until the beginning of the mixed phase with an abrupt increase of the ratio. On the other hand, for $q > 1$, the kaon to anti-kaons ratio is depleted with respect to the standard case ($q = 1$), due to the increase of the antiparticles production. Furthermore, the strong variation of the ratio during the mixed phase transition
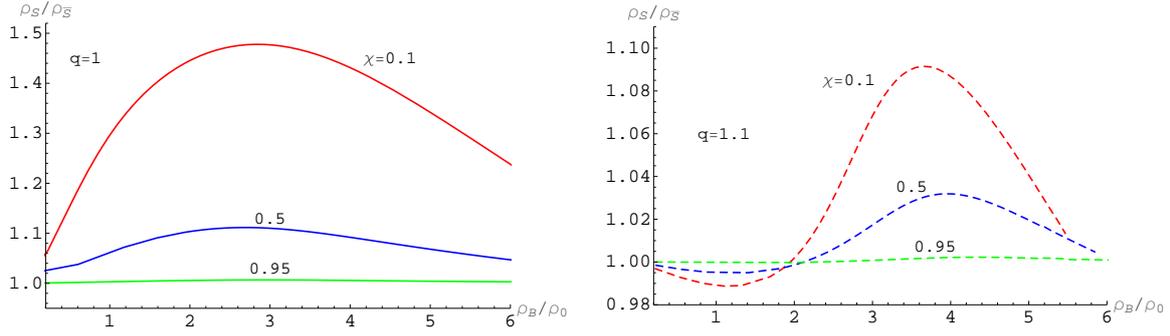
Figure 4.14: Ratio of strange to anti-strange quarks in the quark phase, as a function of the baryon density at different values of the volume fraction of quark-gluon matter χ in the mixed phase for $q = 1$ (left panel) and $q = 1.1$ (right panel).
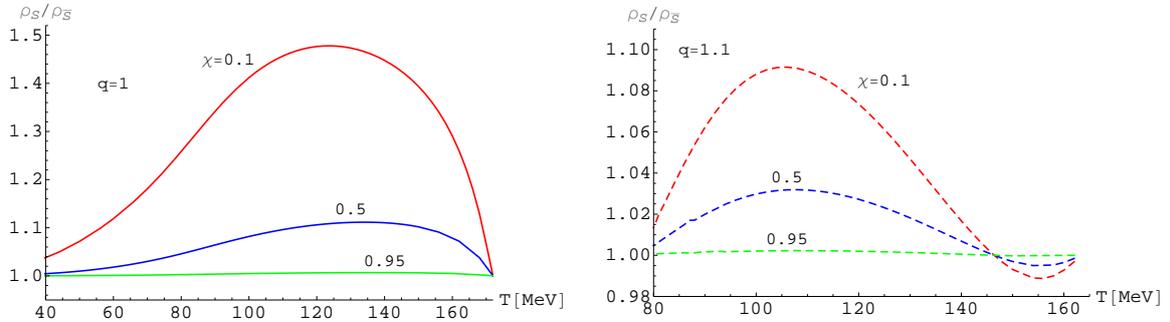
Figure 4.15: The same of figure 4.14 as a function of the temperature

at $q = 1$ results to be very smoothed in presence of nonextensive statistical effects.

In presence of nonextensive statistical effects, the strong enhancement in density of strange particles compared to non-strange can be further observed in figure 4.17 where the K^+/π^+ ratio is reported as a function of baryon density at $T = 120$ MeV (left panel) and as a function of temperature at $\rho_B = 3\,\rho_0$ (right panel). For $q = 1.1$, there is a strong increase of the ratio, while it does not present discontinuities at the beginning of the mixed phase, unlike the case $q = 1$ where a much more antistrangeness excess is present. Finally it is interesting to observe for $q = 1.1$ a continuous decreasing trend of the ratio as a function of temperature at fixed baryon density.

Therefore, in presence of non extensive effects, strange particles are abundantly produced even at moderate temperature and the anti-particles concentration is strongly increased. In particular, for $q > 1$, the phase transition is characterized by an antistrangess content in the hadron phase while the QGP retains a net strangeness excess at large densities

95
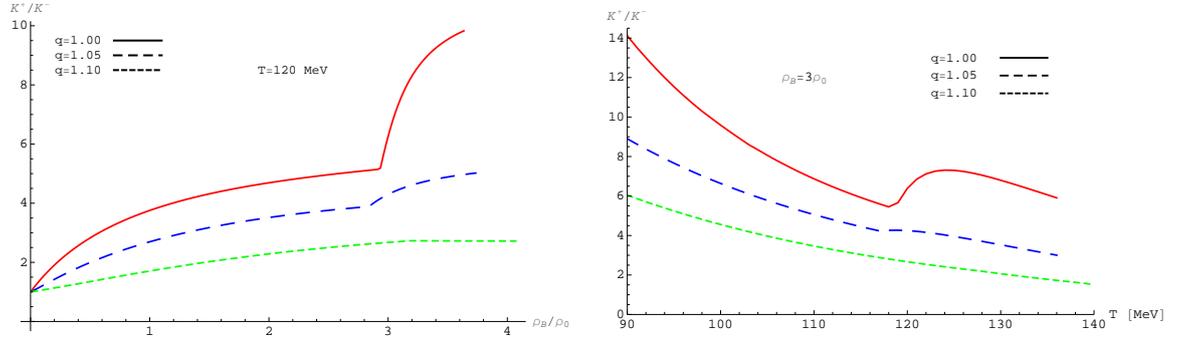
Figure 4.16: Kaon to antikaon ratio as a function of baryon density (left panel) and temperature (right panel) for different values of q in the hadronic phase.
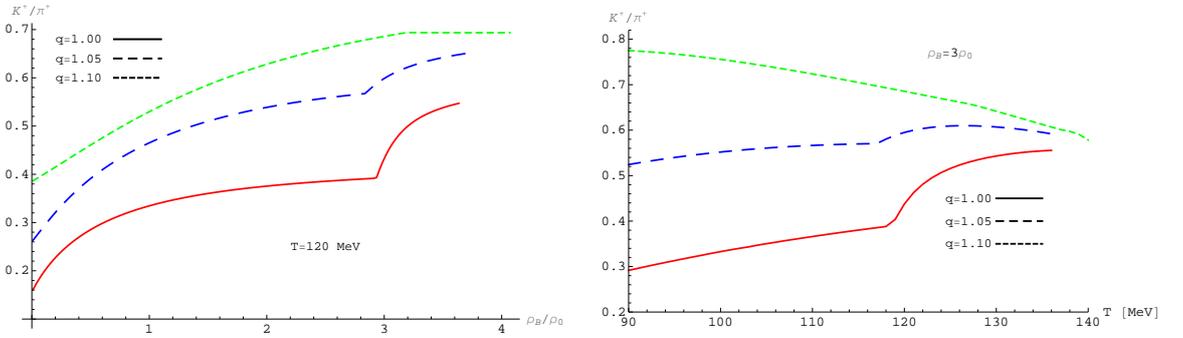
Figure 4.17: The same of figure 4.16 for the K^+/π^+ ratio.

($\rho_B \geq 2\,\rho_0$) and intermediate temperatures ($T \approx 100 \div 120$ MeV), while the other way round occurs at low densities and high temperature. This matter of fact is essentially due to the power law behavior of the mean occupational distribution function which weights differently low and high energy states at different baryon densities and temperatures.

The possibility of separating strange from antistrange matter in the hadron-QGP phase transition can lead to a very significant enrichment of strange quarks in the QGP at high baryon density and intermediate temperature. In fact, in the hadronic sector of the mixed phase, the K^+ and K^0 are enhanced and the hyperons are suppressed. Being mesons much lighter than nucleons and their resonances, they carry away entropy, energy and antistrangeness and, therefore, the prompt kaon emission cools and charges the system with finite net strangeness, leading to an even stronger enhancement of the s quarks in the quark phase. This feature, which also depends strongly on the value of the strange particle densities, favors the formation of metastable or stable droplets of strange quark matter which would contain approximately the same amount of u, d and s quarks. The evidence of such a state of quark matter could be related to the existence of exotic hadron states, like a H-dibaryon state, a deeply bound 6-quark state predicted by Jaffe more than thirty years ago [174]. Although many experimental searches for the H-dibaryon were carried out and so far no convincing signal was found [175], very recently evidence for a bound H-dibaryon was claimed based on lattice QCD calculations [176, 177].

In presence of nonextensive statistical effects, the separation of strange and antistrange quarks in the hadron-QGP mixed phase turns out to be less pronounced than in the standard case due to a more symmetric presence of particle and antiparticle at intermediate temperatures. On the other hand, for $q > 1$, the strangeness fractions Y_S (and, consequently, the densities of strange particles) result to be much greater compared to the $q = 1$ case. This matter of fact could be crucial in the formation and survival of strange quark matter droplets in relativistic heavy ion collisions at high compressed baryonic matter.

4.6 Major conclusions

To summarize, in this Chapter we have studied the main features of the nuclear EOS in the hadronic and quark-gluon phase and the possible formation of a consequent mixed phase in presence of nonextensive statistical effects. We have focused our investigation in regime of finite temperature and baryon chemical potential, reachable in high-energy heavy-ion collisions, for which the deconfinement phase transition can be still considered of the second order by Ehrenfest definition (therefore continuous). From a phenomenological point of view, the nonextensive index q is considered here as a free parameter, even if, actually should not be treated as such because, in principle, it should depend on the physical conditions generated in the reaction, on the fluctuation of the temperature and be related to microscopic quantities (such as, for example, the mean interparticle interaction length, the screening length and the collision frequency into the parton plasma). We have restricted our investigation for small deviations from the standard statistics and for values $q > 1$ because, as quoted in the Introduction, these values were obtained in several phenomenological studies in high energy heavy ion collisions. In this context, it is relevant to observe that by fitting experimental observable at $q > 1$, the temperature (or slope) parameter T is usually minor of the one

obtained in the standard Boltzmann-Gibbs statistics ($q = 1$) [27, 26]. This feature is also present in the considered nuclear equation of state because, at fixed energy per particle E/N, we obtain for $q > 1$ lower values of temperature respect to the standard case. Moreover, let us remember that, in the diffusional approximation, a value $q > 1$ implies the presence of a superdiffusion among the constituent particles (the mean square displacement obeys to a power law behavior $\langle x^2 \rangle \propto t^\alpha$, with $\alpha > 1$) [178].

In the first part of the work (Section. 4.4), we have investigated the hadronic equation of state at not to high temperature, assuming that, for this range of temperatures and baryon densities, the presence of strange particles do not significantly affect the main conclusions regarding the relevance of nonextensive statistical effects to the nuclear EOS. We have then imposed the Gibbs conditions on the global conservation of baryon number and electric charge fraction and we have studied the phase transition from hadronic matter to QGP.
We have shown that, also in presence of small deviations from standard Boltzmann-Gibbs statistics, the meson fields and, consequently, the EOS appear to be sensibly modified. We have then analyzed the QGP proprieties using the MIT Bag model, showing that, also in this case, the EOS becomes stiffer in presence of nonextensive effects. Finally, we have show that nonextensive effects play a crucial role in the deconfinement phase transition. Moreover, although pressure as a function of baryon density is stiffer in the hadronic phase, we have shown that a strong softening in the mixed phase takes place in presence of nonextensive statistics. Such a behavior implies an abruptly variation in the incompressibility and could be considered as a signal of nonextensive statistical effects in high energy heavy ion collisions.

In the second part of this Chapter (Section. 4.5), we have studied an effective nuclear EOS in the framework of nonextensive statistical effects at finite temperature and baryon density. By requiring the Gibbs conditions on the global conservation of the baryon number, electric charge fraction and zero net strangeness. Our investigation is focalized in regime of finite temperature and baryon density relevant for future compressed baryonic matter experiments.

We have shown that strange particles are abundantly produced even at moderate temperature and the anti-particles concentration is strongly increased in presence of nonextensive statistical effects. For $q > 1$, the phase transition is characterized by an antistrangess content in the hadron phase while the QGP retains a net strangeness excess at large densities ($\rho_B \geq 2\,\rho_0$) and intermediate temperatures ($T \approx 100 \div 120$ MeV), while the other way round occurs at low densities and high temperature. This matter of fact is essentially due to the power law behavior of the mean occupational distribution function which weights differently low and high energy states at different baryon densities and temperatures.

The possibility of separating strange from antistrange matter in the hadron-QGP phase transition can lead to a very significant enrichment of strange quarks in the QGP at high baryon density and intermediate temperature. In fact, in the hadronic sector of the mixed phase, the K^+ and K^0 are enhanced and the hyperons are suppressed. Being mesons much lighter than nucleons and their resonances, they carry away entropy, energy and antistrangeness and, therefore, the prompt kaon emission cools and charges the system with finite net strangeness, leading to an even stronger enhancement of the s quarks in the

quark phase. This feature, which also depends strongly on the value of the strange particle densities, favors the formation of metastable or stable droplets of strange quark matter which would contain approximately the same amount of u, d and s quarks. The evidence of such a state of quark matter could be related to the existence of exotic hadron states, like a H-dibaryon state, a deeply bound 6-quark state predicted by Jaffe more than thirty years ago [174]. Although many experimental searches for the H-dibaryon were carried out and so far no convincing signal was found [175], very recently evidence for a bound H-dibaryon was claimed based on lattice QCD calculations [176, 177].

In presence of nonextensive statistical effects, the separation of strange and anti-strange quarks in the hadron-QGP mixed phase turns out to be less pronounced than in the standard case due to a more symmetric presence of particle and antiparticle at intermediate temperatures. On the other hand, for $q > 1$, the strangeness fractions Y_S (and, consequently, the densities of strange particles) result to be much greater compared to the $q = 1$ case. This matter of fact could be crucial in the formation and survival of strange quark matter droplets in relativistic heavy ion collisions at high compressed baryonic matter and can be considered an important feature for the experimental identification of the on-set of nonextensive statistical effects in the nuclear medium.

Chapter 5

Chemical and mechanical instability in a finite temperature and dense nuclear matter.

In this last Chapter, we are planning to investigate the chemical and mechanical instability in a finite temperature and dense nuclear medium, with particular attention to the liquid-gas and nucleon-Δ-matter phase transition and the possible onset of strangeness instability at hight temperature and finite baryon density.

5.1   Introduction

We conclude this Thesis work, with a detailed study of the thermodynamical properties of strongly interacting nuclear matter away from the nuclear ground state. This research field, constitutes one of the most interesting aspects of the experiments on heavy-ion collisions and one of the major tasks of modern high energy nuclear physics.
In this direction, many efforts were focused on searching for possible phase transitions in such collisions. At low temperatures ($T \leq 10$ MeV) and subnuclear densities, a liquid-gas type of phase transition was first predict theoretically [179, 180, 181] and later observed experimentally in a nuclear multifragmentation phenomenon at intermediate-energy nuclear reactions [61, 62].

Because nuclei are made of neutrons and protons, the nuclear liquid-gas phase transition is in a binary system where one has to deal with two independent proton and neutron chemical potentials for baryon number and electric charge conservation. This was made be taking in consideration a very detailed study of Müller and Serot [76] focused on the main thermodynamic properties of asymmetric nuclear matter in the framework of a relativistic mean field model.

A relevant aspect of a system with two conserved charges (baryon and isospin numbers) is that the phase transition is of second order from the viewpoint of Ehrenfest's definition. At variance with the so-called Maxwell construction for one conserved charge, the pressure is not constant in the mixed phase and therefore the incompressibility does not vanish [76, 77].

Such feature plays a crucial role in the structure and in the possible hadron-quark phase transition in compact star objects [78, 79]. Moreover, for a binary system with two phases, the binodal coexistence surface is two dimensional and the instabilities in the mixed liquid-gas phase arise from fluctuations in the proton concentration (chemical instability) and in the baryon density (mechanical instability) [76, 80, 81, 82].

As already discussed in the previous Chapters and in the Introduction, although the equation of state (EOS) at density below the saturation nuclear matter is relatively well known due to the large amount of experimental nuclear data available, at larger density there are many uncertainties; the strong repulsion at short distances of nuclear force makes, in fact, the compression of nuclear matter quite difficult. However, in relativistic heavy-ion collisions the baryon density can reach values of a few times the saturation nuclear density ρ_0 and/or high temperatures.

In this condition, a state of high density resonance matter may be formed and the $\Delta(1232)$-isobar degrees of freedom are expected to play a central role in relativistic heavy ion collisions and in the physics of compact stars [63, 64, 65, 66, 67]. Transport model calculations and experimental results indicate that an excited state of baryonic matter is dominated by the Δ-resonance at the energy from AGS to RHIC [68, 69, 70, 71]. In this direction, very interesting results have been obtained at low energy at the CERN Super Proton Collider (SPS) and at low-energy scan at BNL Relativistic Heavy Ion Collider (RHIC) [112, 113, 114]. Moreover, in symmetric nuclear matter and in the framework of a non-linear Walecka model, it has been predicted that a phase transition from nucleonic matter to Δ-excited nuclear matter can take place and the occurrence of this transition sensibly depends on the Δ-meson coupling constants [72, 73].

The information coming from experiments with heavy ions in intermediate- and high-energy collisions is that the EOS depends on the energy beam but also sensibly on the electric charge fraction y of the colliding nuclei, especially at not too high temperature [74, 75]. Moreover, the study of nuclear matter with arbitrary electric charge fraction results to be important in radioactive beam experiments and in the physics of compact stars.

In this last Chapter, we are planning to study the hadronic equation of state (EOS) at finite temperature and density by means of a relativistic mean-field model with the inclusion Δ-isobars and pion degrees of freedom, by requiring the Gibbs conditions on the global conservation of baryon number and net electric charge. We will also deeply investigated the liquid-gas phase transition both in the extensive and nonextensive context.

Finally, we will present a preliminary study of the possible onset of strangeness diffusional instability, in a multi-component system with two (B, S) and three $(B, C$ and $S)$ conserved charges, over a wide range of baryon density $\rho_0 < \rho_B < 4\rho_0$ and for $T > 70$ MeV.

The main goal of this Chapter is therefore the research and the investigation of the possible phase transitions in the nuclear medium, over a very wide range of temperatures and baryon densities, through the study of the mechanical and chemical instabilities.

This chapter is based on the results obtained in [88, 182].

5.2 Hadronic equation of state

In order to make a complete description of the possible phase transitions in the nuclear medium, at the increasing of the temperature and baryons density, we have to take in consideration different degrees of freedom in the Lagrangian density.
For this reason, we dived this analyze in three parts.

- The first one, at low temperature and baryon density ($T \approx 10$ MeV and $\rho_B \leq 1\rho_0$), where the relevant degrees of freedom are nucleons and a liquid-gas phase transition is expected.

- A second part, at higher temperature and baryon density ($T \leq 50$ MeV and $\rho_0 \leq \rho_B \leq 3\rho_0$), where a phase transition from nucleonic matter to resonance-dominated Δ-matter is expected and the relevant degrees of freedom of the system become nucleons, Δ-isobars and pions.

- Finally, we study the possible on-set of strangeness instability at higher temperature and finite baryon density (70 MeV $< T <$ 140 MeV and $\rho_0 \leq \rho_B \leq 4\rho_0$), where the relevant degrees of freedom are nucleons, pions and strange particles (hyperons and strange mesons), introduced through the effective relativistic mean field model of section 1.4.1 and the chiral one of section 1.4.2.

In this numerical investigation, the meson-nucleon coupling constants and the other parameters (a, b, c) of the Lagrangian density (1.27) will be fixed to the parameters set marked as $TM1$ of Tab. (1.2).

The analyze of the liquid-gas phase transition is performed by requiring the conservation of the baryon number (B) and the electric charge (C), requiring the Gibbs stability condition for the phase coexistence regions. The scalar and vector baryon density and the nuclear EOS are given as usual by eq.s (1.34), (1.35) and (1.39)–(1.40).

The analyze of the Δ-matter phase transition is instead more complicated, primarily due to the presence of Δ-isobars. As known, there is no relativistic quantum theory for the Δ as a spin 3/2 field without any inconsistency when imposing other fields such as the ones with electromagnetic interaction [183]. Anyway, as exposed in Section 1.3.1 and following the Rarita-Schwinger formalism, the spin 3/2 particle, described by means of a vector spinor state, has off-shell spin 1/2 sector. To incorporate Δ-isobars in the framework of effective hadron field theories a formalism was developed treating Δ analogously to the nucleon, taking only the on-shell Δs into account and the mass of the Δs are substituted by the effective one in the RMF approximation [184, 185]. The Δ Lagrangian density, take therefore the form of eq. (1.48).
Following the prescription of Section (1.3), (1.3.1) and (1.4.1), the relevant equations for baryons are given by equations (1.34), (1.35) and (1.39)–(1.40), whereas, for mesons, by eq.s (1.53)–(1.55). Let us observe that the contribution of the lightest non-strange mesons (pions) may not be neglected in regime of temperature and density achieved during the possible Δ-matter phase transition. Taking into account eq. (1.50), from a phenomenological point of view, we can consider the pion degrees of freedom by adding their one-body contribution to the thermodynamical potential, that is, as discussed in Section 1.4.1, the contribution of

an ideal Bose gas with an effective pion chemical potential μ_π^*, depending self-consistently from the meson fields.

Of course, this naive phenomenological approach cannot incorporate the very complex $\pi N \Delta$ interaction at finite temperature and baryon density and a more realistic chiral symmetric model should be implemented. On the other hand, as we will see in Section 5.5, such an effective nuclear EOS has the noticeable advantage of simplifying the very complex numerical analysis involved in seeking of thermodynamic instabilities and in the construction of the mixed phase. Due to this matter of fact, it would be prudent to consider the following results as a preliminary study, that will be investigated in more detail in future, for example with the introduction of a ρ-Δ coupling constant.

In this context, let us observe that, for the range of temperatures and baryon densities considered in this investigation ($T \leq 50$ and $\rho_B \leq 3\,\rho_0$), the contribution of strange hadrons, due to their very low concentration, can be in a good approximation neglected. In fact, unlike compact stars in β-stability regime, since weak-decays cannot take place during the short life-time of high density system, the only possibility of producing strangeness is through associated production but, in the scenario we are discussing, this process has been shown to be very inefficient [186, 165] and, therefore, the study of the possible phase transition can be limited to two conserved charges.

Finally, strangeness instability is investigated in a very high temperature and dense nuclear medium of two (B and S) and three (B, C and S) conserved charges. The inclusion of strange particles (hyperons and strange mesons), was made following the prescription of section 1.3 and through the effective formulation exposed in section 1.4.1 and the chiral model of section 1.4.2.

The hadronic pressure and energy density are given by the sum of the baryon (B) and meson (M) contribution: $\varepsilon = \varepsilon_B + \varepsilon_M$ and $P = P_B + P_M$.

5.3 Phase transition and stability condition

5.3.1 Two conserved charges (B and C)

As already stated, we are dealing with the study of a multi-component system at finite temperature and density with two conserved charges: baryon number (B) and electric charge (C). For such a system, the Helmholtz free energy density F can be written as

$$F(T, \rho_B, \rho_C) = -P(T, \mu_B, \mu_C) + \mu_B \rho_B + \mu_C \rho_C \,, \qquad (5.1)$$

with

$$\mu_B = \left(\frac{\partial F}{\partial \rho_B} \right)_{T, \rho_C} , \quad \mu_C = \left(\frac{\partial F}{\partial \rho_C} \right)_{T, \rho_B} . \qquad (5.2)$$

In a system with N different particles, the particle chemical potentials are expressed as the linear combination of the two independent chemical potentials μ_B and μ_C and, as a consequence, $\sum_{i=1}^{N} \mu_i \rho_i = \mu_B \rho_B + \mu_C \rho_C$. Therefore, the number of particles may change during a process and, at variance of density and temperature, different particle degrees of freedom may be relevant in the description of the system (for example, at low temperature

and density, we have protons and neutrons only, while at higher temperature and density other kind of particles, such as Δ-isobars, can appear). What it is actually relevant for the thermodynamical description under consideration are only the two conserved charges and not the number of different particles constituent the system.

In general, a system can exist in a number of different phases, each of which exhibit quite different macroscopic behavior. The single phase that is realized for a given set of independent variables is the one with the lowest free energy. In a system with two conserved charges, it is possible to have $N_{\max} = 4$ phase coexistence regions in thermodynamical equilibrium [187, 188], even if we have found no evidence for the existence of more than two phases in the regime investigated in this study. By assuming the presence of two phases (denoted as I and II, respectively), the system is stable against the separation in two phases if the free energy of a single phase is lower than the free energy in all two phases configuration. The phase coexistence is given by the Gibbs conditions

$$\mu_B^I = \mu_B^{II}\,, \qquad \mu_C^I = \mu_C^{II}\,, \tag{5.3}$$

$$P^I(T, \mu_B, \mu_C) = P^{II}(T, \mu_B, \mu_C)\,. \tag{5.4}$$

Therefore, at a given baryon density ρ_B and at a given net electric charge density $\rho_C = y\,\rho_B$, the chemical potentials μ_B are μ_C are univocally determined by the following equations

$$\rho_B = (1 - \chi)\,\rho_B^I(T, \mu_B, \mu_C) + \chi\,\rho_B^{II}(T, \mu_B, \mu_C)\,, \tag{5.5}$$

$$\rho_C = (1 - \chi)\,\rho_C^I(T, \mu_B, \mu_C) + \chi\,\rho_C^{II}(T, \mu_B, \mu_C)\,, \tag{5.6}$$

where $\rho_B^{I(II)}$ and $\rho_C^{I(II)}$ are, respectively, the baryon and electric charge densities in the low density (I) and in the higher density (II) phase and χ is the volume fraction of the phase II in the mixed phase ($0 \leq \chi \leq 1$).

An important feature of this conditions is that, unlike the case of a single conserved charge, the pressure in the mixed phase is not constant and, although the total ρ_B and ρ_C are fixed, baryon and charge densities can be different in the two phases, according to Eq.s (5.15) and (5.16).

For such a system in thermal equilibrium, the possible phase transition can be characterized by mechanical (fluctuations in the baryon density) and chemical instabilities (fluctuations in the electric charge density). As usual the condition of the mechanical stability implies

$$\rho_B \left(\frac{\partial P}{\partial \rho_B} \right)_{T, \rho_C} > 0\,. \tag{5.7}$$

By introducing the notation $\mu_{i,j} = (\partial \mu_i / \partial \rho_j)_{T,P}$ (with $i, j = B, C$), the chemical stability can be expressed with the following conditions [188]

$$\mu_{B,B} > 0\,, \quad \mu_{C,C} > 0\,, \quad \begin{vmatrix} \mu_{B,B} & \mu_{B,C} \\ \mu_{C,B} & \mu_{C,C} \end{vmatrix} > 0\,. \tag{5.8}$$

In addition to the above conditions, for a process at constant P and T, it is always satisfied that

$$\rho_B\,\mu_{B,B} + \rho_C\,\mu_{C,B} = 0\,, \tag{5.9}$$

$$\rho_B\,\mu_{B,C} + \rho_C\,\mu_{C,C} = 0\,. \tag{5.10}$$

Whenever the above stability conditions are not respected, the system becomes unstable and the phase transition take place. The coexistence line of a system with one conserved charge becomes in this case a two dimensional surface in (T, P, y) space, enclosing the region where mechanical and diffusive instabilities occur.

5.3.2 Strangeness stability condition

At higher temperature, when strangeness degrees of freedom become important, the Helmholtz free energy density takes the form:

$$F(T, \rho_B, \rho_C, \rho_S) = -P(T, \mu_B, \mu_C, \mu_S) + \mu_B \rho_B + \mu_C \rho_C + \mu_S \rho_S \,, \tag{5.11}$$

with

$$\mu_B = \left(\frac{\partial F}{\partial \rho_B}\right)_{T, \rho_C} \,, \quad \mu_C = \left(\frac{\partial F}{\partial \rho_C}\right)_{T, \rho_B} \,, \quad \mu_S = \left(\frac{\partial F}{\partial \rho_S}\right)_{T, \rho_S} \,. \tag{5.12}$$

In a system with three conserved charges, at most $N_{\mathrm{Max}} = 5$ phase in thermodynamical equilibrium can coexist [187]. However, as for the LG and Δ-matter phase transition, we do not find any evidence of more then two phases.

In this context, the Gibbs condition for the phase coexistence becomes:

$$\mu_B^I = \mu_B^{II} \,, \qquad \mu_C^I = \mu_C^{II} \,, \qquad \mu_S^I = \mu_S^{II} \,, \tag{5.13}$$

$$P^I(T, \mu_B, \mu_C, \mu_S) = P^{II}(T, \mu_B, \mu_C, \mu_S) \,. \tag{5.14}$$

Therefore, at a given baryon density ρ_B and at a given net electric charge density $\rho_C = y\,\rho_B$ and strangeness density $\rho_S = z\,\rho_B$, the chemical potentials μ_B, μ_C and μ_S are univocally determined by the following equations

$$\rho_B = (1 - \chi)\,\rho_B^I(T, \mu_B, \mu_C, \mu_S) + \chi\,\rho_B^{II}(T, \mu_B, \mu_C, \mu_S) \,, \tag{5.15}$$

$$\rho_C = (1 - \chi)\,\rho_C^I(T, \mu_B, \mu_C, \mu_S) + \chi\,\rho_C^{II}(T, \mu_B, \mu_C, \mu_S) \,, \tag{5.16}$$

$$\rho_S = (1 - \chi)\,\rho_S^I(T, \mu_B, \mu_C, \mu_S) + \chi\,\rho_S^{II}(T, \mu_B, \mu_C, \mu_S) \,, \tag{5.17}$$

where $\rho_B^{I(II)}$, $\rho_C^{I(II)}$ and $\rho_S^{I(II)}$ are, respectively, the baryon, the electric charge and the strangeness densities in the low density (I) and in the higher density (II) phase and χ is the volume fraction of the phase II in the mixed phase $(0 \leq \chi \leq 1)$.

In this context, analogously to eq. (5.8), the chemical stability condition can be written as:

$$\mu_{B,B} > 0 \,, \quad \mu_{C,C} > 0 \,, \quad \mu_{S,S} > 0 \,, \quad \begin{vmatrix} \mu_{B,B} & \mu_{B,C} & \mu_{B,S} \\ \mu_{C,B} & \mu_{C,C} & \mu_{C,S} \\ \mu_{S,B} & \mu_{S,C} & \mu_{S,S} \end{vmatrix} > 0 \,, \tag{5.18}$$

where, for a process at constant P and T, we obtain

$$\rho_B\,\mu_{B,B} + \rho_C\,\mu_{C,B} + \rho_S\,\mu_{S,B} = 0 \,, \tag{5.19}$$

$$\rho_B\,\mu_{B,C} + \rho_C\,\mu_{C,C} + \rho_S\,\mu_{S,C} = 0 \,, \tag{5.20}$$

$$\rho_B\,\mu_{B,S} + \rho_C\,\mu_{C,S} + \rho_S\,\mu_{S,S} = 0 \,. \tag{5.21}$$

The mechanical stability condition, is always given by eq. (5.7).

Finally, we will explore the possible onset of strangeness instability in the hadronic system, by requiring the conservation of only two charges (B and S), under the assumption that, at higher temperature, the effects of isospin asymmetry becomes less relevant. Therefore, in analogy to eq.s (5.9) and (5.24), we can write the stability conditions for a process at constant P and T, as:

$$\rho_B \, \mu_{B,B} + \rho_S \, \mu_{S,B} = 0 \,, \tag{5.22}$$

$$\rho_B \, \mu_{B,S} + \rho_S \, \mu_{S,S} = 0 \,. \tag{5.23}$$

As for the LG case or the Δ-matter phase transition, whenever the above stability conditions (eq.s 5.19–5.23) are not respected, the system becomes unstable and a phase transition is expected.

5.4 Liquid-gas phase transition

As already stated in the previous sections, in regime of low temperature and baryon density, relevant in the liquid-gas phase transition, only proton and neutron degrees of freedom take place. In this simple case, for example, Eq.(5.9) can be written as

$$y \left(\frac{\partial \mu_p}{\partial y} \right)_{T,P} + (1 - y) \left(\frac{\partial \mu_n}{\partial y} \right)_{T,P} = 0 \,, \tag{5.24}$$

where $y = \rho_p / \rho_B$. Because we are working with a proton fraction $0 < y \leq 0.5$, the chemical stability conditions (5.8) are therefore satisfied if

$$\left(\frac{\partial \mu_p}{\partial y} \right)_{T,P} > 0 \quad \text{or} \quad \left(\frac{\partial \mu_n}{\partial y} \right)_{T,P} < 0 \,, \tag{5.25}$$

(due the validity of Eq.(5.24), the first above condition implies the second one and viceversa).

As already observed, in presence of two conserved charges the liquid-gas phase transition can be characterized by mechanical and chemical instabilities [76]. In order to better put this feature in focus, we report in Fig. 5.1 the pressure as a function of baryon density for various values of the electric charge fraction y at fixed temperature $T = 10$ MeV. The continuous lines correspond to the solution obtained with the Gibbs construction, whereas the dashed lines are without correction. For a proton fraction $y > 0.2$ a mechanical instability is present, whereas for $y < 0.2$ the system becomes unstable only under chemical-diffusive instability.

The presence of chemical unstable regions are much better evident in Fig. 5.2, where we show the proton and neutron chemical potentials for various isobars at constant temperature, as a function of the proton asymmetry. Below $P = 0.25$ MeV/fm^3, the system becomes unstable because of the presence of regions of negative (positive) slope for μ_p (μ_n).

In order to study the phase coexistence of the system, in the Fig. 5.3, we show the binodal section as a function of the proton asymmetry y at $T = 10$ MeV. Following the same notation of Ref. [76], the binodal surface is divided in two branches by a critical
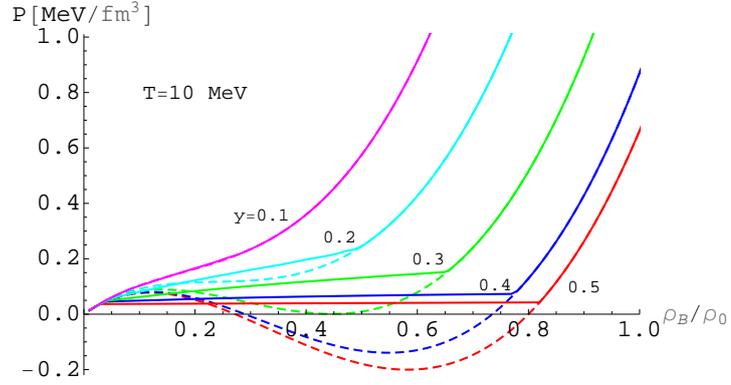
Figure 5.1: Pressure as a function of baryon density for various values of the proton fraction. The continuous/dashed lines correspond to the solution obtained with/without the Gibbs construction.
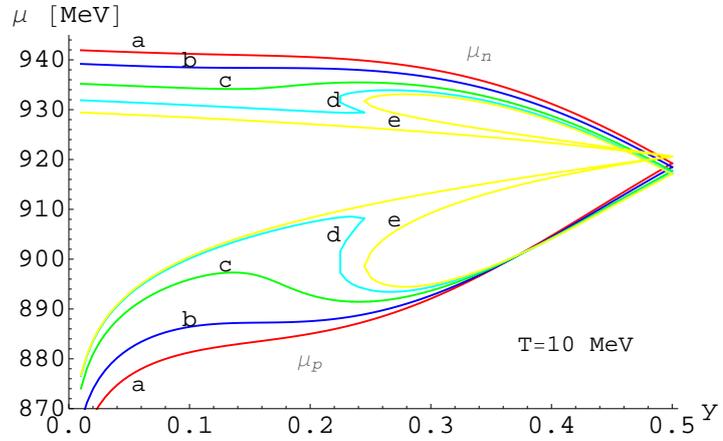
Figure 5.2: Proton and neutron chemical potential as a function of the proton fraction y for various isobars (P=0.25,0.20,0.15,0.10,0.075 MeV/fm^3) (lines from a to e) at T=10 MeV.
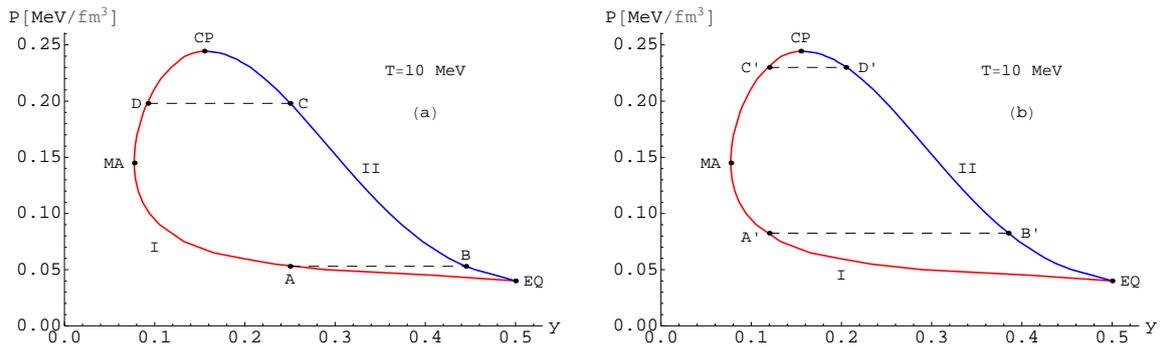
Figure 5.3: Binodal section at $T = 10$ MeV, with in evidence the critical point (CP), the point of maximum asymmetry (MA) and the point of equal equilibrium (EQ). In the left and right panel are reported the evolution of the mixed phase for two different system configurations (see the text for details).

point (CP) and a point of equal equilibrium (EQ) at $y = 0.5$, where protons and neutrons have the same concentration. The left branch of the diagram represents the initial phase configuration of the system at lower density (gas phase, I) and the second branch, at higher density, corresponds to the final phase configuration (liquid phase, II).

The binodal surface encloses the area where the system undergoes to the phase transition. The mixed phase region extends up to small values of the proton asymmetry, whereas the mechanical instability region ends around $y \simeq 0.2$, in agreement with the results of Ref. [76].

During the isothermal compression, the system evolves through configuration at constant y and meets the first branch in a point A. At this point the system becomes unstable and an infinitesimal phase in B appears at the same temperature and pressure of A. In this context, let us remember that, although the proton asymmetry is globally conserved, this is not true for the single phase. In particular, for an asymmetric nuclear system is energetically favorable to separate into a liquid phase (less asymmetric) and a gas phase (more asymmetric), than into two phases with equal proton fraction.

If the point A have a value of y_A greater than the corresponding values y_{CP} of the CP (as in the left panel of Fig. 5.3), the system ends the phase transition in the liquid phase (in the point C). On the other hand, as already observed in Ref. [76], if the system has been prepared in a very asymmetric configuration with $y_{A'} < y_{CP}$ (right panel of Fig. 5.3), it undergoes to a retrograde phase transition. A second liquid-phase in B' is formed but after reaching a point of maximum volume fraction $\chi_{max} < 1$, the system returns to its initial gas phase in the point C'. Note that, this kind of phase transition is possible only for a multi-component system and in this case, is purely diffusive.

In order to better characterize the evolution of the two phases, in Fig. 5.4, the volume fraction χ of the second phase during the phase transition is showed. By increasing the asymmetry parameter of the system under consideration (at lower values of y), the
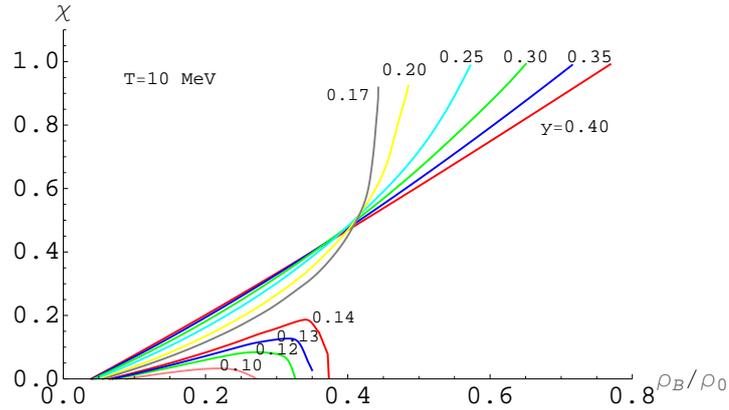
Figure 5.4: Evolution of the volume fraction χ of the second phase as a function of the baryon density, for system with different values of y at $T = 10$ MeV.

maximum density achieved during the mixed phase decreases, until the system undergoes to a retrograde phase transition (for $y < 0.15$).

5.4.1 Nonextensive liquid-gas phase transition

A very interesting aspect of the LG phase transition, due to the low degrees of freedom of the system (only protons and nucleons are presents in our analyze), is the possibility of study such phase transition in the framework of non extensive effects.

In this case, as amply discussed in Chapter (2), the particle thermal distribution function take the form of eq. (2.21) and using the Wilk prescription, we obtain the eq.s (2.22) and (2.23). In this context, the baryon and scalar density and the EOS for the nuclear Lagrangian (1.27), take the form of eq.s (2.24)–(2.25) and (2.28)–(2.29).

The condition for the onset of mechanical and chemical instability are obviously the same of the extensive case, exposed in sections 5.3 and 5.4.1.

The main goal of this analyze, is therefore, to put in evidence the relevance of the possible onset of nonextensive effect in a warm nuclear medium at low baryon density, condition reached during the liquid-gas phase transition.

In particular, in the following, we compare the results obtained for a very small deviation form the standard statistics ($q = 1.02$) to that of the extensive case.

In this context, as amply discussed in Chapters 2 and 4, the relevance of nonextensive effect are bigger as higher is the temperature of the system. However, although during the LG phase transition the temperature of the system is typically of the order of 10 MeV, in presence of nonextensive effects, the pressure and the isobars are sensibly modified(this is probably due to the possible onset of strong-dynamical correlation during the phase transition process).

This is well evident in Fig. 5.5 and Fig. 5.6, where we report, respectively, the pressure as a function of the baryon density for different values of y and q and various isobars as a

function of y in the extensive and nonextensive case.

In particular, in the left panel of Fig. 5.5, we show the variation in the nuclear EOS in presence (dashed lines) and in absence (continuous lines) of nonextensive effects, for different values of y. As can be observed, also in presence of small deviation from the standard BG statistics, the nuclear EOS appears stiffer, favoring in this way the phase transition. In the right panel of the same graphic, we report the the Gibbs construction (continuous lines) for the nonextensive case. Again, below $y = 0.2$, although the system becomes mechanical stable, it continues to undergoes to a phase transition due to a region of chemical instability.

To better clarify the role played by nonextensive effect during the LG phase transition, we
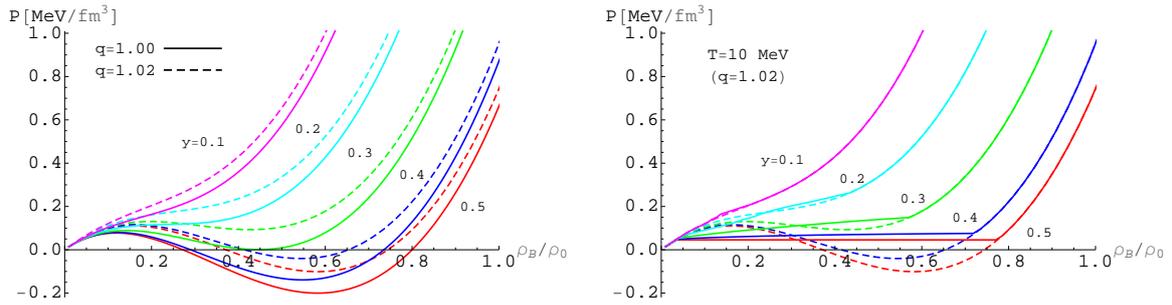
Figure 5.5: Pressure as a function of the baryon density for different proton fraction at $T = 10$ MeV, in presence and in absence of nonextensive effects (left panel) and for $q = 1.02$ (right panel), with and without Gibbs correction, continuous and dashed lines respectively.
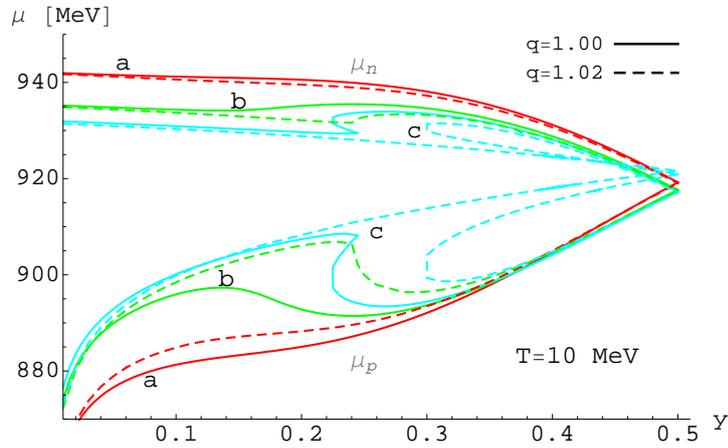
Figure 5.6: Proton and neutron chemical potential as a function of the proton fraction y for various isobars ($P = 0.35, 0.15, 0.10$ MeV/fm^3) (lines from a to c) at $T = 10$ MeV and $q = 1$ and $q = 1.02$.

show in Fig. 5.6, the neutrons and protons chemical potential isobars, at $q = 1$ (continuous lines) and $q = 1.02$ (dashed lines).

Here, we observe again a strong variation of such isobars in particular at $P = 10$ MeV/fm^3, where a strong region of chemical instability, over a wide range of charge asymmetry fraction is present. However, although a remarkable difference in the shape of such isobars, we do not observe a significantly variation in the shape of the binodal diagram, and therefore in the region of mechanical and chemical instability.

This is well evident in Fig 5.7, where we report the binodal section at $T = 10$ MeV in the extensive (continuous line) and nonextensive (dashed line) case.

The two diagrams are almost the same, apart for the fact that, in presence of nonextensive effects, the instability region ends at an higher pressure ($P \approx 27$ MeV/fm^3) and the system achieved a less asymmetric charge configuration. Instead, the point of equal equilibrium and the region of retrograde phase transition, are not strongly modified. This is because at low baryon density (pressure) for these low values of the temperature, nonextensive effects play only a marginal rule and therefore does not change considerably the thermodynamical proprieties of the system.
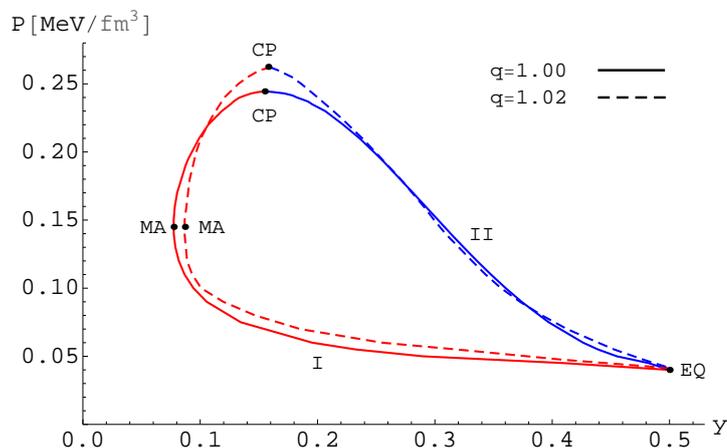
Figure 5.7: Binodal section at $T = 10$ MeV, with in evidence the critical point (CP), the point of maximum asymmetry (MA) and the point of equal equilibrium (EQ), at $T = 10$ MeV, for $q = 1$ and $q = 1.02$.

In order to better characterize the evolution of the two phases, in Fig. 5.7, we report, in analogy to Fig. 5.4, the volume fraction χ of the second phase during the phase transition. It does not change sensibly from the corresponding one at $q = 1$, except for the lower value of the second critical density at which the LG phase transition ends, both for normal and retrograde phase transition. In particular, by increasing the asymmetry parameter of the system (at lower values of y), the maximum density achieved during the mixed phase decreases, until the system undergoes to a retrograde phase transition (for $y < 0.16$), almost the same value of the extensive case. Finally, in Fig. 5.9, we report the phase diagram in presence and in absence of nonextensive effects, respectively marked with dashed and
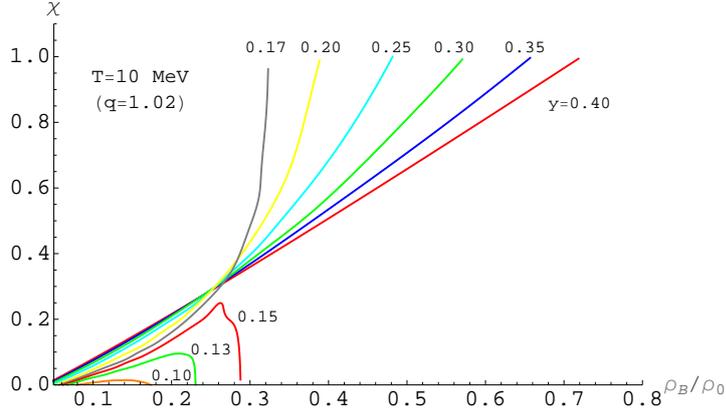
Figure 5.8: Evolution of the volume fraction χ of the second phase as a function of the baryon density, for system with different values of y at $T = 10$ MeV and $q = 1.02$.
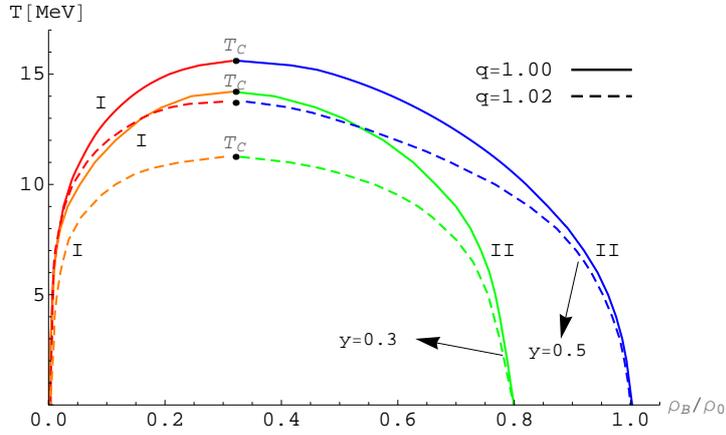
Figure 5.9: Phase diagram of the liquid-gas phase transition for $y = 0.5$ and $y = 0.3$ for the extensive (continuous curves) and non extensive case (dashed curves). The lines labeled with I and II, delimitate the first and second critical density of the coexistence regions, respectively.

continuous lines and for two different proton fractions ($y = 0.5$ and $y = 0.3$).

As one can easily observe, the most important effect in presence of small deviations from the standard statistics, regards the redaction of the critical temperature. In particular, in presence of nonextensive effects, it is lowered of about 1.8 MeV at $y = 0.5$ and of about 2.4 MeV at $y = 0.3$. This implies a reduction in the first and second critical density at moderate temperature. In this sense, the presence of nonextensive effects favor the phase transition, anticipating the onset of the MP and the formation of the liquid phase.

Furthermore, we would like to stress that, at very low temperature for a fixed y, the extensive

and nonextensive formulation converge to the same values of baryon density, therefore the presence of nonextensive effects become negligible.

The reduction in the critical temperature, together with the reduction in the first and second critical density, can be considered as important indication of the possible onset of nonextensive effects in the nuclear medium.

5.5 Δ-matter phase transition

5.5.1 General considerations

By increasing the temperature and the baryon density during the high energy heavy ion collisions ($T \approx 50$ MeV and $\rho_0 \leq \rho_B \leq 3\rho_0$), a multi-particle system with nucleons, Δ-isobar and pion degrees of freedom may take place. The Δ QHD-Lagrangian density and the EOS are defined in Chapter 1.3.1.

To better understand the relevance of Δ-isobars and the dependence of the EOS on the meson-Δ coupling constants ($x_{\sigma\Delta} = g_{\sigma\Delta}/g_{\sigma N}$, $x_{\omega\Delta} = g_{\omega\Delta}/g_{\omega N}$), in Fig. 5.10, we report the energy per baryon as a function of the baryon density at zero temperature and $y = 0.5$, for different values of $x_{\sigma\Delta}$ and $x_{\omega\Delta} = 1$. Let us note that, by increasing the value of $x_{\sigma\Delta}$, a second minimum on the energy per baryon appears.

Following Ref. [98], in setting $x_{\sigma\Delta}$ and $x_{\omega\Delta}$, we have to require that:

i) the second minimum of the energy per baryon lies above the saturation energy of normal nuclear matter, i.e., in the mixed Δ-nucleon matter only a metastable state can occur;

ii) there are no Δ-isobars present at the saturation density;

iii) the scalar field is more (equal) attractive and the vector potential is less (equal) repulsive for Δs than for nucleons, in accordance with QCD finite-density calculations [99].

In this context, it is proper to remember that QCD sum-rule predictions for the scalar self-energy are sensitive to the unknown density dependence of four-quark condensates and due to this, there is no certainly reliable information about the coupling constant of the Δ-isobars with scalar mesons.

Of course, the choice of couplings that satisfies the above conditions is not unique but exists a finite range of possible values (represented as a triangle region in the plane $x_{\sigma\Delta}$-$x_{\omega\Delta}$) which depends on the particular EOS under consideration [98]. Without loss of generality, in the following we can limit our investigation to move only in a side of such a triangle region by fixing $x_{\omega\Delta} = 1$ and varying $x_{\sigma\Delta}$ from unity to a maximum value compatible with the aforementioned conditions. As can be observed in Fig. 5.10, for the TM1 parameter set, such a maximum value corresponds to $x_{\sigma\Delta}^{\max} = 1.33$, while the value $x_{\sigma\Delta}^{\mathrm{II}} = 1.27$ corresponds to the appearance of the second minimum on the energy per baryon with the formation of a metastable state. Analogue behaviors can be obtained with other EOS parameters set (see, for example, Ref. [67] for more details).

In Fig. 5.11, we show in symmetric nuclear matter the relative nucleon (solid lines) and the Δ-isobar (dashed lines) density fraction ($Y_i = \rho_i/\rho_B$), versus the baryon density at $T = 0$ and $T = 50$ MeV, for different values of $x_{\sigma\Delta}$. We observe that Δ-matter becomes
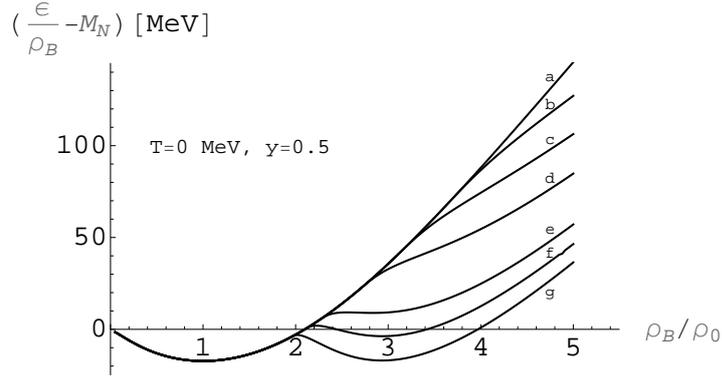
Figure 5.10: The energy per baryon versus baryon density at zero temperature and $y = 0.5$ with (a) without Δ; (b) $x_{\sigma\Delta} = 1.10$; (c) $x_{\sigma\Delta} = 1.15$; (d) $x_{\sigma\Delta} = 1.20$; (e) $x_{\sigma\Delta} = 1.27$; (f) $x_{\sigma\Delta} = 1.30$; (g) $x_{\sigma\Delta} = 1.33$.

dominant with respect to the nucleon concentration at high baryon density and such effect is significantly anticipated by increasing the temperature [1].

In analogy with the liquid-gas case, we are going to investigate the existence of a possible phase transition in the nuclear medium by studying the presence of instabilities (mechanical and/or chemical) in the system.

As already observed in the previous sections, during a phase transition with two conserved charges, the electric charge fraction $y = \rho_C/\rho_B$ is not locally conserved in the single phase but only globally conserved. Therefore, during the compression of the system, the appearance of particles with negative electric charge (such as Δ^-) could, in principle, shift the diffusive instability region to negative values of y, even if the system is prepared with a positive y. Such feature has no counterpart in the liquid-gas phase transition and, as we will see, it turns out to be very relevant in order to properly determine the instability region through the binodal phase diagram.

Taking into account that Eq.(5.24) becomes in this case

$$\left(\frac{\partial \mu_B}{\partial y}\right)_{T,P} + y \left(\frac{\partial \mu_C}{\partial y}\right)_{T,P} = 0 \,, \tag{5.26}$$

the chemical stability condition is satisfied if

$$\left(\frac{\partial \mu_C}{\partial y}\right)_{T,P} > 0 \quad \text{or} \quad \begin{cases} \left(\dfrac{\partial \mu_B}{\partial y}\right)_{T,P} < 0 \,, & \text{if } y > 0 \,, \\[2ex] \left(\dfrac{\partial \mu_B}{\partial y}\right)_{T,P} > 0 \,, & \text{if } y < 0 \,. \end{cases} \tag{5.27}$$

---

[1]Let us remark that the range of baryon density reported in Fig.s 5 and 6 has been chosen in order to better show the effects of different $x_{\sigma\Delta}$ couplings on the formation of Δ-isobars at high baryon density. As we will see, the presence of thermodynamic instabilities will be relevant at lower values of baryon density ($\rho_B \leq 3\,\rho_0$).
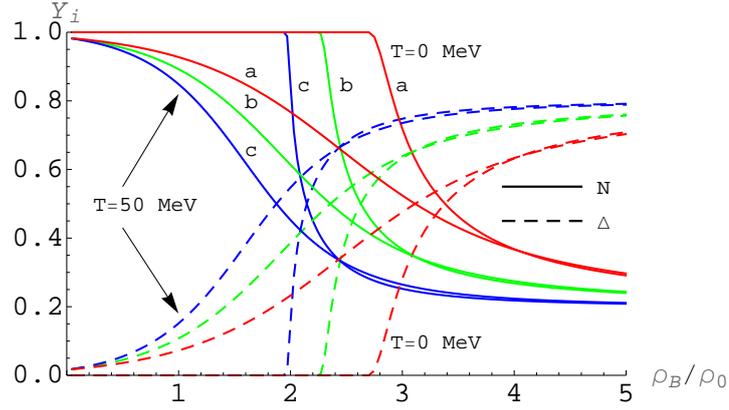
Figure 5.11: The relative nucleons (solid lines) and Δ (dashed lines) densities as a function of the baryon density for different values of temperature with (a) $x_{\sigma\Delta} = 1.2$; (b) $x_{\sigma\Delta} = 1.27$; (c) $x_{\sigma\Delta} = 1.33$.

It is relevant to observe that for the value $x_{\sigma\Delta} = 1$, we do not find any mechanical or diffusive instability. Contrariwise, by increasing the $x_{\sigma\Delta}$ coupling ratio, mechanical and chemical instabilities take place. In particular, in the range: $1 < x_{\sigma\Delta} \leq 1.1$, instabilities are restricted to very low values of temperature and electric charge fraction, but for $x_{\sigma\Delta} > 1.1$, such instabilities start to be much more relevant and extend to higher values of T and y.
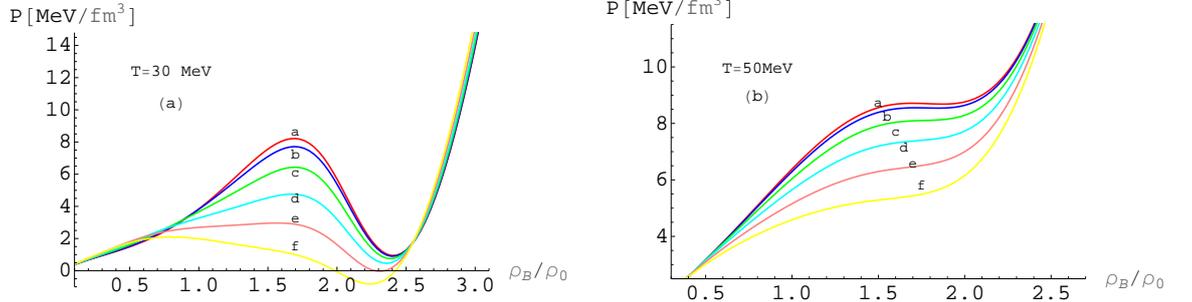
Figure 5.12: Pressure as a function of baryon density for $T = 30$ MeV (left panel) and $T = 50$ MeV (right panel) with $x_{\sigma\Delta} = 1.3$. Letters from a to f correspond to $y = 0.5, 0.4, 0.3, 0.2, 0.1, 0$, respectively.

5.5.2 Mechanical and chemical instability: main results

To better clarify the role played by the σ-Δ coupling constant, we report in Fig. 5.12, the pressure as a function of the baryon density at $T = 30$ MeV (left panel) and $T = 50$ MeV
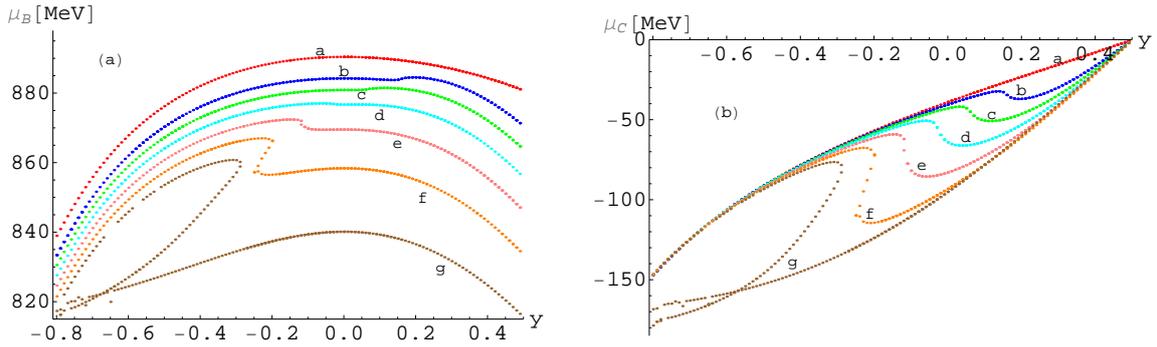
Figure 5.13: Baryon (left panel) and electric charge (right panel) chemical potential isobars as a function of y at $T = 50$ MeV and $x_{\sigma\Delta} = 1.3$. The curves labeled a through g have pressure P=9,7,6,5,4,3,2 MeV/fm^3, respectively.

(right panel), for different values of y and $x_{\sigma\Delta} = 1.3$. In this context it is interesting to observe that at $T = 50$ MeV and below $y = 0.3$, the system becomes mechanically stable, but, in a similar manner to the liquid-gas case, is chemically unstable. This important feature can be better observed in the Fig. 5.13, where we report the baryon and electric charge chemical potential isobars as a function of y, at fixed temperature $T = 50$ MeV and $x_{\sigma\Delta} = 1.3$.

From the analysis of the above chemical potential isobars, we are able to construct the binodal surface relative to the nucleon-Δ matter phase transition. In Fig. 5.14, we show the binodal section at $T = 50$ MeV and $x_{\sigma\Delta} = 1.3$.

The right branch (at lower density) corresponds to the initial phase (I), where the dominant component of the system is given by nucleons. The left branch (II) is related to the final phase at higher densities, where the system is composed primarily by Δ-isobar degrees of freedom (Δ-dominant phase). In presence of Δ-isobars the phase coexistence region results very different from what obtained in the liquid-gas case, in particular it extends up to regions of negative electric charge fraction and the mixed phase region ends in a point of maximum asymmetry with $y = -1$ (corresponding to a system with almost all Δ^--particles, being antiparticles and pions contribution almost negligible in this regime).

Repeating the reasoning made for the liquid-gas phase transition, we analyze the phase evolution of the system during the isothermal compression from an arbitrary initial point A, indicated in Fig. 5.14. In this point the system becomes unstable and starts to be energetically favorable the separation into two phases, therefore an infinitesimal Δ-dominant phase appears in B, at the same temperature and pressure. Let us observe that, although in B the electric charge fraction is substantially negative, the relative Δ^- abundance must be weighed on the low volume fraction occupied by the phase II near the point B ($\chi \approx 0$). During the phase transition ($0 < \chi < 1$), each phase evolves towards a configuration with increasing y, in contrast to the liquid-gas case, where each phase evolves through a configuration with a decreasing value of y (with the exception of the gas phase after the
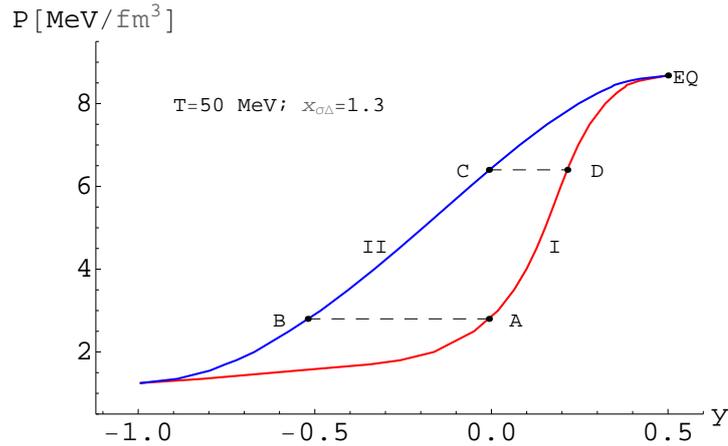
Figure 5.14: Binodal section at $T = 50$ MeV and $x_{\sigma\Delta} = 1.3$.

maximum asymmetry point).

In order to better understand the evolution of the two phases in the mixed phase, we report in Fig. 5.15 the volume fraction χ of the Δ-matter phase as a function of the baryon density. Unlike the liquid-gas case, by decreasing the electric charge fraction y of the system under consideration, the mixed phase involves a greater region of baryon density and extends below the nuclear saturation density.

In the previous example we have consider a fixed value of temperature. The maximum temperature at which the system becomes mechanically stable depends from the particular value of the electric charge fraction. For example, at $y = 0.3$, is about $T_{\max} = 49.5$ MeV and at $y = 0.5$, it is about $T_{\max} = 50.6$ MeV. Furthermore, when $y = 0.5$, the end of the mechanical instability region, obviously, corresponds to the end of the mixed phase region. This is not longer true in presence of two conserved charges. Due to the presence of a diffusive instability region, the mixed phase can extend to slightly higher temperature with respect to the maximum temperature achieved in the symmetric case. Although this feature involves small differences in temperature, is interesting from a conceptual point of view to investigate this aspect in more detail. At this purpose, in Fig. 5.16, we show the pressure as a function of the baryon density and the Gibbs construction (continuous lines) for various values of the electric charge fraction, $x_{\sigma\Delta} = 1.3$ and $T = 51$ MeV (dashed lines are without Gibbs construction). In this case the system is always mechanically stable, while it results unstable for the presence of the chemical-diffusive instability up to $y = 0.35$.

At lower temperatures the mixed phase region becomes more relevant at higher values of y. This feature can be seen in Fig. 5.17 where the binodal section (left panel) and the isothermal pressure as a function of the baryon density (right panel) is reported at $T = 40$ MeV and $x_{\sigma\Delta} = 1.3$. The Gibbs construction corresponds to the curve from A to C; the isothermal curves in B and D (with $y_B \neq y_D$) are also reported. In this case, we assume that the system is initially prepared in the low-density (nucleonic) phase with $y = 0.3$, corresponding to the point A. During the compression each phase evolves following
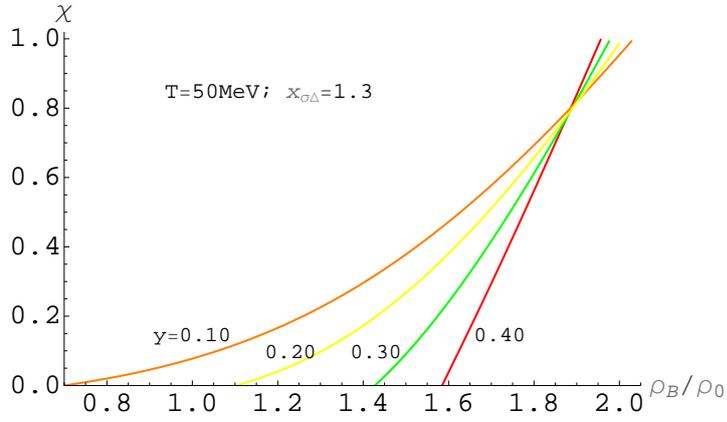
Figure 5.15: Volume fraction of the Δ-matter phase as a function of the baryon density, for system with different values of y.
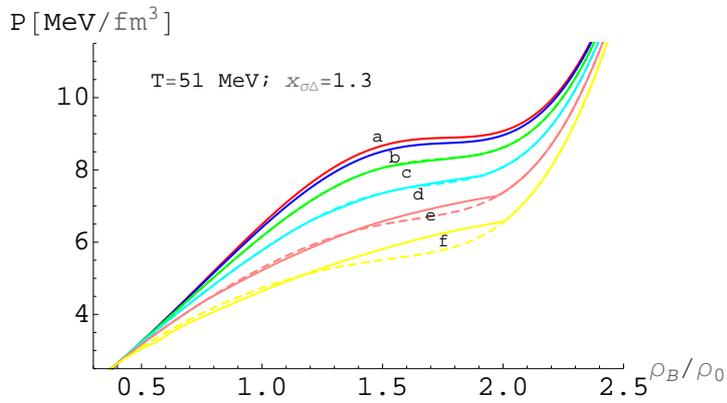
Figure 5.16: Pressure as a function of baryon density at different values of y, from $y = 0.5$ (label a) to $y = 0$ (label f). The continuous/dashed lines correspond to the solution obtained with/without the Gibbs construction.
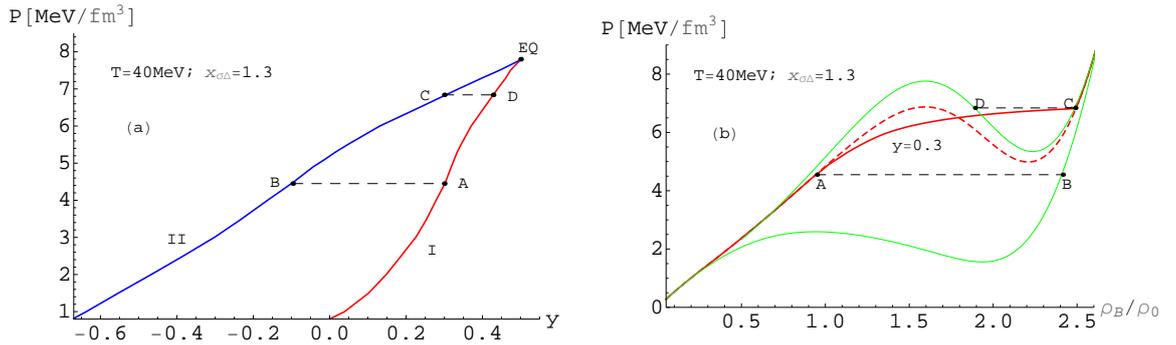
Figure 5.17: Binodal section at $T=$ 40 MeV and $x_{\sigma\Delta} = 1.3$, with in evidence the point of equal equilibrium. Right panel: the corresponding isothermal curves, with in evidence the Gibbs construction (curve from the point A to C) at $y = 0.3$ and the isotherms of the points B and D.

the corresponding curve up to the points C and D, where the system leaves the instability region in the Δ-matter phase.

In Fig. 5.18, we show the Gibbs construction (continuous lines) to the EOS at $y = 0.3$, $x_{\sigma\Delta} = 1.3$ and for different temperatures. By decreasing the temperature, the instability region extends over a wide range of baryon density. In particular, below $T = 40$ MeV, the phase transition starts slightly below the nuclear saturation density.

In order to better characterize the evolution of the system during the isothermal compression of the nuclear medium, we report in Fig. 5.19, the evolution of particles density (in fm^{-3}) before, during and after the phase transition (the dark dashed lines delimits the region of the MP).

In the left panel of Fig. 5.19, we show the particle density as a function of the total baryon density, respectively in the first phase $\rho_i^I = (1-\chi)\rho_i^I$ (continuous lines) and in the second phase $\rho_i^{II} = \chi\rho_i^{II}$ (dashed lines). Δ's particles are negligible in the phase I, but start to be abundantly produced when the system enters in the mixed phase and a II infinitesimal phase, at the same pressure, but in a very asymmetric configuration appears.

In the right panel, we report the total particle density $\rho_i = (1-\chi)\rho_i^I + \chi\rho_i^{II}$ as a function of ρ_B. Δ-isobars start to be the dominant component of the system around $\rho_B \approx 2\rho_0$, and Δ^- becomes the most populated state, due to the high asymmetric configuration reached by the system during the phase transition. Note also the linear grow of Δ's after have reaching the nuclear saturation density.

As already observed, the mixed phase structure results strongly affected not only by the temperature, but also by the particular choice of the $x_{\sigma\Delta}$ coupling. In fact, by decreasing the σ-Δ coupling constant, the mixed phase region shifts to lower temperatures. To better clarify this aspect, we study the phase transition for $x_{\sigma\Delta} = 1.22$ and $T = 20$ MeV (at $T = 50$ MeV, the system results to be mechanically and chemically stable).

In Fig. 5.20, left panel, we report the pressure as a function of the baryon density for
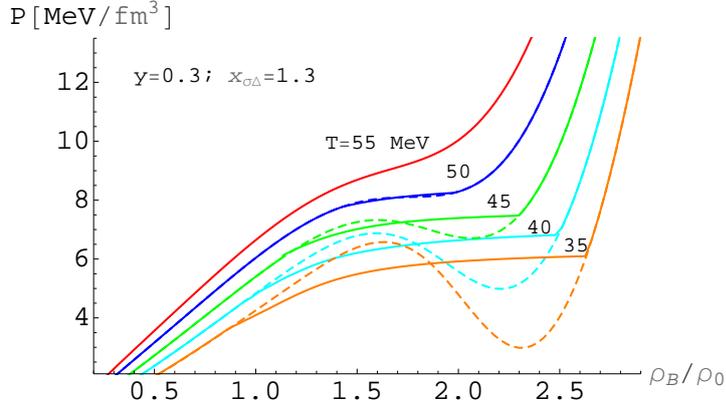
Figure 5.18: Isotherms at constant $y = 0.3$ and $x_{\sigma\Delta} = 1.3$, for various values of temperatures. The solid/dashed lines represent the EOS obtained with/without Gibbs construction.
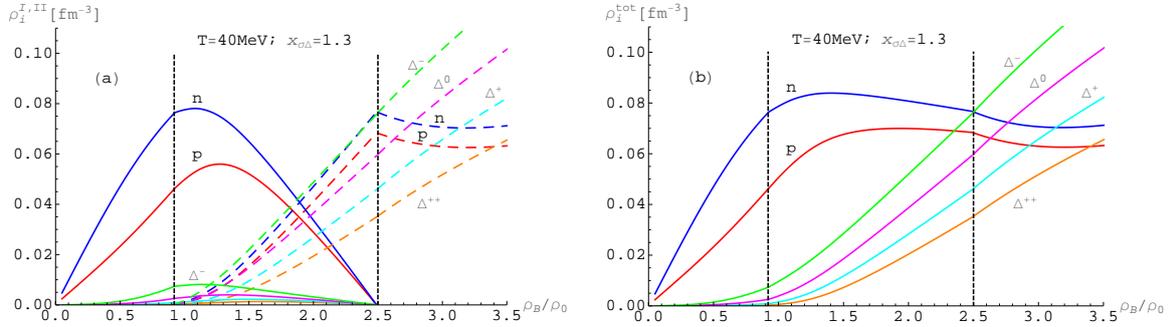
Figure 5.19: Left panel: particles density as a function of the baryon density in the first (continuous lines) and second (dashed lines) phase. Right panel: total particles density as a function of ρ_B ($T = 40$ MeV, $y = 0.3$ and $x_{\sigma\Delta} = 1.3$). The black dashed lines delimits the beginning and the end of the MP.

121
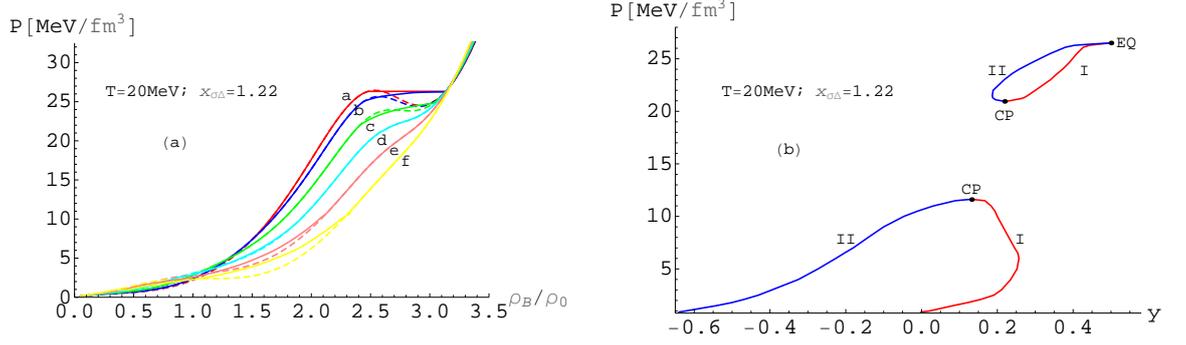
Figure 5.20: Left panel: pressure as a function of the baryon density for different values of y from $y = 0.5$ (label a) to $y = 0$ (label f), with in evidence the instability regions (Gibbs construction in the continuous lines). Right panel: the binodal diagram, with in evidence the point of equal equilibrium and the two critical points. In both the instability sectors a region of retrograde phase transition is present.

different values of y. The continuous lines correspond to the Gibbs construction in the region of instability of the EOS. For this choice of parameters, the binodal section (right panel) is very different with respect to the previous cases and two separate regions of instability are present. The first one extends at lower pressure and it is present only for small value of y, where both mechanical and diffusive instabilities are present. Let us observe that in this lower region, for $y > y_{CP}$, the system undergoes to a retrograde phase transition, likewise to the liquid-gas phase transition. The upper region of instability extends at greater pressures and higher values of y, where mechanical and diffusive instabilities are both present. Also in this second region, on the left of the CP, a retrograde phase transition can occur. However, in this particular case the system is already in a Δ-dominant phase and, at the end of the mixed phase, in which Δ-isobars are partially converted into nucleons, it quickly returns to the Δ-matter phase.

Finally, in Fig. 5.21, we report the phase diagram, in the extensive formulation, with in evidence the coexistence regions of the liquid-gas (at $q = 1$) and the nucleon-Δ matter phase transition for $y = 0.3$ and 0.5 ($x_{\sigma\Delta} = 1.3$). The two coexistence regions are well separated and the features of the two phase transitions are significantly different. In fact, for the liquid-gas, asymmetric nuclear matter implies a reduction of the second critical density and of the critical temperature T_c. Contrariwise, for the Δ-dominant phase transition, we have a slightly increase of the critical temperature and a significant reduction of the first critical density. In particular at moderate temperatures ($T \approx 30 \div 40$ MeV), the system begins the mixed phase at a baryon density of the order of ρ_0. This behavior could be phenomenological relevant in order to identify such phase transition in heavy ion collision experiments.
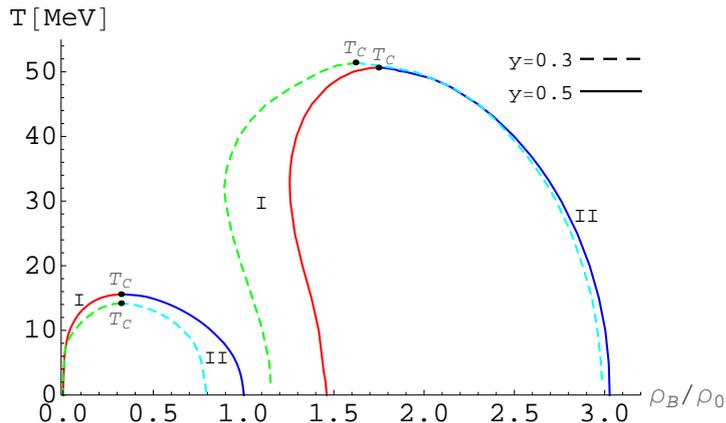
Figure 5.21: Phase diagram of the liquid-gas and the nucleon-Δ matter phase transition for $y = 0.3$ (dashed curves) and $y = 0.5$ (continuous curves). The lines labeled with I and II, delimitate the first and second critical density of the coexistence regions, respectively.

5.6 Strangeness instability

Before concluding this Chapter, we would like to present a preliminary study of the proprieties of strongly interacting nuclear matter at high temperature and baryon density, where strange particles start to be abundantly produced. In fact, during the extreme condition reached in a relativistic heavy ion collision experiment, a net strangeness excess could be generated and chemical fluctuation in strangeness density may take possible.

In particular, in this section, we are planning to investigate the possible onset of strangeness diffusional instability (fluctuation in the strangeness density) at $T > 70$ MeV and $\rho_0 < \rho_B < 4\rho_0$, in a multi-component system with three (B, C, S) and two (B, S) conserved charges.

In this context, we study the nuclear system under different values of strangeness fraction $-0.5 < z < 0.5$, in order to check the possible onset of strangeness diffusional instability in the nuclear medium.

We want to stress that, in this analyze, we do not take in consideration the possible deconfinement phase transition to QGP, as we have done in Chapter. 4, but we treat the nuclear system as if it was in pure hadronic phase.

In this context, in analogy to what obtained in presence of two conserved charges (B and C), for the liquid-gas and Δ-matter phase transition, we construct the mechanical and chemical stability condition. In particular, for a system of two conserved charges (B, S), taking into account that eq. (5.8) becomes

$$\left(\frac{\partial \mu_B}{\partial z}\right)_{T,P} + z \left(\frac{\partial \mu_S}{\partial z}\right)_{T,P} = 0, \tag{5.28}$$

123

the chemical stability condition is satisfied if

$$\left(\frac{\partial \mu_S}{\partial z}\right)_{T,P} > 0 \quad \text{or} \quad \begin{cases} \left(\dfrac{\partial \mu_B}{\partial z}\right)_{T,P} < 0 \,, & \text{if } z > 0 \,, \\[4mm] \left(\dfrac{\partial \mu_B}{\partial z}\right)_{T,P} > 0 \,, & \text{if } z < 0 \,. \end{cases} \tag{5.29}$$

Analogously, in presence of three conserved charges, eq. (5.8) becomes

$$\left(\frac{\partial \mu_B}{\partial z}\right)_{T,P} + y \left(\frac{\partial \mu_C}{\partial z}\right)_{T,P} + z \left(\frac{\partial \mu_S}{\partial z}\right)_{T,P} = 0 \,, \tag{5.30}$$

$$\left(\frac{\partial \mu_B}{\partial y}\right)_{T,P} + y \left(\frac{\partial \mu_C}{\partial y}\right)_{T,P} + z \left(\frac{\partial \mu_S}{\partial y}\right)_{T,P} = 0 \,, \tag{5.31}$$

and the condition for the chemical stability reads

$$\left(\frac{\partial \mu_S}{\partial z}\right)_{T,P} > 0 \quad \text{and} \quad \begin{cases} \left(\dfrac{\partial \mu_B}{\partial z}\right)_{T,P} > \text{ or } < 0 \,, \\[4mm] \left(\dfrac{\partial \mu_C}{\partial z}\right)_{T,P} > \text{ or } < 0 \,, \end{cases} \tag{5.32}$$

and

$$\left(\frac{\partial \mu_C}{\partial y}\right)_{T,P} > 0 \quad \text{and} \quad \begin{cases} \left(\dfrac{\partial \mu_B}{\partial y}\right)_{T,P} > \text{ or } < 0 \,, \\[4mm] \left(\dfrac{\partial \mu_S}{\partial y}\right)_{T,P} > \text{ or } < 0 \,, \end{cases} \tag{5.33}$$

so the mixed derivatives can be both positive or negative, independently by the value of z and y, whereas $\partial \mu_S / \partial z$ and $\partial \mu_C / \partial y$, must be always positive.

The mechanical stability condition is obviously given by eq. (5.7).

5.6.1 Strangeness instability (three conserved charges)

.

The analyze is performed using the effective relativistic formulation of Section. 1.4.1 and the Chiral one of Section 1.4.2 and by fixing the nucleon meson coupling constant to TM1 parameter sets of Tab. 1.2.

In this analysis the relevant degrees of freedom of the system are the baryons octet (n, p, Λ, Σ^+, Σ^0, Σ^-, Ξ^-, Ξ^0) and the lightest pseudo-scalar (π, K, $\overline{K}$, η, η') and vector mesons (ρ, ω, K^*, $\overline{K}^*$, ϕ).

Strange particles are in fact abundantly produced at higher temperature and baryon density and, during the extreme condition reached in the relativistic heavy ion collision experiments, chemical fluctuation in strangeness density may be possible, generating in this case a region of chemical instability.

For this reason we analyze the nuclear medium, in the pure hadronic phase, over a very wide range of temperatures (70 MeV $< T <$ 140 MeV) and baryon densities ($\rho_0 < \rho_B < 4\rho_0$). Anyway, for this range of parameter set, we do not find any mechanical or chemical instability regions.

Therefore, in agreement with eq.s (5.32) and (5.33), we conclude that, in presence of three conserved charges, there are no regions of mechanical or chemical instability in the range of temperature and baryons density explored in this study.

5.6.2   Strangeness instability (two conserved charges)

.

In presence of two conserved charges (B and S), we limit ourself to consider a small number of degrees of freedom of the system, without losing of generality.
In this sense, we analyze the nuclear medium through the effective relativistic formulation and the minimal coupling scheme, considering only the baryons octet (n, p, Λ, Σ^+, Σ^0, Σ^-, Ξ^-, Ξ^0), the pions and the K^+ and K^- strange mesons in both the models (in the minimal coupling scheme pions are included as a free bose gas). The anti-kaon coupling constant is fixed to $U_{K^-} = -160$ MeV and $U_{K^-} = -50$ MeV.

In this condition, as for the previous case, we do not find any mechanical instability region over the range of temperatures (70 MeV $< T <$ 140 MeV) and baryon densities ($\rho_0 < \rho_B < 4\rho_0$) explored here, eq. (5.29) is always satisfied.
However, especially for moderate temperature $T \approx (70 \div 80)$ MeV and high baryon density ($2 \div 3\rho_0$) we found a region of chemically instability for moderate values of $z \approx 0.4$.
In this region the system becomes instable due to fluctuations of strangeness density, therefore eq. (5.29) is not respected and the system is expected to undergoes to a phase transition.

In Fig. 5.22, we report an example of such instability region for the Chiral model. In analogy to the LG case and the Δ matter phase transition (Fig.s 5.2 and 5.13), here we report various isobars at $T = 70$ MeV and $U_{K^-} = -50$ MeV. At the increasing of the temperature, the region of chemical instability rapidly moves to higher values of z and after disappear. Contrariwise, by increasing of the baryon density, the chemical instability region moves to lower z. In presence of a stronger attractive potential depth U_{K^-}, we observe a strong reduction in μ_B and μ_S and at $U_{K^-} = -160$ MeV the instability region cease to exists in the range of strangeness density explored in this study.

A similar behavior is obtained for the effective relativistic formulation. Unfortunately, in this case, due to the absence of an effective mass, the kaons condensate just before the onset of strangeness diffusional instability.
We would like to underline that this is only a preliminary study, anyway, from the above considerations, strangeness diffusional instability seems to be present in systems with two conserved charges, over a region of moderate temperature and hight baryon density. By increasing of the temperature, strange particles are abundantly produced, but the conditions for the onset of chemical instability moves to higher z and after disappear.
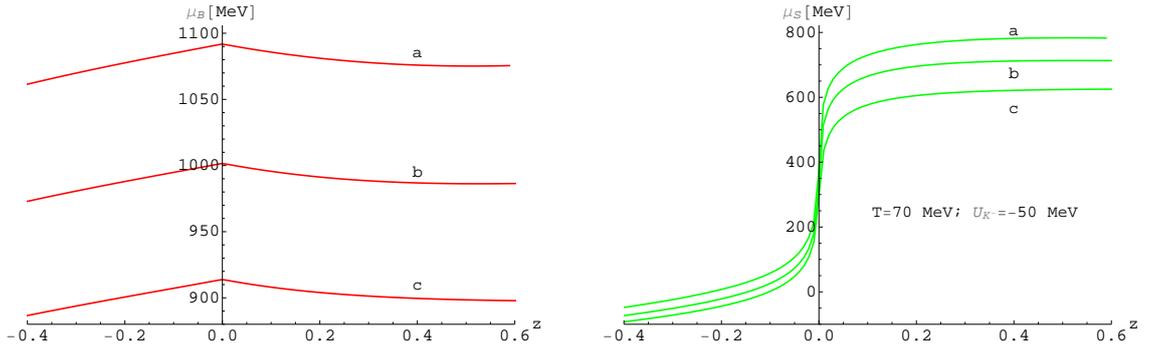
Figure 5.22: Baryon (left panel) and strange (right panel) chemical potential isobars as a function of z at $T = 70$ MeV and different pressure $P = (85, 50, 25)$ MeV/fm^3 (label from a and c).

5.7 Major conclusions

The main goal of this Chapter is to show the possible existence of chemical and mechanical instability at finite temperature and dense nuclear matter. At this scope we have firstly studied the relativistic nuclear EOS for the liquid-gas phase transition and with the inclusion of Δ-isobars, by requiring the global conservation of baryon and electric charge numbers, through the Lagrangian density 1.27 and TM1 parameter set Tab. (1.2) .
In this context, we have also investigated the nuclear medium at low temperature and baryon density in presence of nonextensive effects and we have compared the obtained results with that of extensive case, showing a remarkable reduction of the critical temperature and of the first and second critical density, especially in presence of asymmetric matter.
Similarly to the liquid-gas phase transition in a warm and low density nuclear matter, also a nucleon-Δ matter phase transition can occur at higher temperature and density ($T \leq 50$ MeV, $\rho \approx 1 \div 3\,\rho_0$). We have shown that for asymmetric nuclear matter both mechanical and chemical instability take place. This latter plays a crucial role in the characterization of the phase transition and can also imply very low values of the electric charge fraction y during the mixed phase region.

The nucleon-Δ matter phase transition depends significantly on the value of the σ-Δ coupling constant and we have seen that the presence of instabilities may become relevant from a phenomenological point of view only for a limited range of the possible $x_{\sigma\Delta}$ couplings.

Whether metastable Δ-excited nuclear matter exists or not is still a controversial issue because little is actually known about the Δ-coupling constants with the scalar and vector mesons, even if QCD finite-density sum rule results predict a larger net attraction for a Δ-isobar than for a nucleon in the nuclear medium [99]. Although we have seen that instabilities are already present for $x_{\sigma\Delta} > 1$, they become phenomenological more relevant at greater values of $x_{\sigma\Delta}$, involving larger region of mixed phase and greater values of the electric charge fraction.

The analysis of the instability regions with different Δ-coupling constants turns out to be not trivial from the numerical point of view, especially at lower values of $x_{\sigma\Delta}$ where a complex structure of the mixed phase can be formed. For example, we have shown that, in the case of $x_{\sigma\Delta} = 1.22$, two separate regions of instability are present. Moreover, the case $x_{\sigma\Delta} = 1.3$ has been studied for different values of temperature and we have seen that in asymmetric nuclear matter the mixed phase transition involves a large range of baryon density.

Similarly to the liquid-gas phase transition, the nucleonic and the Δ-matter phase have a different electric charge fraction in the mixed phase. The electric charge fraction in the nucleonic phase reflects a system with higher values of y than the Δ-matter phase. In the liquid-gas phase transition, the process of producing a larger neutron excess in the gas phase is referred to as isospin fractionation [62, 81, 82]. A similar effects can occur in the nucleon-Δ matter phase transition essentially due to a Δ^- excess in the Δ-matter phase with lower values of y. As already observed, due to the uncertainty on the meson-Δ coupling constants, we have not considered in this investigation the coupling of the Δ with the isovector ρ-meson field, because much less explored in literature. We have verified that the presence of such a coupling could further increase the isospin asymmetry in the mixed phase and lower the critical temperature of the nucleon-Δ matter phase transition.

In this context, it is proper to observe that Coulomb interaction and finite size effects, not considered in this study, can significantly alter the structure of the phase transition. Moreover, as already observed, we outline that our effective EOS cannot incorporate the complex $\pi N \Delta$ dynamics and should be very interesting to investigate the presence of chemical and mechanical instabilities in the framework of a more realistic chiral hadronic EOS. Taking also into account the large uncertainty on the possible values of Δ-meson field couplings, it is caution to highlight at this stage the pedagogical character of this study.

Many effects discussed in this paper may be more evident at low values of y, obtainable in principle with radioactive ion beam facilities. On the other hand, it is rather unlikely, at least in the near future, that neutron rich nuclei can be accelerated to energies larger than a few GeV per nucleon. However, some precursor signals of the considered instabilities could be observed even in collisions of stable nuclei at intermediate energies. For example, in Ref. [74], the simulation of the reaction ^{238}U$+^{238}$U (average $y = 0.39$), at 1 A GeV and semicentral impact parameter $b = 7$ fm, shows that a rather exotic nuclear matter can be formed in a transient time of the order of 10 fm/c, with baryon density up to $3\,\rho_0$, $T \leq 50 \div 60$ MeV and $y \approx 0.35 \div 0.40$. Such conditions would meet fully the nucleon-Δ mixed phase region (see Fig. 5.21).

A possible signature of the nucleon-Δ matter phase transition could be find via observables particularly sensitive to the expected different isospin content of the two phases. For example, at the AGS energies, the Δ-resonance was predicted to be the dominant source for pions of small transverse momenta [63]. In this case, an increase of the negative pions π^- of small trasverse momenta at a greater asymmetry of the beam could be a good indicator of a Δ isospin fractionation effect.

Finally, we have presented a preliminary study of the possible onset of strangeness diffusional instability, in an hadronic system, at high temperature and over a wide range of baryon densities. In this context, we have found no mechanical or chemical instability

regions for a system of three conserved charges (B, C and S). Whereas, in presence of two conserved charges (B and S), we have showed the onset of a chemical-diffusive instability region around $z \approx 0.4$, for temperature and baryon density of the order of $T \approx 70$ MeV and $\rho_B = (2 \div 3)\rho_0$ and $U_{K^-} = -50$ MeV. The system is very sensitive to the changes of the temperature, in particular by increasing of the T and/or of the anti-kaon potential depth, the diffusive instability region rapidly disappear, whereas by increasing of ρ_B the instability region is shifted at lower z, with possible signature in high energetic and high compressed relativistic heavy ion collision experiments.

Future studies will be necessary in order to better estimate the possible onset of strangeness instability in relativistic heavy ion collision experiments or in the core of compact objects.

Chapter 6

Conclusions

In the present dissertation, we have analyzed the proprieties of strongly interacting nuclear matter at high baryon density and finite temperature.

In this condition, due to the complexity of the microscopic many-body interaction, which determine the macroscopic thermodynamical variables and EOS, is of fundamental importance to develop statistical approaches and introduce some approximations (mean-field and no-sea approximations) in order to treat the complexity of such interactions. To this regard, in Chapter 1, we have introduced the Lagrangian formalism, in the framework of non-linear relativistic mean-field theory, where the nuclear interaction is mediated by the exchange of virtual isoscalar - scalar (σ), isoscalar - vector (ω) and isovector - vector (ρ) meson fields [87, 86, 85] and the coupling constants of the model are related with the bulk proprieties of nuclear matter (Tab. 1.2). Quantum hadron dynamics (QHD), constitute in this sense, a relativistic covariant theory of hot and dense hadronic matter.

However, as has been showed, the extraction of information about the equation of state (EOS) at different densities and temperatures, by means of intermediate and high-energy heavy-ion collisions, is a very difficult task and can be realized only indirectly by comparing the experimental data with different theoretical models, such as, for example, fluid-dynamical models. In this condition and in the absence of a converging method to approach QCD at finite density and temperature, one has often to resort to effective and phenomenological models investigations to obtain qualitative results.

The study and the implementation of such effective models (effective relativistic mean-field model and nonextensive statistical mechanics) is one of the major results of this thesis.

Effective relativistic mean-field model, has been introduced in section 1.4.1, in order to include in the hadronic Lagrangian density, the contribution of the lightest pseudo-scalar (π, K, $\overline{K}$, η, $\eta^{'}$) and vector mesons (ρ, ω, K^*, $\overline{K}^{*}$, ϕ), through an effective chemical potential depending on the self-consistent interaction between baryons. This approach, allows us to overcome some theoretical and experimental difficulties in the measure of the mesons coupling constants. Following this scheme, we have analyzed the strangeness production at finite temperature and baryon density, with particular attention to the kaon and anti-kaon production, comparing the obtained results with that of the minimal coupling scheme of section 1.4.2. We have found a good correspondence between the two models for moderate value of the anti-kaon optical potential ($U_{K^-} = -50$ MeV), as suggested by recent

self-consistent calculation based on chiral Lagrangian and G-matrix theory [46, 47, 48]. In particular, we have showed that, the strong difference in the kaon to anti-kaon ratio, could be considered as a relevant feature in the determination of the real part of the anti-kaon optical potential, in the range of temperature and density reached in the future compressed baryonic matter (CBM) experiment of facility of antiproton and ion research (FAIR) at GSI [55, 57, 58]. Finally, we have found that the kaons chemical potential is always less then the corresponding kaon threshold energy ($\omega^\pm$). This matter of fact seems to suggest, in agreement with the results obtained within modern transport codes [53], that kaon condensation does not take place at any temperature and density in those systems in rapid evolution, like the relativistic heavy ion collision, where the zero net strangeness condition is conserved.

The implementation of the nuclear equation of state with effective and phenomenological model, appears particularly important during the extreme condition reached in the relativistic heavy ion collision experiments, where QCD become highly non-perturbative and strongly dynamical correlations, memory effects and long-range color interactions can take place [18, 2, 19].
Regarding this and in agreement with several authors and experimental observations [23, 24, 25, 26, 27, 28, 28, 29], in Chapter 2, we have introduced and implemented the nuclear EOS in the framework of nonextensive statistical mechanics, proposed firstly by Tsallis [20, 21, 22]. Following this line, in Chapter 4, we have presented a detailed study of the deconfinement phase transition from hadron matter to quark-gluon plasma, in regime of finite temperature and baryon density, reachable in high-energy heavy-ion collisions, for which the deconfinement phase transition can be considered of the first order.
Let us remember that, in this numerical investigation, we have considered the nonextensive index q as a free parameter, even if, in principle, it should depends on the physical conditions generated in the reaction, on the fluctuation of the temperature and be related to microscopic quantities (such as, for example, the mean interparticle interaction length, the screening length and the collision frequency into the parton plasma).
The mixed phase has been obtained by applying the Gibbs conditions to systems of more than one conserved charge (Section 4.2) by requiring the global conservation of the baryon number (B), electric charge (C) and strangeness number (S). Let us remark that, one of the most important aspect of a multi-component system, implies a global and not a local charge conservation. Therefore, the charge densities ρ_B, ρ_C and ρ_S are fixed only as long as the system remains in one of the two pure phases. In the mixed phase, the charge concentration in each of the regions of one phase or the other may be different.

Following this line, we have showed that, even in presence of small deviation from the standard BG statistics, the meson fields and, consequently, the EOS appear to be sensibly modified. In fact, by varying temperature and density, the EOS reflects in terms of the macroscopic thermodynamical variables the microscopic interactions of the different phases of nuclear matter. In particular, although pressure as a function of baryon density is stiffer in the hadronic phase, we have found a strong softening in the mixed phase in the presence of nonextensive statistics. Such behavior implies an abrupt variation in the incompressibility and could be considered as a signal of nonextensive statistical effects in high-energy heavy-ion collisions. Furthermore, the first and second critical densities are in general reduced, favoring in this way the formation of the mixed phase and consequently, the deconfinement

phase transition to quark gluon plasma.

One of the most important results obtained in this analysis, was to demonstrate the strong enhancement of strange particles and anti-particles, at high temperatures $T = (120 \div 170)$ MeV and baryon densities $\rho_B = (1 \div 3)\rho_0$. In particular, we have found that, in presence of nonextensive effects, the phase transition is characterized by an antistrangeness content in the hadron phase while the QGP retains a net strangeness excess at large densities ($\rho_B \geq 2\rho_0$) and intermediate temperatures ($T \approx 100 \div 120$ MeV), while the other way round occurs at low densities and high temperature. The separation of strange and anti-strange quarks in the hadron-QGP mixed phase turns out to be less pronounced than in the standard case due to a more symmetric presence of particle and antiparticle at intermediate temperatures. On the other hand, for $q > 1$, the strangeness fraction Y_S (and, consequently, the density of strange particles) results to be much greater compared to the $q = 1$ case.

This matter of fact, as explained, is essentially due to the power law behavior of the mean occupational distribution function which weighs differently low and high energy states at different baryon densities and temperatures.

Therefore, the possibility of separating strange from antistrange matter in the hadron-QGP phase transition, can lead to a very significant enrichment of strange quarks in the QGP at high baryon density and intermediate temperature. In fact, in the hadronic sector of the mixed phase, K^+ and K^0 are enhanced and the hyperons are suppressed. Being mesons much lighter than nucleons and their resonances, they carry away entropy, energy and antistrangeness and, therefore, the prompt kaon emission cools and charges the system with finite net strangeness, leading to an even stronger enhancement of the s quarks in the quark phase. This feature, which also depends strongly on the value of the strange particle densities, favors the formation of metastable or stable droplets of strange quark matter which would contain approximately the same amount of u, d and s quarks. The evidence of such a state of quark matter could be related to the existence of exotic hadron states, like a H-dibaryon state, a deeply bound 6-quark state predicted by Jaffe more than thirty years ago [174]. Although many experimental searches for the H-dibaryon were carried out and so far no convincing signal was found [175], very recently evidence for a bound H-dibaryon was claimed based on lattice QCD calculations [176, 177].

This matter of fact could be crucial in the formation and survival of strange quark matter droplets in relativistic heavy ion collisions at high compressed baryonic matter.

The influence of nonextensive effects, has also been investigated at finite temperature and in β-stable nuclear matter, in presence and in absence of hyperons and trapped neutrinos, in astrophysical systems (Chapter 3). In this context, we have analyzed the mechanical and thermodynamical proprieties of strongly interacting nuclear matter over a wide range of temperatures and baryon densities. We have found a strong variation in the main physical parameter of the PNS in presence of nonextensive effects. In particular, using the Wilk prescription [33], when $q < 1$ we have found a remarkable reduction in the stellar temperature at fixed baryon density with respect to the standard case ($q = 1$). Especially in the maximum heating phase, the EOS becomes slightly softer and higher central baryon densities at fixed total baryon mass are reached, influencing the neutrino diffusion during the deleptonization process. In the case of sub-extensive effects, hyperons start later but have a bigger concentration at high baryon density, allowing to sustain a higher neutrino

luminosity at late times. The other way round takes place in the case of $q > 1$. We have an increase of the temperature as a function of the baryon density and lower central densities at fixed baryon masses are reached. The hyperons on-set is shifted at lower baryon densities and a greater hyperons concentration at low baryon masses is present. On the other hand, a significant reduction of the hyperons concentration at high stellar masses take place, contributing to a lower luminosity at late times. Furthermore, we have found that, in presence of super-extensive statistical effects and hyperon degrees of freedom, it is favored the realization of a metastable phase, with an enhancement of a possible black hole formation after the deleptonization era (Tab 3.1).

Finally, in the last part of this dissertation (Chapter 5), we have concentrated our analysis on a detailed study of the thermodynamical proprieties of strongly interacting and dense nuclear matter. This constitutes, one of the most interesting aspects and one of the most difficult tasks of modern high-energy nuclear physics.
In this context, we have investigated a multi-component system, with two (B and C) and three conserved charges (B, C and S), over a wide range of temperatures ($0 < T < 140$ MeV) and baryon densities ($0 < \rho_B < 4\rho_0$), looking for the possible onset of mechanical and chemical instability (fluctuation of the baryon density and in the electric or strangeness density, respectively) associated to different phase transitions in the nuclear medium.
This was made following the very detailed study of Müller and Serot [76]. In agreement with other previous works [76, 72, 73, 164], we have found two different types of phase transitions. The first one, at low temperatures ($T \leq 10$ MeV) and subnuclear densities, where a nucleonic liquid-gas phase transition was first predicted theoretically [179, 180, 181] and later observed experimentally in a nuclear multifragmentation phenomenon at intermediate-energy nuclear reactions [61, 62]. A second one, at higher temperature and baryon density ($T \leq 50$ MeV and $\rho_0 \leq \rho_B \leq 3\rho_0$), from a nucleonic fluid to a resonance-dominated Δ-matters.
We have then generalized and extended these studies in presence of asymmetric nuclear matter and, in the simple case of the LG phase transition, we have also explored such phase transition in presence of nonextensive effects, showing that, despite to the low temperature at which it takes place, the nuclear isobars and the phase diagram are sensibly modified.
As amply discussed in Chapter 5, the relevant aspect of a multi-component system, is that the phase transition is of second order from the viewpoint of Ehrenfests definition. In particular, the system is stable against the separation in two phases, until the free energy of a single phase is lower than the free energy in all two phases configuration. In this condition, the mixed phase is obtained in the usual way, by applying the Gibbs condition and by requiring the global conservation of each charge in the total phase.
Furthermore, in agreement with [76], we have shown that, in presence of asymmetric nuclear matter, a phase transition can occur not only via mechanical instability, but also via chemical/diffusive instability, even if the system results mechanically stable. This fact determines a strong variation in the phase diagram, in fact, in presence of an isospin asymmetry, the critical temperature and the critical density of the liquid-gas phase transition are sensibly reduced and the phase transition is favored.

Furthermore, by increasing of the temperature of the system, we have shown that new degrees of freedom appear. In this condition, the implementation of the nuclear equation of state, with the inclusion of the Δ-isobars and pions, allowed us to explore the phase transition

and the instability regions over a wider range of baryon densities and temperatures. In this context, as for the LG case, we have shown that, for asymmetric nuclear matter, both mechanical and chemical instabilities take place. The latter plays a crucial role in the characterization of the phase transition and can also imply very low values of the electric charge fraction y during the mixed-phase region. The binodal diagram, in fact, extends up to very negative region of charge fraction, corresponding to a system with almost all Δ^--particles, being antiparticles, strange hadrons and pions contribution almost negligible in this regime. The strong Δ^- excess in the Δ-matter phase, is phenomenologically similar to the isospin fractioning process which produced a larger neutron excess in the gas phase of the LG phase transition [62, 81, 82].

Anyway, the analysis of the instability regions with different Δ-coupling constants, was found to be not trivial from the numerical point of view, especially at lower values of $x_{\sigma\Delta}$ where a complex structure of the mixed phase can be formed. For example, we have shown that, for $x_{\sigma\Delta} = 1.22$, two different regions of instability are present. Conversely, below $x_{\sigma\Delta} < 1.1$, such instabilities are restricted to very low values of temperature and electric charge fraction and therefore do not contribute significantly to the nuclear medium proprieties.

In this context, it is proper to observe that Coulomb interaction and finite size effects, not considered in this study, can significantly alter the structure of the phase transition. Moreover, as already observed, we outline that our effective EOS cannot incorporate the complex $\pi N\Delta$ dynamics and should be very interesting to investigate the presence of chemical and mechanical instabilities in the framework of a more realistic chiral hadronic EOS. Anyway, in the framework of effective relativistic mean-field model, we have obtained significant results, especially for moderate and hight values of $x_{\sigma\Delta} = (1.2 \div 1.3)$. In particular, the case $x_{\sigma\Delta} = 1.3$ has been extensively studied for different values of temperature, showing that, in asymmetric nuclear matter, the mixed phase transition is sensibly modified and involves a larger range of baryon density. In particular, we have observed a significant reduction of the first critical density and a slight increase of the critical temperature. This is because, the region of diffusive instability, extends above the maximum temperature at which the system becomes mechanically stable and this determines an increase of the mixed phase region. Furthermore, at moderate temperature and for strong asymmetric nuclear matter ($T \approx 30$ MeV and $y \approx 0.3$), we have found that the system begins the mixed phase at a baryon density of the order of nuclear saturation density ρ_0. This behavior could be phenomenologically relevant in order to identify such phase transition in heavy ion collision experiments.

Many effects discussed in this analysis can be more evident at low values of y, obtainable in principle with radioactive ion beam facilities. On the other hand, it is rather unlikely, at least in the near future, that neutron rich nuclei can be accelerated to energies larger than a few GeV per nucleon. However, some precursor signals of the considered instabilities could be observed even in collisions of stable nuclei at intermediate energies. For example, in Ref. [74], the simulation of the reaction ^{238}U$+^{238}$U (average $y = 0.39$), at 1 A GeV and semicentral impact parameter $b = 7$ fm, shows that a rather exotic nuclear matter can be formed in a transient time of the order of 10 fm/c, with baryon density up to $3\,\rho_0$, $T \leq 50 \div 60$ MeV and $y \approx 0.35 \div 0.40$. Such conditions would meet fully the nucleon-Δ mixed phase region (see Fig. 5.21).

Furthermore, a possible signature of the nucleon-Δ matter phase transition could be found via observables particularly sensitive to the expected different isospin content of the two phases. For example, at the AGS energies, the Δ-resonance was predicted to be the dominant source for pions of small transverse momenta [63]. In this case, an increase of the negative pions π^- of small trasverse momenta at a greater asymmetry of the beam could be a good indicator of a Δ isospin fractioning effect.

Finally, we have also explored the possible onset of strange-diffusive instability at high temperature and finite baryon density. We have found that, for a binary system of two conserved charges (B and S), a diffusive instability region appears around $z \approx 0.45$, for temperature and baryon density of the order of $T \approx 70$ MeV and $\rho_B = (2 \div 3)\rho_0$. At the increasing of the temperature, the region of chemical instability rapidly moves to higher values of z and after disappears, on the contrary, by increasing of the baryon density, the chemical instability region moves to lower z.
We have found no indication of chemical or mechanical instability region for a system of three conserved charges (B, C, S).

I am confident that the future CBM (compressed baryonic matter) experiment of the FAIR (Facility of Antiproton and Ion Research) project at GSI Darmstadt will make it possible to create compressed baryonic matter with a high net baryon density [55, 58, 57], allowing the experimental identification of such phase transitions and a precise measure of the strangeness production and of the quark-gluon plasma phase transition at high temperature and finite baryon density.

List of publications

PUBLICATION IN SCIENTIFIC JOURNALS:

1. Lavagno A., Pigato D. and Quarati P. *Journal of Physics G: Nuclear and Particle Physics*, **37**, 115102 (2010).

2. Lavagno A. and Pigato D. *European Physical Journal A* **47**, 101140 (2011).

3. Iazzi F., Introzzi R., Lavagno A., Pigato D. and Younis M. H. *International Journal of Modern Physics E* **21**, 1250028 (2012).

4. Lavagno A. and Pigato D. *Physical Review C* **86**, 024917 (2012).

5. Lavagno A. and Pigato D. *Journal of Physics G: Nuclear and Particle Physics*, **39**, 125106 (2012).

CONFERENCE PROCEEDINGS:

1. Gervino, G., Lavagno, A., and Pigato, D. *Journal of Physics Conference Series* **206**, 012070 (2011).

2. Gervino, G., Lavagno, A., and Pigato, D. *Central European Journal of Physics* **10**, 102478 (2011).

3. Iazzi F., Lavagno A., Pigato D. *Hyperfine Interaction*, 101007 (2011).

4. Lavagno A. and Pigato D. *European Physical Journal Web of Conferences* **37**, 09022 (2012).

5. Lavagno A. and Pigato D. *2nd European Nuclear Physics Conference*, 17-21 September 2012, Bucarest.

Bibliography

[1] Hwa, R. and Wang, X. *Quark Gluon Plasma 3* . (World Scientific Publishing Co. Pvt. Ltd., Singapore, 2004).

[2] Biro', T. S. *Journal of Physics G: Nuclear and Particle Physics* **35**(4), 044056 (2008).

[3] Braun-Munzinger, P. and Wambach, J. *Rev. Mod. Phys.* **81**, 1031–1050 Jul (2009).

[4] Castorina, P., Redlich, K., and Satz, H. *The European Physical Journal C - Particles and Fields* **59**, 67–73 (2009). 10.1140/epjc/s10052-008-0795-z.

[5] Cahn, R. and Goldhaber, G. *The Experimental Foundations of Particle Physics (Cambridge: Cambridge University Press)* (1989).

[6] Gell-Mann, M. *Physical Review* **125**, 1067–1084 February (1962).

[7] Ne'Eman, Y. *Nuclear Physics A* **26**, 222–229 August (1961).

[8] Gell Mann, M. *Physics Letter* **8**, 214–215 (1964).

[9] Feynman, R. P., Gell-Mann, M., and Zweig, G. *Physical Review Letters* **13**, 678–680 November (1964).

[10] Barnes, V. E. and Connolly, e. a. *Physical Review Letters* **12**, 204–206 February (1964).

[11] Greenberg, O. W. *Physical Review Letters* **13**, 598–602 November (1964).

[12] Fritzsch, H., Gell-Mann, M., and Leutwyler, H. *Physics Letters B* **47**, 365–368 November (1973).

[13] Politzer, H. D. *Physical Review Letters* **30**, 1346–1349 June (1973).

[14] Gross, D. J. and Wilczek, F. *Physical Review Letters* **30**, 1343–1346 June (1973).

[15] Augustin, J. E. and et al., B. *Phys. Rev. Lett.* **33**, 1406–1408 Dec (1974).

[16] Aubert, J. J., Becker, U., Biggs, P. J., and et al., B. *Phys. Rev. Lett.* **33**, 1404–1406 Dec (1974).

[17] Glendenning, N. *Compact Stars* Springer (2000).

[18] Schmidt, S. e. a. *Phys. Rev. D.* (1997).

[19] Biró, T. S. *Journal of Physics G Nuclear Physics* **35**(4), 044056 April (2008).

[20] Tsallis, C. *J. Stat. Phys.* **52**, 479 (1997).

[21] Gell-Mann, M. and Tsallis, C. *Nonextensive Entropy: Interdisciplinary Applications* , (New York:Oxford University Press) (2004).

[22] Tsallis, C. *Introduction to Nonextensive Statistical Mechanics* , (New York:Oxford University Press) (2009).

[23] Beck, C. *European Physical Journal A* **40**, 267–273 June (2009).

[24] Biró, T. S. and Purcsel, G. *Physical Review Letters* **95**(16), 162302 October (2005).

[25] Kodama, T. and Koide, T. *European Physical Journal A* **40**, 289–297 June (2009).

[26] Wilk, G. and Włodarczyk, Z. *European Physical Journal A* **40**, 299–312 June (2009).

[27] Alberico, W. M. and Lavagno, A. *European Physical Journal A* **40**, 313–323 June (2009).

[28] Cleymans, J. *Journal of Physics G Nuclear Physics* **37**(9), 094015 September (2010).

[29] Chinellato, D., Takahashi, T., and Bediaga, I. *J. Phys. G: Nucl. Part. Phys.* **37**, 094042 (2010).

[30] Conroy, J. M. and Miller, H. G. *Physical Review D* **78**(5), 054010 September (2008).

[31] Ferro, F., Lavagno, A., and Quarati, P. *European Physical Journal A* **21**, 529–534 September (2004).

[32] Pereira, F. I. M., Silva, R., and Alcaniz, J. S. *Phys. Rev. C* **76**(1), 015201 July (2007).

[33] Rożynek, J. and Wilk, G. *Journal of Physics G Nuclear Physics* **36**(12), 125108 December (2009).

[34] Lavagno, A., Pigato, D., and Quarati, P. *Journal of Physics G Nuclear Physics* **37**(11), 115102 November (2010).

[35] Lavagno, A. and Pigato, D. *European Physical Journal A* **47**, 52 April (2011).

[36] Lavagno, A. and Pigato, D. *Journal of Physics G: Nuclear and Particle Physics* **39**(12), 125106 (2012).

[37] Lavagno, A., Scarfone, A. M., and Narayana Swamy, P. *Journal of Physics A Mathematical General* **40**, 8635–8654 July (2007).

[38] Harris, J. W., Sandoval, A., Stock, R., Stroebele, H., Renfordt, R. E., Geaga, J. V., Pugh, H. G., Schroeder, L. S., Wolf, K. L., and Dacal, A. *Physical Review Letters* **47**, 229–232 July (1981).

[39] Schnetzer, S., Lombard, R. M., Lemaire, M.-C., Moeller, E., Nagamiya, S., Shapiro, G., Steiner, H., and Tanihata, I. *Physical Review C* **40**, 640–653 August (1989).

[40] Banik, S., Greiner, W., and Bandyopadhyay, D. *Physical Review C* **78**(6), 065804 December (2008).

[41] Friedman, E., Gal, A., and Batty, C. J. *Nuclear Physics A* **579**, 518–538 October (1994).

[42] Batty, C. J., Friedman, E., and Gal, A. *Physical Report P* **287**, 385–445 August (1997).

[43] Friedman, E., Gal, A., Mareš, J., and Cieplý, A. *Physical Review C* **60**(2), 024314 August (1999).

[44] Glendenning, N. K. and Schaffner-Bielich, J. *Physical Review C* **60**(2), 025803 August (1999).

[45] Pons, J. A., Reddy, S., Ellis, P. J., Prakash, M., and Lattimer, J. M. *Physical Review C* **62**(3), 035803 September (2000).

[46] Tolós, L., Ramos, A., and Polls, A. *Physical Review C* **65**(5), 054907 May (2002).

[47] Lutz, M. F. M. and Korpa, C. L. *Nuclear Physics A* **700**, 309–329 March (2002).

[48] Lutz, M. F. M. and Kolomeitsev, E. E. *Nuclear Physics A* **700**, 193–308 March (2002).

[49] Zakout, I., Greiner, W., and Jaqaman, H. R. *Nuclear Physics A* **759**, 201–226 September (2005).

[50] Pal, S., Bandyopadhyay, D., and Greiner, W. *Nuclear Physics A* **674**, 553–577 July (2000).

[51] Thorsson, V., Prakash, M., and Lattimer, J. M. *Nuclear Physics A* **572**, 693–731 May (1994).

[52] Kaplan, D. B. and Nelson, A. E. *Physics Letters B* **175**, 57–63 July (1986).

[53] Hartnack, C., Oeschler, H., Leifels, Y., Bratkovskaya, E. L., and Aichelin, J. *Physical Report P* **510**, 119–200 January (2012).

[54] Knorren, R., Prakash, M., and Ellis, P. J. *Physical Review C* **52**, 3470–3482 December (1995).

[55] Senger, P. *Journal of Physics G Nuclear Physics* **30**, 1087 August (2004).

[56] Henning, W. F. *Nuclear Physics A* **805**, 502–510 June (2008).

[57] Arsene, I. C., Bravina, L. V., Cassing, W., Ivanov, Y. B., Larionov, A., Randrup, J., Russkikh, V. N., Toneev, V. D., Zeeb, G., and Zschiesche, D. *Physical Review C* **75**(3), 034902 March (2007).

139

[58] Bravina, L. V., Arsene, I., Nilsson, M. S., Tywoniuk, K., Zabrodin, E. E., Bleibel, J., Faessler, A., Fuchs, C., Bleicher, M., Burau, G., and Stöcker, H. *Physical Review C* **78**(1), 014907 July (2008).

[59] Botvina, A. S. and Mishustin, I. N. *European Physical Journal A* **30**, 121–128 October (2006).

[60] D'Agostino, M., Bruno, M., Gulminelli, F., Cannata, F., Chomaz, P., Casini, G., Geraci, E., Gramegna, F., Moroni, A., and Vannini, G. *Nuclear Physics A* **749**, 55–64 March (2005).

[61] Pochodzalla, J., Möhlenkamp, T., and Rubehn, e. a. *Phys. Rev. Lett.* **75**, 1040–1043 Aug (1995).

[62] Xu, H. S., Tsang, M. B., and Liu, e. a. *Phys. Rev. Lett.* **85**, 716–719 Jul (2000).

[63] Hofmann, M., Mattiello, R., Sorge, H., Stöcker, H., and Greiner, W. *Phys. Rev. C* **51**, 2095–2098 Apr (1995).

[64] Zabrodin, E. E., Arsene, I. C., and et al., B. *Journal of Physics G Nuclear Physics* **36**(6), 064065 June (2009).

[65] Xiang, H. and Hua, G. *Phys. Rev. C* **67**, 038801 Mar (2003).

[66] Chen, Y., Yuan, Y., and Liu, Y. *Phys. Rev. C* **79**, 055802 May (2009).

[67] Lavagno, A. *Phys. Rev. C* **81**, 044909 Apr (2010).

[68] Bass, S. A., Gyulassy, M., Stöcker, H., and Greiner, W. *Journal of Physics G Nuclear Physics* **25**, 1 March (1999).

[69] Mao, G., Neise, L., Stöcker, H., and Greiner, W. *Phys. Rev. C* **59**, 1674–1699 Mar (1999).

[70] Fachini, P. *Journal of Physics G: Nuclear and Particle Physics* **35**(4), 044032 (2008).

[71] Abelev, B. I., Aggarwal, M. M., and Ahammed, Z. e. a. *Phys. Rev. C* **78**, 044906 Oct (2008).

[72] Waldhauser, B. M., Theis, J., Maruhn, J. A., Stöcker, H., and Greiner, W. *Phys. Rev. C* **36**, 1019–1026 Sep (1987).

[73] Li, Z., Mao, G., Zhuo, Y., and Greiner, W. *Phys. Rev. C* **56**, 1570–1575 Sep (1997).

[74] Toro, M. D., Drago, A., Gaitanos, T., Greco, V., and Lavagno, A. *Nuclear Physics A* **775**, 102 – 126 (2006).

[75] Li, B.-A., Chen, L.-W., Ma, H.-R., Xu, J., and Yong, G.-C. *Phys. Rev. C* **76**, 051601 Nov (2007).

[76] Müller, H. and Serot, B. D. *Phys. Rev. C* **52**, 2072–2091 Oct (1995).

[77] Bonanno, L., Drago, A., and Lavagno, A. *Phys. Rev. Lett.* **99**, 242301 Dec (2007).

[78] Glendenning, N. K. *Phys. Rev. D* **46**, 1274–1287 Aug (1992).

[79] Drago, A. and Lavagno, A. *Physics Letters B* **511**(2âĂŞ4), 229 – 234 (2001).

[80] Barranco, M. and Buchler, J. R. *Phys. Rev. C* **22**, 1729–1737 Oct (1980).

[81] Das, C., Gupta, S. D., Lynch, W., Mekjian, A., and Tsang, M. *Physics Reports* **406**(1), 1 – 47 (2005).

[82] Baran, V., Colonna, M., Di Toro, M., and Greco, V. *Phys. Rev. Lett.* **86**, 4492–4495 May (2001).

[83] Machleidt, R. *Relativistic Dynamics and Quark Nuclear Physics* edited by M. B. Johnson and A. Picklesimer John Wiley and Son (1986).

[84] Serot, B. and Walecka, J. *Adv. Nuc. Phys* **16**(1), 1 (1986).

[85] Boguta, J. and Bodmer, A. R. *Nuclear Physics A* **292**, 413–428 December (1977).

[86] Walecka, J. D. *Annals of Physics* **83**, 491–529 (1974).

[87] Glendenning, N. K. and Moszkowski, S. A. *Physical Review Letters* **67**, 2414–1417 October (1991).

[88] Lavagno, A. and Pigato, D. *Physical Review C* **86**(2), 024917 August (2012).

[89] Bodmer, A. *Nuclear Physics A* **526**, 703 – 721 (1991).

[90] Schaffner, J., Dover, C., and Gal, A. e. a. *Physical Review Letters* **71**, 674–678 August (1993).

[91] Schaffner, J., Dover, C. B., Gal, A., Greiner, C., Millener, D. J., and Stocker, H. *Annals of Physics* **235**, 35–76 October (1994).

[92] Schaffner, J. and Mishustin, I. N. *Phys. Rev. C* **53**, 1416–1429 Mar (1996).

[93] Bunta, J. K. and Gmuca, Š. *Physical Review C* **70**(5), 054309 November (2004).

[94] Millener, D. J., Dover, C. B., and Gal, A. *Phys. Rev. C* **38**, 2700–2708 Dec (1988).

[95] Schaffner-Bielich, J. and Gal, A. *Physical Review C* **62**(3), 034311 September (2000).

[96] Yang, F. and Shen, H. *Phys. Rev. C* **77**, 025801 Feb (2008).

[97] Mattiello, R., Sorge, H., Stöcker, H., and Greiner, W. *Phys. Rev. Lett.* **63**, 1459–1462 Oct (1989).

[98] Kosov, D., Fuchs, C., Martemyanov, B., and Faessler, A. *Physics Letters B* **421**, 37 – 40 (1998).

[99] Jin, X. *Phys. Rev. C* **51**, 2260–2263 Apr (1995).

[100] Cavagnoli, R., Providência, C., and Menezes, D. P. *Physical Review C* **83**(4), 045201 April (2011).

[101] Gal, A. *Nuclear Physics A* **691**, 268–277 August (2001).

[102] Iazzi, F., Introzzi, R., Lavagno, A., Pigato, D., and Younis, M. H. *International Journal of Modern Physics E* **21**, 50028 May (2012).

[103] Iazzi, F., Lavagno, A., and Pigato, D. In *EXA 2011, by Bühler, Paul; Hartmann, Olaf; Marton, Johann; Suzuki, Ken; Widmann, Eberhard; Zmeskal, Johann, ISBN 978-94-007-4889-7. Springer Science+Business Media Dordrecht, 2012, p. 273*, Bühler, P., Hartmann, O., Marton, J., Suzuki, K., Widmann, E., and Zmeskal, J., editors, 273, (2012).

[104] Lavagno, A. and Pigato, D. In *European Physical Journal Web of Conferences*, volume 37 of *European Physical Journal Web of Conferences*, 9022, December (2012).

[105] Greiner, C., Koch, P., and Stocker, H. *Physical Review Letters* **58**, 1825–1828 May (1987).

[106] Greiner, C. and Stöcker, H. *Physical Review D* **44**, 3517–3529 December (1991).

[107] Kaczmarek, O., Karsch, F., Laermann, E., and Lütgemeier, M. *Phys. Rev. D* **62**, 034021 Jul (2000).

[108] Drago, A., Lavagno, A., and Pagliara, G. *Physical Review D* **69**(5), 057505 March (2004).

[109] Bonanno, L., Drago, A., and Lavagno, A. *Physical Review Letters* **99**(24), 242301 December (2007).

[110] Toneev, V. D., Nikonov, E. G., Friman, B., Nörenberg, W., and Redlich, K. *European Physical Journal C* **32**, 399–415 January (2003).

[111] Lavagno, A. *Physica A Statistical Mechanics and its Applications* **305**, 238–241 March (2002).

[112] Alt, C., Anticic, T., Baatar, B., Barna, D., and Bartke, e. a. *Phys. Rev. C* **77**, 024903 Feb (2008).

[113] STAR Collaboration, Aggarwal, M. M., Ahammed, Z., Alakhverdyants, A. V., Alekseev, I., and Anderson, e. a. *ArXiv e-prints* July (2010).

[114] Richardson, E. and for the PHENIX Collaboration. *ArXiv e-prints* June (2012).

[115] Heiselberg, H. and Wang, X.-N. *Phys. Rev. C* **53**, 1892–1902 Apr (1996).

[116] Teweldeberhan, A. M., Miller, H. G., and Tegen, R. *International Journal of Modern Physics E* **12**(03), 395–405 (2003).

[117] Drago, A., Lavagno, A., and Quarati, P. *Physica A: Statistical Mechanics and its Applications* **344**(3âĂŞ4), 472 – 477 (2004). <ce:title>Proceedings of the International Workshop on 'Trends and perspectives in extensive and non-extensive statistical mechanics', in honor of the 60th birthday of Constantino Tsallis</ce:title>.

[118] Tsallis, C. *Journal of Statistical Physics* **52**, 479 (1988).

[119] E.M.F., C. and Tsallis, C. *Journal of Physics A* **24**, 3187 (1991).

[120] C., T., R.S., M., and A.R., P. *Physica A* **261**(3), 534–554 (1998).

[121] Wilk, G. and Włodarczyk, Z. *Physical Review Letters* **84**, 2770–2773 March (2000).

[122] Tirnakli, U., Buyukkilic, F., and Demirhan, D. *Physics Letters A* **245**, 62 – 66 (1998).

[123] Silva, R., Anselmo, D. H. A. L., and Alcaniz, J. S. *EPL (Europhysics Letters)* **89**(1), 10004 (2010).

[124] Russkikh, V. N. and Ivanov, Y. B. *Phys. Rev. C* **74**, 034904 Sep (2006).

[125] Lavagno, A. *Physics Letters A* **301**, 13–18 August (2002).

[126] Osada, T. and Wilk, G. *Phys. Rev. C* **77**, 044903 Apr (2008).

[127] Biró, T. S., Purcsel, G., and Ürmössy, K. *European Physical Journal A* **40**, 325–340 June (2009).

[128] Greiner, W. and Rischke, D. H. *Physics Reports* **264**(1âĂŞ5), 183 – 204 (1996).

[129] Meyer-Ortmanns, H. *Rev. Mod. Phys.* **68**, 473–598 Apr (1996).

[130] Buballa, M. *Physics Reports* **407**(4âĂŞ6), 205 – 376 (2005).

[131] Braun-Munzinger, P. and Wambach, J. *Rev. Mod. Phys.* **81**, 1031–1050 Jul (2009).

[132] Prakash, M., Lattimer, J. M., Pons, J. A., Steiner, A. W., and Reddy, S. In *Physics of Neutron Star Interiors,* Blaschke, D., Glendenning, N. K., and Sedrakian, A., editors, volume 578 of *Lecture Notes in Physics, Berlin Springer Verlag*, 364, (2001).

[133] Prakash, M., Cooke, J. R., and Lattimer, J. M. *Rhysical Review D* **52**, 661–665 July (1995).

[134] Pons, J. A., Steiner, A. W., Prakash, M., and Lattimer, J. M. *Physical Review Letters* **86**, 5223–5226 June (2001).

[135] Pons, J. A., Reddy, S., Prakash, M., Lattimer, J. M., and Miralles, J. A. *Atrohpysical Journal* **513**, 780–804 March (1999).

[136] Prakash, M., Bombaci, I., Prakash, M., Ellis, P. J., Lattimer, J. M., and Knorren, R. *Physical Reviwe p* **280**, 1–77 (1997).

[137] Drago, A. and Lavagno, A. *Physics Letters B* **511**, 229–234 July (2001).

[138] Berezhiani, Z., Bombaci, I., Drago, A., Frontera, F., and Lavagno, A. *Atrohpysical Journal* **586**, 1250–1253 April (2003).

[139] Drago, A., Lavagno, A., and Parenti, I. *Astrohpysical Journal* **659**, 1519–1535 April (2007).

[140] Schimft S et al., journal = Physical Review D, y. . . v. . . d. . P. .

[141] Biró, T. S. and Greiner, C. *Physical Review Letters* **79**, 3138–3141 October (1997).

[142] Biró, T. S. *Journal of Physics G Nuclear Physics* **35**(4), 044056 April (2008).

[143] Bediaga, I., Curado, E. M. F., and de Miranda, J. M. *Physica A Statistical Mechanics and its Applications* **286**, 156–163 October (2000).

[144] Alberico, W. M., Lavagno, A., and Quarati, P. *European Physical Journal C* **12**, 499–506 February (2000).

[145] Lavagno, A., Scarfone, A. M., and Narayana Swamy, P. *Journal of Physics A Mathematical General* **40**, 8635–8654 July (2007).

[146] Beck, C. *Physica A Statistical Mechanics and its Applications* **286**, 164–180 October (2000).

[147] Lavagno, A. and Quarati, P. *Physics Letters B* **498**, 47–52 January (2001).

[148] Lavagno, A. and Quarati, P. *Nuclear Physics B Proceedings Supplements* **87**, 209–211 June (2000).

[149] Ferro, F., Lavagno, A., and Quarati, P. *European Physical Journal A* **21**, 529–534 September (2004).

[150] Alberico, W. M., Czerski, P., Lavagno, A., Nardi, M., and Somá, V. *Physica A Statistical Mechanics and its Applications* **387**, 467–475 January (2008).

[151] Cleymans, J., Hamar, G., Levai, P., and Wheaton, S. *Journal of Physics G Nuclear Physics* **36**(6), 064018 June (2009).

[152] Landau, S. J., Mosquera, M. E., and Vucetich, H. *Astrohpysical Journal* **637**, 38–52 January (2006).

[153] Quarati, P. and Scarfone, A. M. *Astrohpysical Journal* **666**, 1303–1310 September (2007).

[154] Carvalho, J., do Nascimento, J., Silva, R., and Medeiros, J. *Astrohpysical Journal* **696**, L48 (2009).

[155] Livadiotis, G. and McComas, D. J. *Astrohpysical Journal* **714**, 971–987 May (2010).

[156] Leubner, M. P. *Astrohpysical Journal* **632**, L1–L4 October (2005).

[157] Burrows, A., Mazurek, T. J., and Lattimer, J. M. *Astrohpysical Journal* **251**, 325–336 December (1981).

[158] Benvenuto, O. and Lugones, G. *Royal Astro. Soc.* **304**, 25 (2008).

[159] Steiner, A. W., Prakash, M., and Lattimer, J. M. *Physics Letters B* **486**, 239–248 August (2000).

[160] Fischer, T., Whitehouse, S. C., Mezzacappa, A., Thielemann, F.-K., and Liebendörfer, M. *Astronomy and Astrophysics* **499**, 1–15 May (2009).

[161] Schaefer, B.-J. and Wagner, M. *Physical Review D* **79**(1), 014018 January (2009).

[162] Fodor, Z. and Katz, S. D. *Journal of High Energy Physics* **4**, 50 April (2004).

[163] Kekelidze, V. D. e. a. *Phys. Atomic Nuclei* **75**, 542 (2012).

[164] Biró, T. S. and Greiner, C. *Physical Review Letters* **79**, 3138–3141 October (1997).

[165] Fuchs, C. *Progress in Particle and Nuclear Physics* **56**(1), 1 – 103 (2006).

[166] Ferini, G., Colonna, M., Gaitanos, T., and Toro, M. D. *Nuclear Physics A* **762**, 147 – 166 (2005).

[167] di Toro, M., Drago, A., Gaitanos, T., Greco, V., and Lavagno, A. *Nuclear Physics A* **775**, 102–126 August (2006).

[168] Gervino, G., Lavagno, A., and Pigato, D. *Journal of Physics Conference Series* **306**(1), 012070 July (2011).

[169] Gervino, G., Lavagno, A., and Pigato, D. *Central European Journal of Physics* **10**, 594–601 June (2012).

[170] Sahu, P. and Cassing, W. *Nuclear Physics A* **712**(3âĂŞ4), 357 – 369 (2002).

[171] StÃűcker, H. and et al., E. L. B. *Journal of Physics G: Nuclear and Particle Physics* **31**(6), S929 (2005).

[172] Isse, M., Ohnishi, A., Otuka, N., Sahu, P. K., and Nara, Y. *Phys. Rev. C* **72**, 064908 Dec (2005).

[173] Lavagno, A., Pigato, D., and Quarati, P. *Journal of Physics G Nuclear Physics* **37**(11), 115102 November (2010).

[174] Jaffe, R. L. *Physical Review Letters* **38**, 195–198 January (1977).

[175] Yoon, C. J., Akikawa, H., and Aoki, K. e. a. *Physical Review C* **75**(2), 022201 February (2007).

[176] Beane, S. R., Chang, E., and Detmold, W. a. *Physical Review Letters* **106**(16), 162001 April (2011).

[177] Inoue, T., Ishii, N., and Aoki, S. e. a. *Physical Review Letters* **106**(16), 162002 April (2011).

[178] Tsallis, C. and Bukman, D. J. *Phys. Rev. E* **54** (1996).

[179] Jaqaman, H., Mekjian, A. Z., and Zamick, L. *Phys. Rev. C* **27**, 2782–2791 Jun (1983).

[180] Goodman, A. L., Kapusta, J. I., and Mekjian, A. Z. *Phys. Rev. C* **30**, 851–865 Sep (1984).

[181] Bondorf, J., Donangelo, R., Mishustin, I., and Schulz, H. *Nuclear Physics A* **444**(3), 460 − 476 (1985).

[182] Lavagno, A. and Pigato, D. 2nd European Nuclear Physics Conference, 17–21 September 2012, Bucarest.

[183] Johnson, K. and Sudarshan, E. *Annals of Physics* **13**(1), 126 − 145 (1961).

[184] de Jong, F. and Malfliet, R. *Phys. Rev. C* **46**, 2567–2581 Dec (1992).

[185] Boguta, J. *Physics Letters B* **109**(4), 251 − 254 (1982).

[186] Ferini, G., Colonna, M., Gaitanos, T., and Toro, M. D. *Nuclear Physics A* **762**, 147 − 166 (2005).

[187] Landau, L. D. and E. M. Lifshitz, Butterworth-Heinemann, O. U. . *Statistical Physics* .

[188] L. E. Reichl, University of Texas Press, A. . *A Modern Course in Statistical Physics* .